

INVESTIGATION OF THE DYNAMIC PROPERTIES OF FERROELECTRIC
CRYSTALS CLOSE TO PHASE TRANSITIONS

A THESIS SUBMITTED TO
THE GRADUATE SCHOOL OF NATURAL AND APPLIED SCIENCES
OF
MIDDLE EAST TECHNICAL UNIVERSITY

BY

ALI KİRACI

IN PARTIAL FULFILLMENT OF THE REQUIREMENTS
FOR
THE DEGREE OF DOCTOR OF PHILOSOPHY
IN PHYSICS

JULY 2015

Approval of the thesis:

**INVESTIGATION OF THE DYNAMIC PROPERTIES OF
FERROELECTRIC CRYSTALS CLOSE TO PHASE TRANSITIONS**

submitted by **ALİ KİRACI** in partial fulfillment of the requirements for the degree
of **Doctor of Philosophy in Physics Department, Middle East Technical
University** by,

Prof. Dr. Gülbin Dural Ünver
Dean, Graduate School of **Natural and Applied Sciences**

Prof. Dr. Mehmet Zeyrek
Head of Department, **Physics**

Prof. Dr. Hamit Yurtseven
Supervisor, **Physics Dept., METU**

Examining Committee Members:

Prof. Dr. Bekir Sıtkı Kandemir
Physics Dept., Ankara University

Prof. Dr. Hamit Yurtseven
Physics Dept., METU

Assoc. Prof. Dr. Alpan Bek
Physics Dept., METU

Prof. Dr. Barış Akaoğlu
Physics Eng. Dept., Ankara University

Assoc. Prof. Dr. Barış Emre
Physics Eng. Dept., Ankara University

Date:

I hereby declare that all information in this document has been obtained and presented in accordance with academic rules and ethical conduct. I also declare that, as required by these rules and conduct, I have fully cited and referenced all material and results that are not original to this work.

Name, Last Name: ALI KIRACI

Signature :

ABSTRACT

INVESTIGATION OF THE DYNAMIC PROPERTIES OF FERROELECTRIC CRYSTALS CLOSE TO PHASE TRANSITIONS

Kiracı, Ali

Ph.D., Department of Physics

Supervisor : Prof. Dr. Hamit Yurtseven

July 2015, 94 pages

In this thesis we investigated the dynamical properties of some ferroelectric crystals and ceramics under various temperature and pressure conditions close to the phase transitions. In particular, we focused on the Raman frequencies, damping constant and the activation energy of soft modes with the pseudospin-phonon coupling in some ferroelectric crystals exhibiting phase transitions. We predicted the critical behavior of the frequency related to the order parameter (spontaneous polarization) in the ferroelectric and/or paraelectric phases of potassium dihydrogen phosphate (KDP), barium titanate (BaTiO_3), lead titanate (PbTiO_3), lead zirconate titanate (PZT), strontium zirconate (SrZrO_3), cadmium niobate ($\text{Cd}_2\text{Nb}_2\text{O}_7$) and lithium niobate (LiNbO_3). For these predictions, our calculations have been performed by using the mean field theory (MFT).

We analyzed the damping constant as a function of temperature and/or pressure for the ferroelectrics studied in this thesis by using the pseudospin-phonon coupled model and the energy fluctuation model. We also calculated the temperature dependence of the relaxation time of BaTiO₃, PZT and LiNbO₃ using our results of the order parameter and the damping constant described from both models studied here. We also used the Landau phenomenological theory to describe the observed behavior of the dielectric constant (or susceptibility) in the ferroelectric and paraelectric phases of BaTiO₃ and in the ferroelectric phase of LiNbO₃.

As a part of this thesis, we calculated the temperature dependence of the frequency of Raman modes for NaNO₂ through the Grüneisen parameter. By analyzing the experimental data from the literature, the observed behavior of those ferroelectric crystals is described on the basis of the models studied here.

Keywords: Order Parameter, Damping Constant, Activation Energy, Ferroelectric

Materials, Dielectric Constant

ÖZ

FAZ GEÇİŞLERİ YAKININDA FERROELEKTRİK KRİSTALLERİN DİNAMİK ÖZELLİKLERİNİN ARAŞTIRILMASI

Kıracı Ali

Doktora, Fizik Bölümü

Tez Yöneticisi: Prof. Dr. Hamit Yurtseven

Temmuz 2015, 94 sayfa

Bu tezde bazı ferroelektrik kristal ve seramiklerin faz geçişleri yakınında çeşitli sıcaklık ve basınç koşulları altında dinamik özelliklerini inceledik. Özellikle, faz geçişi gösteren bazı ferroelektrik kristallerde sanki spin-fonon çiftlenimiyle yumuşak kiplerin Raman frekansları, sönüm katsayıları ve aktivasyon enerjilerine odaklandık. Ferroelektrik ve/veya paraelektrik fazlarda düzen parametresi (kendiliğinden polarizasyon) ile ilintili frekansların kritik davranışlarını potasyum sülfat (KDP), baryum titanat (BaTiO_3), kurşun titanat (PbTiO_3), kurşun zirkonat titanat (PZT), stronsiyum zirkonat (SrZrO_3), kadmiyum niyobat ($\text{Cd}_2\text{Nb}_2\text{O}_7$) ve lityum niyobat (LiNbO_3) için öngördük. Bu öngörüler için yapılan hesaplamalar ortalama alan teorisi (MFT) kullanılarak gerçekleştirilmiştir.

Sanki spin-fonon çiftlenimi modeli ile enerji dalgalanma modelini kullanarak bu tezde çalışılan ferroelektriklerin sönüm katsayısını sıcaklığın ve/veya basıncın

fonksiyonu olarak analiz ettik. Aynı zamanda, $BaTiO_3$, PZT ve $LiNbO_3$ ' ün durulma zamanının sıcaklık bağımlılığını, düzen parametresi ve burada çalışılan iki modelden bulunan sönüm katsayısı sonuçlarından hesapladık. $BaTiO_3$ ' ün ferroelektrik ve paraelektrik fazlarında ve $LiNbO_3$ ' ün ferroelektrik fazında dielektrik sabitinin (yada duygunluğun) gözlenen davranışını tanımlamak için Landau fenomenolojik teoriyi kullandık.

Bu tezin bir parçası olarak, $NaNO_2$ için Grüneisen parametresi aracılığı ile Raman kiplerinin sıcaklığa bağımlı frekanslarını hesapladık. Literatürden deneysel veri analiziyle bu ferroelektrik kristallerin gözlenen davranışı, burada çalışılan modeller temeli üzerinde betimlenmiştir.

Anahtar Kelimeler: Düzen Parametresi, Sönüm Katsayısı, Aktivasyon Enerji Ferroelektrik Malzemeler, Dielektrik Katsayısı.

To my beloved wife.

ACKNOWLEDGEMENTS

I would like to express my special appreciation and thanks to my advisor Prof. Dr. HAMİT YURTSEVEN, for his excellent supervision, patient guidance, encouragement, friendly attitude, being accessible and continuous support. Your advice on both research as well as on my career have been priceless. I would also like to thank my committee members, Prof. Dr. BEKİR SITKI KANDEMİR, Assoc. Prof. Dr. ALPAN BEK, Assoc. Prof. Dr. BARIŞ AKAOĞLU and Assoc. Prof. Dr. BARIŞ EMRE for serving as my committee members even at hardship. I also want to thank you for letting my defense be an enjoyable moment, and for your brilliant comments and suggestions, thanks to you.

I would also like to thank to Assoc. Prof. Dr. HÜSEYİN KARAÇALI for his encouragement and support during my research period.

A special thanks to my family. Words cannot express how grateful I am to my mother, my father and my sisters. I would also like to thank all of my friends who supported me in writing, and incited me to strive towards my goal. At the end I would like express appreciation to my beloved wife EMEL ALTAŞ KİRACI who spent sleepless nights with and was always my support in the moments when there was no one to answer my queries.

I would like to thank The Scientific and Technological Research Council of Turkey (TÜBİTAK) for supporting me 4 years in Turkey as a scholar during my Ph. D. thesis.

TABLE OF CONTENTS

ABSTRACT	v
ÖZ	vii
ACKNOWLEDGMENTS	x
TABLE OF CONTENTS	xi
LIST OF TABLES	xiv
LIST OF FIGURES	xviii
CHAPTERS	
1 INTRODUCTION	1
1.1 History of ferroelectrics	2
1.2 Classificaion of ferroelectric materials	3
1.3 Properties of ferroelectric materials.	5
1.3.1 Hysterisis Loop and polarization switching	5
1.3.2 Phase transitions	5
1.3.3 Domains	6
1.3.4 Dielectric constant and susceptibility	6
1.4 Barium titanate (BaTiO ₃)	7
1.5 Lead titanate (PbTiO ₃)	7
1.6 Potassium Dihydrogen Phosphate (KDP, KH ₂ PO ₄)	8
1.7 Sodium Nitrite (NaNO ₂)	8

1.8	Lead Zirconate Titanate (PZT, $\text{PbZr}_{1-x}\text{Ti}_x\text{O}_3$)	9
1.9	Strontium Zirconate (SrZrO_3)	9
1.10	Cadmium pyroniagate ($\text{Cd}_2\text{Nb}_2\text{O}_7$, CNO)	10
1.11	Lithium niobate (LiNbO_3 , LN)	10
2	THEORY	11
2.1	Landau phenomenological theory	11
2.2	Soft mode concept	12
2.3	Damping constant (Linewidth)	12
2.4	Order parameter (spontaneous polarization)	16
2.5	Grüneisen parameter	17
2.6	Activation energy	18
3	RESULTS AND DISCUSSION	19
3.1	Calculation of the raman frequency and the damping constant of a coupled mode in the ferroelectric and paraelectric phases in KH_2PO_4	19
3.2	Calculation of the damping constant for the soft-optic and acoustic mode in hexagonal barium titanate.	25
3.3	Temperature dependence of the Raman frequency, damping constant and the activation energy of a soft-optic mode in ferroelectric barium titanate	32
3.4	Damping constant calculated as a function of temperature for the tetragonal Raman mode close to the paraelectric-ferroelectric transition in BaTiO_3	37
3.5	Temperature dependence of the polarization and the dielectric constant near the paraelectric- ferroelectric transitions in BaTiO_3	40

3.6	Calculation of the damping constant and the order parameter for the lattice mode in ferroelectric PbTiO_3	49
3.7	Calculation of the infrared frequencies as a function of temperature using the volume data in the ferroelectric phase of NaNbO_3	52
3.8	Temperature dependence of the Brillouin frequency shift and the linewidth of the LA mode in the ferroelectric phase of PZT-x ($\text{PbZr}_{1-x}\text{Ti}_x\text{O}_3$)	56
3.9	Calculation of the damping constant, relaxation time and the activation energy for lead titanate zirconate in the paraelectric phase	59
3.10	Temperature dependence of the Raman frequency, damping constant and the activation energy of a soft mode in $\text{Cd}_2\text{Nb}_2\text{O}_7$	64
3.11	Calculation of the damping constant and the activation energy of the E_g soft phonon mode in ferroelectric SrZrO_3	67
3.12	Temperature dependence of the order parameter, damping constant, relaxation time and the activation energy of the $A_1(\text{TO}_1)$ soft phonon mode in ferroelectric LiNbO_3	70
3.13	Summary	77
4	CONCLUSIONS	79
4.1	Summary	84
	REFERENCES	85
	CURRICULUM VITAE	91

LIST OF TABLES

TABLES

Table 1.1	Important events in ferroelectricity [8]	3
Table 3.1	Comparison of the transition temperatures T_C calculated from Eq. (3.1) and $T_C^2 = 710(17.1 - P)$ [113] at various pressures [1].	19
Table 3.2	Values of the maximum observed [42] frequencies ω_0 , fitted parameters of Eq. (3.2) and the activation energies U for KDP [1].	22
Table 3.3	Values of the fitted parameters of Eq. (3.4) and the activation energies U (Eq. 2.26) at constant pressure of KDP at temperatures $T > T_C$ [1].	23
Table 3.4	Values of the coefficients obtained by fitting the order parameter P to the bilinear constant A according to Eq. (3.5) ($T < T_0$) for the hexagonal barium titanate [2]	25
Table 3.5	Values of the coefficients obtained by fitting κ to the inverse relaxation time τ according to Eq. (3.8) ($T < T_0$) for the hexagonal barium titanate. The κ values were calculated from Eq. (3.7) through the damping constant Γ (Eqs. 2.16 and 2.19), as indicated [1]	27
Table 3.6	Values of the activation energy U according to Eq. (2.26) where the damping constant Γ calculated from equations indicated, was used in the temperature range ($T < T_0$) for the hexagonal barium titanate. $k_B T_0$ value is also given here [2].	28
Table 3.7	Values of the coefficients a and b according to Eq. (3.12) in the phase above the transition temperature ($T_0 = 221.5K$) of the hexagonal $BaTiO_3$ [3].	33
Table 3.8	Values of the activation energy extracted from Eq. (2.26) where the calculated Γ_{sp} (Eqs. 2.16 and 2.19) were used in the temperature interval indicated in the phase above the transition temperature T_C ($T_0 = 222K$) of the hexagonal $BaTiO_3$. $k_B T_C$ value is also given here [3].	34

Table 3.9	The values of the background bandwidth Γ'_0 (Γ_0) and the amplitude A' (A) for the Raman mode indicated for BaTiO ₃ according Eqs. 2.16 and 2.19 [4]	37
Table 3.10	Values of the temperature T_C , the parameters α and a_4 (Eq. 3.26) for the ferroelectric-paraelectric transition for the thin films indicated in BaTiO ₃ [5]	42
Table 3.11	Values of the coefficients a_0 , a_1 and a_2 determined for the soft mode of E (1TO) within the temperature interval indicated in the ferroelectric phase of PbTiO ₃ according to Eq. (3.36) [6]	49
Table 3.12	Values of the coefficients b_0 , b_1 and b_2 determined for the soft mode of E (1TO) within the temperature interval indicated in the ferroelectric phase of PbTiO ₃ according to Eq. (3.37) [6]	50
Table 3.13	Values of the background damping constant (Γ'_0, Γ_0) and the coefficient (A', A) for the soft mode E (1TO) in the temperature intervals indicated according to the pseudospin-phonon coupled model (Eq. 2.16) and the energy fluctuation model (Eq. 2.19) for the ferroelectric phase of PbTiO ₃ [6]	51
Table 3.14	Values of the fitting parameters of Eq. (3.39) for the observed volume data [135]	53
Table 3.15	Constant volume V_1 , constant frequencies ν_1 values of lattice modes in NaNO ₂ . Values of the constant “Grüneisen parameter” γ_P is also given here [60]	53
Table 3.16	Coefficients of Eq. (3.38), whose values detected from the fitting procedure of Eq. (2.24) and observed frequency data [60] in bulk NaNO ₂ [7]	53
Table 3.17	Values of the fitted parameters for the damping constant Γ_{SP} (Eqs. 2.16 and 2.19) using the observed data [70] in the Ferroelectric phase ($T < T_C$) of PbZr _{1-x} Ti _x O ₃ ($x=0.45$).	57
Table 3.18	Values of the activation energy (U) which were calculated using the models within the temperature range indicated for the ferroelectric phase ($T < T_C$) of PbZr _{1-x} Ti _x O ₃ ($x=0.45$). $k_B T_C$ value at $T_C = 657$ K is also given here	58
Table 3.19	Coefficients of Eqs. 2.16 and 2.19 using the observed data [70] in the paraelectric phase ($T > T_C$) of PbZr _{1-x} Ti _x O ₃ ($x=0.45$).	60
Table 3.20	Coefficients of Eq. (3.42) for the inverse relaxation time τ^{-1} using the observed data [70] in the paraelectric phase ($T > T_C$) of PbZr _{1-x} Ti _x O ₃ ($x=0.45$).	61

Table 3.21	Values of the activation energy (U) which were calculated using the models within the temperature range indicated for the paraelectric phase ($T > T_C$) of $\text{PbZr}_{1-x}\text{Ti}_x\text{O}_3$ ($x=0.45$). $k_B T_C$ value at $T_C = 657$ K is also given here.	62
Table 3.22	Values of the coefficients a and b according to Eq. (3.37) below the transition temperature ($T_C = 196$ K) of $\text{Cd}_2\text{Nb}_2\text{O}_7$	64
Table 3.23	Values of the fitted parameters for the damping constant Γ (Eqs. 2.16 and 2.19) using the observed data [91] in the ferroelectric phase ($T < T_C$) of the $\text{Cd}_2\text{Nb}_2\text{O}_7$	65
Table 3.24	Values of the activation energy (U) which were calculated using the models within the temperature ranges indicated for the ferroelectric phase ($T < T_C$) of cadmium pyroniobate. $k_B T_C$ value at $T_C = 196$ K is also given here.	66
Table 3.25	Values of the fitted parameters for the damping constant Γ (Eqs. 2.16 and 2.19) using the observed data [81] in the ferroelectric phase ($T < T_C$) of the SrZrO_3	68
Table 3.26	Values of the activation energy (U) which were calculated using the models within the temperature ranges indicated for the ferroelectric phase ($T < T_C$) of SrZrO_3 . $k_B T_C$ value at $T_C = 1443$ K is also given here.	69
Table 3.27	Values of the fitted parameters (Eq. 3.44) for the lowest Raman mode $A_1(\text{TO}_1)$ in the LiNbO_3 below the transition temperature ($T_C = 1260$ K).	71
Table 3.28	Values of the fitted parameters (Eq. 3.44) for the lowest Raman mode $A_1(\text{TO}_1)$ in the LiNbO_3 below the transition temperature ($T_C = 1260$ K).	72
Table 3.29	Values of the fitted parameters (Eq. 3.47) for the lowest Raman mode $A_1(\text{TO}_1)$ in the LiNbO_3 below the transition temperature ($T_C = 1260$ K).	73
Table 3.30	Values of the fitted parameters for the damping constant Γ (Eqs. 2.16 and 2.19) using the observed data [81] in the ferroelectric phase ($T < T_C$) of the LiNbO_3	74
Table 3.31	Values of the coefficients obtained by fitting κ to the inverse relaxation time τ according to Eq. (3.48) ($T < T_C$) for LiNbO_3 . The κ values were calculated from Eq. (3.7) through the damping constant Γ (Eqs. 2.16 and 2.19), as indicated.	75

Table 3.32	Values of the activation energy (U) which were calculated using the models within the temperature ranges indicated for the ferroelectric phase ($T < T_C$) of SrZrO_3 . $k_B T_C$ value at $T_C = 1443 \text{ K}$ is also given here.	75
Table 3.33	Values of the activation energy U, which were calculated within the temperature ranges indicated for some ferroelectric materials studied in this here. $k_B T_C$ values are also given for comparison.	78

LIST OF FIGURES

FIGURES

Figure 1.1 Crystal structure of a perovskite type ferroelectric material with general formula ABO_3	4
Figure 1.2 Structural units of KH_2PO_4 . The arrows indicate the direction of the atomic displacements that give rise to the development of a dipole moment parallel to the c axis.	4
Figure 1.3 “ P - E hysteresis loop” for a typical ferroelectric material [15].	5
Figure 3.1 Figure 3.1 Pressure dependence of the observed [42] and calculated [1] (Eq. 3.2) of ω_-/ω_0 for KDP at $T=80$ K.	20
Figure 3.2 Figure 3.1 Pressure dependence of the observed [42] and calculated [1] (Eq. 3.2) of ω_-/ω_0 for KDP at $T=90$ K.	21
Figure 3.3 Pressure dependence of Γ_- calculated through P-P model (Eq. 2.16) and the E-F model (Eq. 2.19) below the transition temperature of KDP at $T=80$ K [1].	21
Figure 3.4 Pressure dependence of Γ_- calculated through P-P model (Eq. 2.16) and the E-F model (Eq. 2.19) below the transition temperature of KDP at $T=90$ K [1].	22
Figure 3.5 Image for the fitting procedure (Eq. 3.4) of the observed [42] and the calculated [1] (Eq. 2.19) damping constant Γ_- at constant pressure of KDP at temperatures $T > T_C$. The best fit is shown by a solid line.	22
Figure 3.6 Temperature dependent Γ_- calculated [1] from Eqs. (2.16) and (2.19) at temperatures $T > T_C$. The observed Γ_- that is deduced from the relaxation rate data [42] of KDP was also given in this graph.	23
Figure 3.7 Temperature dependent order parameter both observed [21] and calculated [2] (Eq. 2.16) for the hexagonal barium titanate at temperatures $T < T_C$	26
Figure 3.8 The damping constant Γ calculated [2] from Eqs. (2.16) and (2.19) for the hexagonal barium titanate at temperatures $T < T_C$ ($T_0 = 222K$).. . . .	27

Figure 3.9	Temperature dependent κ values calculated [2] from Eq. (3.7) through the damping constant Γ (Eqs. 2.16 and 2.19) for the hexagonal barium titanate ($T_0 = 222K$). Experimental data [21] for the relaxation time (Eq. 3.6) are also shown here..	28
Figure 3.10	Figure 3.10 Arrhenius plot (Eq. 2.26) by using Eq. (2.16) [2] in the temperature interval of 204.7 to 217K (Table 3.6) for the hexagonal barium titanate. ($T_0 = 222K$)..	29
Figure 3.11	Figure 3.10 Arrhenius plot (Eq. 2.26) by using Eq. (2.19) [2] in the temperature interval of 204.7 to 217K (Table 3.6) for the hexagonal barium titanate. ($T_0 = 222K$)..	29
Figure 3.12	The order parameter P fitted to the experimental data [114] for the frequency ratio ω_0/ω_{\max} of the soft phonon according to Eq. (3.11) at various temperatures above the transition temperature ($T_0 = 222K$) of the hexagonal $BaTiO_3$ [3]	34
Figure 3.13	The damping constant Γ_{sp} calculated [3] from Eqs. (2.16) and (2.19) of the hexagonal $BaTiO_3$ at temperatures $T > T_C$ ($T_0 = 222K$). The observed Γ data [114] are also given here..	35
Figure 3.14	Temperature dependence of the full width at half maximum (FWHM) of the 308 cm^{-1} line [4]. The observed data for thin films of 60 nm and 200 nm [116] of this mode are shown, respectively. The observed [114] Raman bandwidths of the soft-optic mode in the hexagonal $BaTiO_3$ are also shown for comparison.	38
Figure 3.15	Temperature dependent $(\omega/\omega_{\max})^2$ values of the 310 cm^{-1} Raman mode (correlated to the spontaneous polarization P) for the ferroelectric (FE) – paraelectric (PE) transition using the thin film of 60 nm according to Eq. (3.30) in $BaTiO_3$ [5].. The observed data [125] are also shown here.	43
Figure 3.16	Temperature dependent $(\omega/\omega_{\max})^2$ values of the 310 cm^{-1} Raman mode (correlated to the spontaneous polarization P) for the ferroelectric (FE) – paraelectric (PE) transition using the thin film of 200 nm according to Eq. (3.30) in $BaTiO_3$ [5]. The observed data [125] are also shown here.	43

Figure 3.17 Temperature dependent χ^{-1} values for the ferroelectric (FE) – paraelectric (PE) transition using the thin film of 60 nm according to Eq. (3.27) (FE) and Eq. (3.28) (PE) in BaTiO ₃ [5]	44
Figure 3.18 Temperature dependent χ^{-1} values for the ferroelectric (FE) – paraelectric (PE) transition using the thin film of 200 nm according to Eq. (3.27) (FE) and Eq. (3.28) (PE) in BaTiO ₃ [5].. . . .	44
Figure 3.19 The observed spontaneous polarization P_S^2 of single-crystal BaTiO ₃ [127]. P_S^2 was normalized with respect to its maximum value.. . . .	45
Figure 3.20 Inverse susceptibility (χ^{-1}) obtained from the observed dielectric constant (ϵ) [128] as a function of the temperature for barium titanate ceramics with different porosities and pore size (5%) [5].	46
Figure 3.21 Variation of the inverse susceptibility (χ^{-1}) obtained from the experimental dielectric constant (ϵ) [129] with the temperature at three frequencies (10, 100 and 100 kHz) of Ba _{1-x} Ce _x TiO ₃ for x=0 (BaTiO ₃) [5].. . . .	47
Figure 3.22 Raman frequencies of the soft mode E (1TO) which were calculated as a function of temperature using the molecular field theory (Eq. 2.20) by fitting to the experimental data [33] in the ferroelectric phase of PbTiO ₃ (T _C = 493 °C) [6].. . . .	50
Figure 3.23 Damping constant Γ calculated [6] using both the pseudospin-phonon coupled model (Eq. 2.16) and the energy fluctuation model (Eq. 2.19) for the soft mode of E (1TO) in the ferroelectric phase of PbTiO ₃ (T _C = 493 °C)..	51
Figure 3.24 Temperature dependence of the observed volume [135] for bulk NaNO ₂ . The best line is shown by a solid line [7].. . . .	52
Figure 3.25 Temperature dependence of the calculated Eq. (2.24) and observed [60] longitudinal optic and transverse optic frequencies of A ₁ mode in NaNO ₂ [7].. . . .	54
Figure 3.26 Temperature dependence of the calculated Eq. (2.24) and observed [60] longitudinal optic and transverse optic frequencies of B ₁ mode in NaNO ₂ [7].. . . .	54
Figure 3.27 Temperature dependence of the calculated Eq. (2.24) and observed [60] longitudinal optic and transverse optic frequencies of B ₂ mode in NaNO ₂ [7].. . . .	55
Figure 3.28 Temperature dependence of the observed Brillouin frequencies of the LA mode in the ferroelectric (T<T _C) of PbZr _{1-x} Ti _x O ₃ [70] (T _C = 657 K)..	56

Figure 3.29	Temperature dependent Γ_{sp} values calculated (Eqs. 2.16 and 2.19) using the observed Brillouin frequency data [70] for the ferroelectric phase ($T < T_C$) of $\text{PbZr}_{1-x}\text{Ti}_x\text{O}_3$ ($x=0.45$). Observed FWHM [70] are also shown here ($T_C= 657$ K).	57
Figure 3.30	Temperature dependence of the observed Brillouin frequencies of the LA mode in the paraelectric ($T > T_C$) of $\text{PbZr}_{1-x}\text{Ti}_x\text{O}_3$ [70] ($T_C= 657$ K).	60
Figure 3.31	Temperature dependent Γ_{sp} values calculated (Eqs. 2.16 and 2.19) using the observed Brillouin frequency data [70] for the paraelectric phase ($T > T_C$) of $\text{PbZr}_{1-x}\text{Ti}_x\text{O}_3$ ($x=0.45$). Observed FWHM [70] are also shown here.	61
Figure 3.32	Temperature dependence of the relaxation time calculated (Eq. 3.41) using the observed Brillouin frequency data [70] for the paraelectric phase ($T > T_C$) of $\text{PbZr}_{1-x}\text{Ti}_x\text{O}_3$ ($x=0.45$). Observed relaxation time [70] also shown here.	62
Figure 3.33	Calculated (Eq. 3.37) and observed [91] values of the soft mode frequency at temperatures $T < T_C$ for CNO.	64
Figure 3.34	Comparison of the calculated (Eqs. 2.16 and 2.19) and observed Γ [91] values at temperatures $T < T_C$ for CNO.	65
Figure 3.35	The temperature dependent frequency ratio squared $(\omega/\omega_{\max})^2$ values of the Eg mode of SrZrO_3 at temperatures $T < T_C$. ($T_C= 1443$ K).	67
Figure 3.36	The calculated Γ values using both the P-P model (Eq. 2.16) and the EF model (Eq. 2.19) for the Raman mode of SrZrO_3 in the ferroelectric phase. Observed damping constant [81] is also shown here. Solid curve is a guide to eye.	68
Figure 3.37	The best linear fit for the square of the observed frequency (normalized) data [92] as a function of temperature difference for the lowest Raman mode $A_1(\text{TO}_1)$ in the LiNbO_3 below the transition temperature ($T_C= 1260$ K).	71
Figure 3.38	The best fit (quadratic) for the inverse dielectric susceptibility χ^{-1} (Eq. 3.46) as a function of the temperature difference for the lowest Raman mode $A_1(\text{TO}_1)$ in the LiNbO_3 below the transition temperature ($T_C= 1260$ K).	72
Figure 3.39	Temperature dependence of the normalized observed frequencies (squared) and the calculated values of P^2 (Eq. 3.18) for the lowest Raman mode $A_1(\text{TO}_1)$ in the LiNbO_3 below the transition temperature ($T_C= 1260$ K).	73

Figure 3.40 Damping constant Γ calculated as a function of temperature using both the pseudospin-phonon coupled model (Eq. 2.16) and the energy fluctuation model (Eq. 2.19) for the Raman mode of LiNbO_3 in the ferroelectric phase. Observed damping constant [92] are also shown here. . . 73

Figure 3.41 Temperature dependence of the relaxation time κ calculated from Eq. (3.7) through the damping constant Γ (Eqs. 2.16 and 2.19) for the LiNbO_3 . Experimental data τ^{-1} [92] for the relaxation time are also shown here. The solid line is a guide to eye. 74

CHAPTER 1

INTRODUCTION

Ferroelectric materials are special materials which possess a spontaneous polarization P_S in the absence of the electric field. Their spontaneous polarization can be determined through the polarization-electric field (P-E) hysteresis loop. Increasing temperature up to the Curie temperature leads to the rapidly decreasing of spontaneous polarization. They have some characteristics. By applying a suitable electric field, the spontaneous polarization can be reversed (switching process, reversible polarization). They have very high dielectric constant (permittivity) and around a phase transition temperature called Curie point, the electric permittivity exhibits a sharp peak (anomaly) which obeys, frequently, the Curie-Weiss law. Another important “fingerprint” of ferroelectrics is the non-linear behavior. This non-linear property allows us to make ferroelectric capacitors with adjustable capacitance. Ferroelectric domains, regions of uniform orientation of polarization, play an important role in the phase transitions through the motion of domain walls.

Although ferroelectrics have been known and been studied over a century, they are still widely investigated because of their diverse potential applications in sensor technology and microelectronic devices. Some applications of the ferroelectrics are ferroelectric capacitor (medical ultrasound machines), radio-frequency identification (RFID), dynamic random-access memory (DRAM), ferroelectric random access memory (FeRAM, lower power usage and faster write performance when compared with DRAM), high quality infrared cameras, fire sensors, sonar vibration sensor and ferroelectric tunnel junction (nanometer-thick ferroelectric). Various experimental techniques have been reported in the literature to understand the structural phase transitions in ferroelectrics, including dielectric measurements, neutron scattering, Raman scattering, infrared reflectivity and absorption, light scattering, nuclear

magnetic resonance (NMR), elastic, specific heat, x-ray, ultrasonic and Brillouin scattering, differential thermal analysis and electro-optic measurements. There are also some theoretical approaches to analyze the observed behavior of ferroelectric materials. In particular, mean field theories of Landau, Devonshire and Ginzburg, which are based on the symmetry criteria. Also, Cochran's lattice dynamical theory (W. Cochran, Adv. Phys 10, 401, 1961) and Cowley's microscopic anharmonic theory (R.A Cowley, Adv. Phys. 12, 421, 1963) have been reported in the literature to explain the soft mode concept as also explained by Landau, Devonshire and Ginzburg theories. Another concept is the mode coupling theory in which the two damped harmonic oscillators are considered to describe the coupled susceptibility of this interacted system by Cowley (R.A Cowley, J. Phys. Soc. Jap. Supp. 28, 239, 1970).

In this thesis, in particular we analyzed and predicted the damping constant below and above the transition temperature for some ferroelectric materials studied here. The origin of these two models was described by Matsushita for ammonium halides (See Ref. 102). We have published [1-7] on the dynamical properties some papers included in this thesis. Lately, we carried out some other studies for the lead titanate zirconate (PZT), $\text{Cd}_2\text{Nb}_2\text{O}_7$, SrZrO_3 and LiNbO_3 which have not been published yet but discussed in this thesis. All experimental data used and the details of our studies are given in Chapter 3, "Results and Discussions".

1.1 History of Ferroelectrics

The brief history of ferroelectrics was reported by L. E. Cross and R. E. Newnham in their study [8]. The early developments of ferroelectrics are mainly divided into three parts as given in their study. In the early 1880's, Pierre and Jacques Curie brothers observed that when quartz subjected to an external electric field, it changed its shape. This phenomenon was named as piezoelectricity. In 1920, Valasek discovered that the polarization of $\text{NaKC}_4\text{H}_4\text{O}_6 \cdot 4\text{H}_2\text{O}$, Rochelle salt, reoriented due to the external electric field below a certain transition temperature (Curie temperature) [9]. This property was later called ferroelectricity. In 1935, potassium

dihydrogen phosphate (KDP), KH_2PO_4 , was reported to be a ferroelectric material by G. Busch and P. Scherrer [10]. “perovskite era” has began with the discovery of barium titanate, BaTiO_3 , in the early 1940’s by Wainer and Solomon [11]. With the discovery of BaTiO_3 , researches on ferroelectrics accelerated in the middle of the 1940’s. Historical development in ferroelectrics is given briefly in Table 1.1 [8].

Table 1.1 Important events in ferroelectricity [8].

1920-1930	Rochelle salt period: discovery of ferroelectricity
1930-1940	KDP age: Thermodynamic and atomic models of ferroelectricity
1940-1950	Early barium titanate era: High-K capacitors developed
1950-1960	Period of proliferation: Many new ferroelectrics discovered
1960-1970	Age of high science: soft modes and order parameters
1970-1980	Age of diversification: Ferroelectrics, electro-optics, thermistors
1980-1990	Age of integration: Packages, composites and integrated optics
1990-2000	Age of miniaturization: size effect, manipulated modes and dipoles

1.2 Classification of ferroelectric materials

Ferroelectrics can be classified as two limiting forms. Changing of the dipole systems in a crystal from randomly direction to a favored direction is the order-disorder type, while the opposite movement of the positive and negative ions is displacive type. In the first order transitions, the polarization (order parameter) and the enthalpy are discontinuous at the transition temperature while they are continuous in the second order transition.

Perovskites type of ferroelectrics with generic formula of ABO_3 is the displacive type. Some examples of perovskite type ferroelectrics are BaTiO_3 , PbTiO_3 , KNbO_3 , PbZrO_3 , LiNbO_3 and $\text{Pb}(\text{Zr}, \text{Ti})\text{O}_3$ (PZT). Figure 1.1 shows the lattice for perovskite type. A perovskite has a cubic crystal structure at the high temperatures. The polarization occurs when B atom is displaced from the cubic center along any symmetry axes [12,13].

Sodium nitrite, NaNO_2 , and KH_2PO_4 (KDP) are typical examples of order-disorder type ferroelectrics. Structural unit of KH_2PO_4 is given in Figure 1.2 [14].

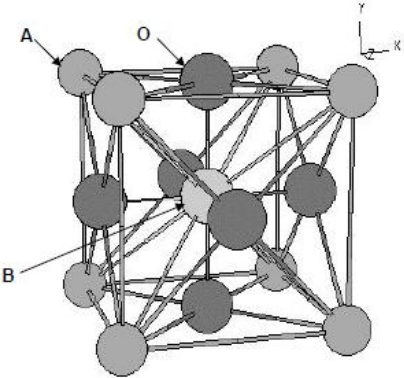


Figure 1.1 Crystal structure of a perovskite type ferroelectric material with general formula ABO_3 .

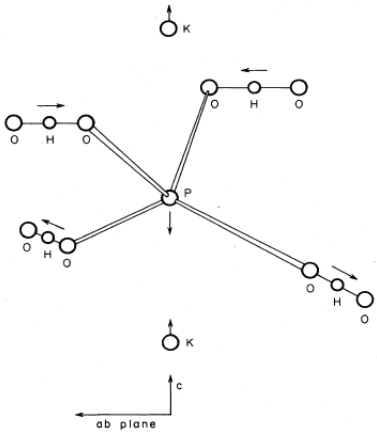


Figure 1.2 Structural units of KH_2PO_4 . The arrows indicate the direction of the atomic displacements that give rise to the development of a dipole moment parallel to the c axis.

1.3 Properties of Ferroelectric Materials

1.3.1 Hysteresis Loop and polarization switching

Polarization switching (reversal) is observed when a ferroelectric material subjected to a periodic external field. This applied field starts to change the polarization due to the reorientation of electric dipoles in domains. This phenomenon is one of the main characteristic of ferroelectrics. Schematic illustration of polarization is given in Figure 1.3 (P-E hysteresis loop) [15]. P_R shown in the figure is remanant polarization, it is the value of the polarization at $E=0$. Spontaneous polarization P_S is the saturation polarization (extrapolation of point C in the figure.)

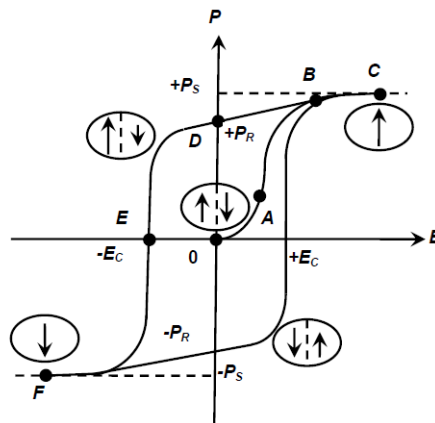


Figure 1.3 “P-E hysteresis loop” for a typical ferroelectric material [15].

1.3.2 Phase transitions

A structural phase transition takes place from the high temperatures (disordered phase) into the low temperatures (ordered phase) at a specific temperature T_C (Curie temperature). Below this temperature, the spontaneous polarization appears as an order parameter and at temperatures higher than T_C the spontaneous polarization is

equal to zero. Ferroelectrics show anomalies in the dielectric, elastic, thermal and other thermodynamic properties very close to the Curie temperature T_C [16].

1.3.3 Domains

Ferroelectric crystals generally have polarization in many directions. If there is no electric field and mechanical stress, many small regions called domains will form inside the crystal with decreasing temperature below T_C . Ferroelectric domain is the region within each of which the polarization aligns in the equal orientation. In adjacent domains, the polarization is in different directions [17]. The resultant polarization is the summation of the all different oriented dipoles in all domains. The movement of the domain wall, caused by an applied electric field, contribute to the dynamical properties of ferroelectric material.

1.3.4 Dielectric Constant and Susceptibility

Susceptibility, χ , is a quantity characterizing the capability of a material to be polarized under the changing external field. $\chi = \epsilon - 1$, where ϵ is the dielectric constant. In ferroelectric materials, the dielectric constant (susceptibility) is temperature dependent. At temperatures above T_C , most ferroelectrics obey Curie-Weiss relation given by

$$\epsilon(T) = \epsilon_0 + \frac{C}{T - T_0} \quad (1.1)$$

where C is the Curie-Weiss constant. T_0 is the constant Curie-Weiss temperature. At $T_0 < T_C$, the transition is first order while at $T_0 = T_C$, it is second order. ϵ_0 is the permittivity of the air (very small value). Ferroelectrics materials, in general, have high values of the dielectric constant.

1.4 Barium titanate (BaTiO₃)

BaTiO₃ is the most known perovskite type ferroelectric crystal. At temperatures higher than the transition temperature ($T_C = 400$ K), it has paraelectric cubic phase with point group O_h while it has a tetragonal ferroelectric phase with point group C_{4v} at temperatures lower than the transition temperature [18]. With decreasing the temperature below T_C , the titanium and oxygen atoms move with respect to the barium atom, which changes the symmetry of lattice (displacive type phase transition). BaTiO₃ undergoes successive phase transitions from cubic to tetragonal (paraelectric-ferroelectric), tetragonal to orthorhombic (ferro-ferro) and orthorhombic to rhombohedral (ferro-ferro) as also indicated in a T-P phase diagram [19]. In their study, Sawaguchi [20] reported that, hexagonal barium titanate (h-BaTiO₃) exhibits successive structural phase transitions at 222 K and 74 K showing both ferroelectric and ferroelastic property below 74 K. Above this temperature, h-BaTiO₃ is in the paraelectric phase and it shows piezoelectric properties below 222 K [21]. A lot of measurements have been carried out for BaTiO₃ such as the measurements of dielectric [22,23], neutron scattering [24], Raman scattering [25-28], infrared reflectivity [29], light scattering [21], NMR [30], elastic [31], and specific heat [32].

1.5 Lead titanate (PbTiO₃)

Lead titanate is another ferroelectric material with a type of perovskite structure. It has a potential applications in sensor technology and microelectronic devices since it exhibits ferroelectricity and piezoelectricity. PbTiO₃ undergoes a first order transition of displacive type at 766 K, which is associated with the soft modes [33]. Lead titanate has a tetragonal crystal structure with a space group $P4mm$ [34] in the ferroelectric phase ($T < T_C$) while it has a cubic crystal structure with a space group $Pm3m$ [35] in the paraelectric phase ($T > T_C$). Studies on the soft modes of PbTiO₃ have been carried out experimentally [33,36,37] and theoretically on the basis of mean-field and self-consistent phonon model calculations [38].

1.6 Potassium Dihydrogen Phosphate (KDP, KH_2PO_4)

Potassium dihydrogen phosphate is one of the well known hydrogen-bonded FE (ferroelectric) material. It undergoes an order-disorder phase transition ($T_C=123$ K) [39]. KDP has a tetragonal structure above 123 K (paraelectric phase) $1\bar{4}2d$ (D_{2d}^{12}) space group and it has an orthorhombic structure below 123 K (ferroelectric phase) with $Fdd2$ (C_{2v}^{19}) space group. A lot of experimental works have been carried out for KDP since its ferroelectric properties have known almost a century. Some theoretical works have been reported to clarify the phase transition mechanism in KDP such as, dynamical coupling theory [40] and tunneling model [41]. Also, some other works have been performed to investigate the coupled mode systems in KDP [42-46].

1.7 Sodium Nitrite (NaNO_2)

The phase transition in sodium nitrite is an order-disorder type which occurs at 436.2 K [47]. At temperatures $T < T_C$ (ferroelectric phase), it is in the orthorhombic structure and it has $C_{2v}^{25} Immm$ space group [48]. It is in the “antiferroelectric phase” between the temperature range of 438.5 K (Neel temperature) and 437.1 K (Curie temperature). [49]. Above the 438.5 K, it is in the disordered paraelectric phase with the space group $D_{2h}^{25} - Immm$ (orthorhombic structure) [50]. After the discovery of the ferroelectric behaviour of NaNO_2 [51], a lot of experimental and theoretical works have been reported to explain the phase transition mechanism in NaNO_2 . Some examples of experimental works are “x-ray” [52,53], “dielectric” [54,55], “thermal expansion” [56,57], “Raman spectra” [58,59], “infrared absorption” [60,61], “ultrasonic and Brillouin scattering” [62,63], “NMR” [64] and “neutron scattering” [65,66].

1.8 Lead Zirconate Titanate (PZT, $\text{PbZr}_{1-x}\text{Ti}_x\text{O}_3$)

Lead zirconate titanate is a solid mixture of lead zirconate (PbZrO_3) and lead titanate (PbTiO_3) with different concentrations (x). PZT has a phase boundary between the rhombohedral ($R3m$) and tetragonal ($P4mm$) phases which is known as morphotropic phase boundary (MPB) [67]. Growing a high-quality PZT single crystal is not easy, so that the exact crystal symmetry and the nature of phase transition near the MPB region over the whole composition in a wide temperature range remains still unclear [68,69]. As given in a recent study [70], a good-quality PZT single crystal was grown for the concentrations of $x=0.45$ and $x=0.42$. It is observed that ($x=0.45$) at 657 K, PZT undergoes a phase transition from the paraelectric cubic to a ferroelectric tetragonal and at 592 K, it exhibits a tetragonal-monoclinic phase transition. Structural, electrical and optical studies on PZT single crystals near MPB have been reported [71-73]. Also, a series of studies for the elastic properties and mechanical losses have been carried out [74-77].

1.9 Strontium zirconate (SrZrO_3)

Strontium zirconate, SrZrO_3 , is a member of the high temperature perovskite type ferroelectric material. It has been reported that [78], it has a structural phase transition from cubic ($Pm3m$) to tetragonal ($I4/mcm$) at the transition temperature of 1443 K, from tetragonal ($I4/mcm$) to orthorhombic ($Cmcm$) at 1103 K and from orthorhombic ($Cmcm$) to orthorhombic ($Pbnm$) at 973 K, respectively. X-ray diffraction [79], neutron scattering [78], heat capacity and thermal expansion [80] and ultraviolet Raman spectroscopy [81] are some of those studies reported in the literature.

1.10 Cadmium pyroniagate ($\text{Cd}_2\text{Nb}_2\text{O}_7$, CNO)

Cadmium pyroniagate, $\text{Cd}_2\text{Nb}_2\text{O}_7$, is a member of low temperature pyrochlore-type (with general formula of $\text{A}_2\text{B}_2\text{O}_7$) ferroelectric material. It has a complex phase transition sequences below the room temperature. Above 205 K, it has a cubic crystal structure ($\text{Fd}\bar{3}\text{m}$) [82,83] and CNO transforms to orthorhombic [84] or tetragonal [85] at 205 K (improper ferroelastic). CNO undergoes a phase transition at 196 K (proper ferroelectric) [84], another phase transition occurs at 85 K (incommensurate) [85] which follows the transition taking place at 46 K (commensurate) [82]. Investigations of the dielectric properties [86-88], domain structure [86], electrooptic [89], specific heat [90] and Raman scattering [91] are some of those studies reported in the literature for CNO.

1.11 Lithium niobate (LiNbO_3 , LN)

Lithium niobate, LiNbO_3 , is another member of high temperature perovskite type ferroelectric material. The structural phase transition of LN is still unclear despite several works reported in the literature. The transition temperature from paraelectric to the ferroelectric phase depends on the composition of lithium and niobate ions. LN is widely used for the applications in optoelectronics and nonlinear optics. Some reported studies on lithium niobate are, the Raman scattering [92], infrared spectroscopy [93], neutron scattering [94], differential thermal analysis (DTA) [95], x-ray diffraction [96] and the permittivity measurements [97].

CHAPTER 2

THEORY

2.1 Landau phenomenological theory

In 1937, Landau defined a theory of second-order phase transition depending on the symmetry criteria in the absence of external electric field. It is observed that the periodicity (with temperature) of density of a simple one dimensional lattice changes at temperatures below the transition temperature. This periodic charge density can be written in terms of polarization [14]. He assumed that the free energy F can be expanded in a power series near transition temperature T_C as follows

$$F = F_0 + \frac{1}{2}AP^2 + \frac{1}{3}BP^3 + \frac{1}{4}CP^4 + \dots \quad (2.1)$$

where P is the polarization (order parameter). There are two conditions for stability, $\frac{\partial F}{\partial P} = 0$ (first) and $\frac{\partial^2 F}{\partial P^2} < 0$ (second). First condition requires the elimination of any linear terms while the second condition requires that the coefficient A should be positive. The symmetry criterion eliminates any odd term in in Eq. (2.1). Only coefficient A has been assumed to be temperature dependent as,

$$A = A_0(T - T_C) \quad (2.2)$$

The coefficient A_0 in Eq. (2.2) is a positive constant. The relation between P and phonon frequency ω is reported as [98],

$$m\omega^2 = \frac{\partial^2 F}{\partial P^2} = A \quad (2.3)$$

By combining Eqs. (2.2) and (2.3), one gets

$$\omega = \omega_0(T - T_C)^{\frac{1}{2}} \quad (2.4)$$

The forces in ferroelectrics are mainly coulombic. Thus one can expect Eq. (2.4) to hold for the soft-mode behavior, as discussed below in section 2.2 with the soft mode concept in ferroelectrics.

Landau's theory can also be used to investigate the first-order phase transition by expanding the free energy F up to the sixth order. To sum up, the free energy can be considered in general as

$$F = F_0 + \frac{1}{2}A_0(T - T_0)P^2 + \frac{1}{4}CP^4 + \frac{1}{6}DP^6 \quad (2.5)$$

for $C > 0$ and $T_0 = T_C$, phase transition is second-order type, while for $C < 0$ and $T_0 \neq T_C$ phase transition is of a first-order type and when $C = 0$, transition is tricritical.

2.2 Soft mode concept

In 1959, Cochran reported that the anomaly behavior of dielectric constant in the neighborhood of T_C can be associated with an optical phonon mode (soft-mode) in which the crystal acquires periodic translational symmetry (displacive-type). At T_C , this soft phonon frequency ω_s decreases to zero. It is shown that, this concept can be applied also to the order-disorder type of ferroelectrics by de Gennes [100]. ω_s has been expressed as

$$\omega_s^2 \sim (T - T_C) \quad (2.6)$$

2.3 Damping constant (Linewidth)

Yamada et al. [101] developed a coupled model to investigate the temperature dependence of the damping constant by only considering one pseudospin and one phonon for NH_4Br , in 1972. In 1976, Matsushita extended this model by taking into

account more than one pseudospin and more than one phonon interactions [102]. He reported his Hamiltonian as

$$\begin{aligned}
H = & \frac{1}{2} \sum_{\vec{k}\nu} \left[P^*(\vec{k}\nu)P(\vec{k}\nu) + \omega_0^2(\vec{k}\nu)Q^*(\vec{k}\nu)Q(\vec{k}\nu) \right] - \frac{1}{2} \sum_{\vec{q}} J_{eff}(\vec{q})\sigma^*(\vec{q})\sigma(\vec{q}) \\
& + \sum_{\vec{k} \vec{q} \nu \nu'} K_{1,eff}(\vec{k} \vec{q} \nu \nu') \sigma(\vec{q}) Q^*(\vec{k}\nu) Q(\vec{k}-\vec{q}, \nu') \\
& + \sum_{\vec{k} \vec{q} \vec{q}' \nu \nu'} K_{2,eff}(\vec{k} \vec{q} \vec{q}' \nu \nu') \sigma(\vec{q}) \sigma(\vec{q}') Q^*(\vec{k}\nu) \times Q(\vec{k}-\vec{q}-\vec{q}', \nu')
\end{aligned} \tag{2.7}$$

where

$$J_{eff}(\vec{q}) = J(\vec{q}) + \sum_{\nu} \left| g(\vec{q}\nu) \right|^2 \tag{2.8}$$

This Hamiltonian has four terms, the ‘‘phonon energy’’ is described by the first two terms, P is the momentum of the phonon with the wave vector \vec{k} and mode ν , Q is its coordinate in the canonical form and, ω_0 is the characteristic frequency of the corresponding phonon. J_{eff} , appearing in the second term, is the interaction energy between the two pseudospins. The term with the coefficient $K_{1,eff}$ represents the interaction between one pseudospin and two phonons, while the term with the coefficient $K_{2,eff}$ corresponds to the interaction between two pseudospins and two phonons. Matsushita has derived the damping constant Γ_{SP} by using his Hamiltonian. It is given as,

$$\begin{aligned}
\Gamma_{\vec{x}}(\vec{k}\nu, \omega) = & \sum_{\vec{q} \nu'} \frac{\left| K_1(\vec{k}, \vec{q}, \nu, \nu') \right|^2}{8\omega\omega_0(\vec{k}-\vec{q}, \nu')} \times \left(\left\langle \frac{n(\omega_0(\vec{k}-\vec{q}, \nu'))}{n(\omega-\omega_0(\vec{k}-\vec{q}, \nu'))} + 1 \right\rangle \times S(\vec{q}, \omega-\omega_0(\vec{k}-\vec{q}, \nu')) \right. \\
& \left. + \left\langle \frac{n(\omega_0(\vec{k}-\vec{q}, \nu')) + 1}{n(\omega+\omega_0(\vec{k}-\vec{q}, \nu'))} + 1 \right\rangle \times S(\vec{q}, \omega+\omega_0(\vec{k}-\vec{q}, \nu')) \right)
\end{aligned} \tag{2.9}$$

Here, K_1 is proportional to the force constant. The “dynamic scattering function” $S(\vec{q}, \omega)$ is a Lorentzian shape function which is related to the full width at half maximum (FWHM or damping constant). So, $S(\vec{q}, \omega)$ describes the anomaly behavior of damping constant near transition temperature T_c . Laulicht and Luknar [103] have indicated the following approximations to get simpler form of Eq. (2.9). Namely,

- 1) At central peak (transition point) $\omega_v = \omega_0(\vec{k}, \nu) \approx \omega_0(\vec{k} - \vec{q}, \nu)$ and $\Gamma_{sp}(\vec{k}, \nu, \omega) \approx \Gamma_{sp}(\vec{k}, \nu, \omega_v)$.
- 2) The parameters ω , K_1 and n can be neglected in the neighborhood of T_c .
- 3) Replace integration instead of summation
- 4) $S[\vec{q}, \omega_v(\vec{k}) - \omega_v(\vec{k} - \vec{q}), \nu'] \cong S(\vec{q}, \omega \approx 0)$
- 5) $S(\vec{q}, \omega + \omega_0(\vec{k} - \vec{q}, \nu')) \approx 0$
- 6) The “dynamic scattering function” defined as

$$S(\vec{q}, \omega) = \langle n(\omega) + 1 \rangle \frac{\chi(\vec{q}, 0) \omega \tau_q}{1 + (\omega \tau_q)^2} \quad (2.10)$$

Using those approximations given above, Laulicht [104] has reached the following damping constant expression, given as

$$\Gamma_{sp}(\omega_v) \approx A \int_{BZ} S(\vec{q}, \omega) \left[\frac{n(\omega_v)}{n(\omega) + 1} + 1 \right] d^3q + B \quad (2.11)$$

. Laulicht has also considered the following approximations,

$$n(\omega) + 1 = (kT/\hbar\omega), \quad (\omega \tau_q)^2 \ll 1 \quad \text{and} \quad n(\omega_v)/[n(\omega) + 1] \ll 1 \quad \text{for} \quad \omega \approx 0,$$

By using these approximations and the definition of the “dynamic scattering function” (Eq. 2.10), Laulicht [104] has rewritten Eq. (2.11) as,

$$\Gamma_{sp} \simeq \frac{AkT}{\hbar} \int_{BZ} \chi(q,0) \tau_q d^3q + B \quad (2.12)$$

Laulicht and Luknar [103] have reported the following expression by using the “dynamic Ising model”

$$\chi(q,0)\tau_q = \frac{C(1-P^2)}{T} \frac{\tau_q^2}{\tau} \quad (2.13)$$

where $P = P_s/P_{\max}$ is the order parameter. It is also reported that [103],

$$\Gamma_{sp} \propto (1-P^2) \langle \tau_q^2 / \tau \rangle \quad (2.14)$$

where, $\langle \tau_q^2 / \tau \rangle$ is the “effective correlation time of the polarization”

In their study, Lahajnar et al.[105] have calculated the integration of Eq. (2.12) by using the Eq. (2.13) for KDP. They have reported that, the damping constant Γ_{sp} is proportional to the relaxation time T_1 , given as

$$\Gamma_{sp} \propto \frac{1}{T_1} = k\tau(1-P^2) \ln\left[\frac{T_c}{T-T_c(1-P^2)}\right] \quad (2.15)$$

Finally, the expression of the damping constant can be expressed as,

$$\Gamma_{sp} = \Gamma_0 + A(1-P^2) \ln\left[\frac{T_c}{T-T_c(1-P^2)}\right] \quad (2.16)$$

where Γ_0 and A are constants.

Schaack and Winterfelt [106] have also derived a statement for Γ_{sp} . They considered that, the damping constant is related to the fluctuation of the frequencies ($P = 0$) at zero wavevector value. They expressed this relation as,

$$\Gamma_{sp}^2 \propto \frac{kT\chi(0)}{V} \quad (2.17)$$

by using the definition of the dielectric susceptibility $\chi(0)$ (Eq. 2.13), they have reported that

$$\Gamma_{sp}^2 \propto \frac{T(1-P^2)}{T-T_C(1-P^2)} \quad (2.18)$$

Eq. (2.18) can be written as an expression

$$\Gamma_{sp} = \Gamma'_0 + A' \left[\frac{T(1-P^2)}{T-T_C(1-P^2)} \right]^{\frac{1}{2}} \quad (2.19)$$

where Γ'_0 and A' are constants, as given in Eq. (2.16).

To sum up, Eqs. (2.16), “pseudospin-phonon (P-P) coupled model”, and (2.19), “energy fluctuation (EF) model”, can be employed to compute temperature and/or pressure dependent Γ_{sp} in the paraelectric-ferroelectric phase transition, as we did for some ferroelectric materials such as BaTiO₃, PbTiO₃, PZT and KDP.

2.4 Order parameter (“spontaneous polarization”)

Order parameter is the orderness of a sample. It can take any value between 0 and 1. At temperatures well below the transition temperature T_C , in the ferroelectric phase, sample is completely ordered and the order parameter is equal to 1. As the temperature increases the order parameter decreases and at the temperature higher than T_C , in the paraelectric phase, sample is disordered and the value of order parameter becomes zero. So, the temperature dependent of the order parameter in Eqs. (2.16) and (2.19) need to be calculated in order to predict Γ_{sp} values from the P-P coupled model and EF model studied in this thesis. Brout [107] has reported an expression for order parameter as,

$$P \approx \begin{cases} 1 - 2\exp\left(\frac{-2T_C}{T}\right) & T \ll T_C \\ \left\{ 3 \left(1 - \frac{T}{T_C} \right) \right\}^{\frac{1}{2}} & 0 \ll (T_C - T) \ll T_C \\ 0 & T_C \ll T \end{cases} \quad (2.20)$$

2.5 Grüneisen parameter

Grüneisen parameter (γ) as a dimensionless quantity, can be used to set limitations for the thermal properties of solids varying with temperature and pressure. It has both macroscopic and microscopic definitions [108]. The macroscopic definition is related to the thermodynamic properties, which in principle may be obtained experimentally and the microscopic definition is related to the motion in atoms of any solid and vibrational frequency of those atoms. In their study Gillet et al. [109] have calculated the same mode Grüneisen parameter of forsterite (Mg_2SiO_4) by using the two definitions under the limitations of the anharmonic approximation.

By the definition (anharmonic approximation), the “mode Grüneisen parameter” given as

$$\gamma = -\frac{d \ln \nu}{d \ln V} \quad (2.21)$$

The temperature dependent “Grüneisen parameter” γ_P (isobaric) and the pressure dependent “Grüneisen parameter” γ_T (isothermal) can be represented as

$$\gamma_P = -\frac{V}{\nu} \frac{(\partial \nu / \partial T)_P}{(\partial V / \partial T)_P} \quad (2.22)$$

and

$$\gamma_T = -\frac{V}{\nu} \frac{(\partial \nu / \partial P)_T}{(\partial V / \partial P)_T} \quad (2.23)$$

From the representation of γ_P (Eq. 2.22), one can obtain the vibrational frequency ν_P , as a function of temperature, as

$$\nu_P(T) = A(T) + \nu_1 \left[\left(\frac{V_P(T)}{V_1} \right) \right]^{-\gamma_P} \quad (2.24)$$

The values of $\nu_P(T)$ and $V_P(T)$, at zero pressure and at a constant temperature, are ν_1 and V_1 , respectively. The temperature dependent term $A(T)$ in Eq. (2.24) can be deduced from the observed data of frequency.

2.6 “Activation energy”

Orientation of ion group can be considered as pseudospins. Activation energy is energy barrier between the pseudospins. The total linewidth (damping constant), including the activation energy U , as a function of temperature has been reported by Rakov [110] and Bartoli and Litovitz [111] as follows:

$$\Gamma \cong \Gamma_{vib} + C \exp\left(\frac{-U}{k_B T}\right) \quad (2.25)$$

The first term in Eq. (2.25) is due to the vibrational relaxation process while the second term corresponds to the reorientational relaxation process. Satiah and Bist [112] reported that, the first term can be treated as temperature independent over a short range of temperatures close to the transition temperature T_C . With this approximation one can get the following relation to calculate the activation energy U at various temperatures close to the phase transition temperature T_C as

$$\ln \Gamma = -\left(\frac{U}{k_B T}\right) \quad (2.26)$$

CHAPTER 3

RESULTS AND DISCUSSION

3.1 “Calculation of the Raman frequency and the damping constant of a coupled mode in the ferroelectric and paraelectric phases in KH_2PO_4 ”

We calculated the pressure dependent of frequencies and the damping constant, of ω_- mode below the transition temperature at 80 K and 90 K for KDP ($T_c = 122\text{K}$ at $P = 0$) [1]. Firstly, we examined the phase diagram of KDP ($T_c - P$) given by Samara [113] and we exposed a linear relation given by

$$T_c = 123 - 5P \quad (3.1)$$

We compared the transition temperatures of KDP calculated from Eq. (3.1) and an empirical formula $T_c^2 = k(P^* - P)$ [113] with constant k and P^* values of 710 K^2/kbar and 17.1 kbar, respectively, between 0 and 4 kbar as given in Table 3.1.

Table 3.1 Comparison of the transition temperatures T_c calculated from Eq. (3.1) and $T_c^2 = 710(17.1 - P)$ [113] at various pressures [1].

P (kbar)	Eq. (3.1) T_c (K)	$T_c^2 = k(P^* - P)$ T_c (K)
0	123	110.2
1	118	106.9
2	113	103.5
3	108	100.1
4	103	96.4

Table 3.2 Values of the maximum observed [42] frequencies ω_0 , fitted parameters of Eq. (3.2) and the activation energies U for KDP [1].

P (kbar)	T_c (K)	T (K)	ω_0 (cm ⁻¹)	a_0	a_1	Eq.(2.16) $-U$ (eV)	Eq.(2.19) $-U$ (eV)	$k_B T_c$ (eV)
0	122	80	145.21	0.494	0.505	0.106	0.063	0.011
		90	142.75	0.446	0.636	0.106	0.056	

Eq. (3.1) was inserted in Eq. (2.20) to compute order parameter S (P in Eq. 2.20) for fixed temperatures (Table 3.2) of KDP. We then related the calculated order parameter S with the observed (normalized) soft mode frequency ω_-/ω_0 according to a linear relation given as,

$$\omega_-/\omega_0 = a_0 + a_1 S \quad (3.2)$$

The maximum observed values of the Raman frequencies, ω_0 , the constants a_0 and a_1 for constant 80 K and 90 K temperatures were given in Table 3.2. The calculated (Eq. 3.2) and the observed [42] values of ω_-/ω_0 , as a function of pressure, were given in Fig. 3.1 (for T= 80 K) and Fig. 3.2 (for T= 90 K).

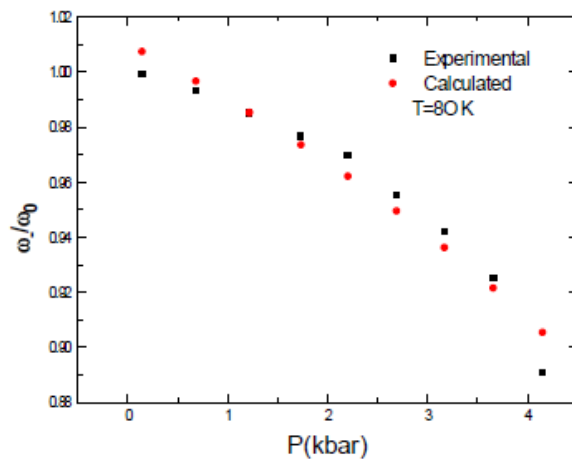


Figure 3.1 Pressure dependence of the observed [42] and calculated [1] (Eq. 3.2) of ω_-/ω_0 for KDP at T=80 K.

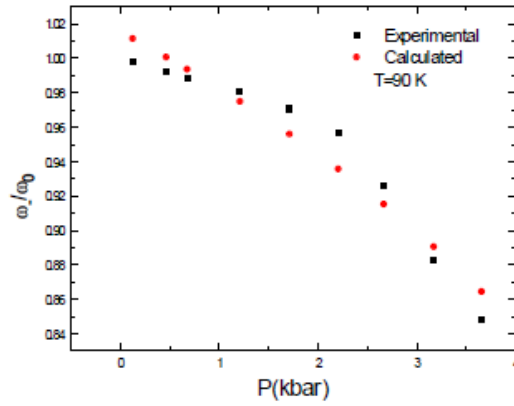


Figure 3.2 Pressure dependence of the observed [42] and calculated [1] (Eq. 3.2) of ω_-/ω_0 for KDP at T= 90 K.

Those calculated values of the order parameter S led us to predict the damping constant Γ_- of this Raman mode through the P-P model (Eq. 2.16) and the EF model (Eq. 2.19). Our prediction for the damping constant Γ_- of ω_- , as a function of pressure, were shown in Fig. 3.3 ($P = 0, T = 80 K$) and Fig. 3.4 ($P = 0, T = 90 K$). By inserting Eq. (3.1) in to the Eq. (2.26) where $T = T_C$, we deduced the U values of the coupled mode for constant 80 K and 90 K temperatures and zero pressure of KDP. These U values were given in Table 3.2.

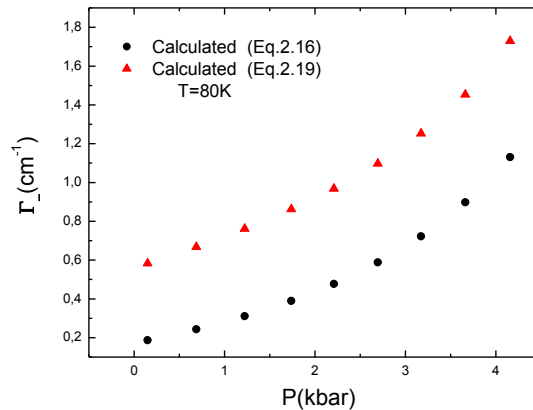


Figure 3.3 Pressure dependence of Γ_- calculated through P-P model (Eq. 2.16) and the E-F model (Eq. 2.19) below the transition temperature of KDP at T=80 K [1].

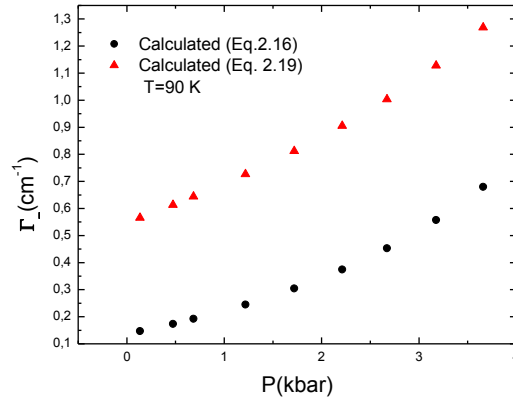


Figure 3.4 Pressure dependence of Γ_- calculated through P-P model (Eq. 2.16) and the E-F model (Eq. 2.19) below the transition temperature of KDP at $T=90$ K [1].

We also calculated the temperature dependent of the Raman frequencies and the damping constant of this coupled mode ω_- of KDP at temperatures $T > T_C$. It was observed experimentally [42] that ω_-^2 is directly proportional to the temperature, that is consistent with the soft mode concept. This linearity was reported as [42],

$$\omega_-^2 = 46.8(T - 86K) \text{ cm}^{-2} \quad (3.3)$$

We normalized (ω_-/ω_0) the observed frequencies [42] of this mode by using the maximum value $\omega_0 = 86.65 \text{ cm}^{-1}$ at $P = 6.54$ kbar.

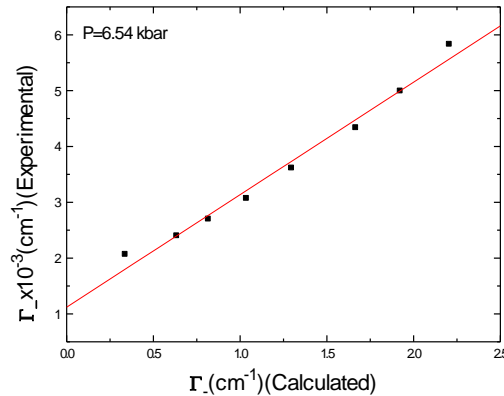


Figure 3.5 Image for the fitting procedure (Eq. 3.4) of the observed [42] and the calculated (Eq. 2.19) damping constant Γ_- at constant pressure of KDP at temperatures $T > T_C$. [1]. The best fit is shown by a solid line.

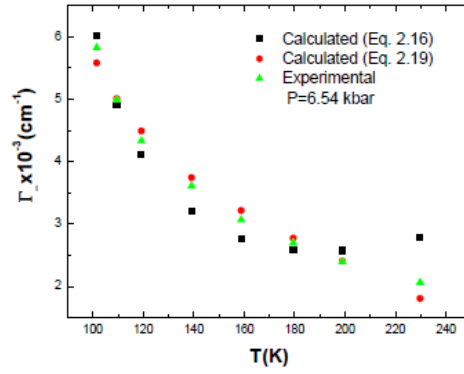


Figure 3.6 Temperature dependent Γ_- calculated [1] from Eqs. (2.16) and (2.19) at temperatures $T > T_C$. The observed Γ_- that is deduced from the relaxation rate data [42] of KDP was also given in this graph.

These normalized values of frequencies were then inserted in Eqs. (2.16) and (2.19) to calculate the Γ_- values of KDP where we replaced the order parameter S by ω_-/ω_0 . We also extracted the experimental data of Γ_- from the observed relaxation rate τ_-^{-1} through $\tau_-^{-1} = \omega_-^2/\Gamma_-$. We then fitted the observed and calculated values of Γ_- according to

$$\Gamma_-(obs) = a\Gamma_-(cal) + b \quad (3.4)$$

as given in Fig. 3.5. In this figure, the values of the $\Gamma_-(cal)$ were found from the “energy fluctuation model” (Eq. 2.19). The fitted parameters of Eq. (3.4) are given in Table 3.3. Fig. 3.6 shows the temperature dependence of the both observed and calculated values of Γ_- at constant pressure of KDP at temperatures $T > T_C$. The activation energy that is deduced from the Arrhenius plot of Eq. (2.26) is also given in Table 3.3 above the transition temperature of KDP.

Table 3.3 Values of the fitted parameters of Eq. (3.4) and the activation energies U (Eq. 2.26) at constant pressure of KDP at temperatures $T > T_C$ [1].

P (kbar)	T_C (K)	Equation	$a \times 10^{-3}$	$b \times 10^{-3} (\text{cm}^{-1})$	Eq. (2.26) $-U$ (eV)
6.54	91.6	2.16	2.97	2.13	0.013
		2.19	1.12	2.02	0.016

In his study Peercy [42] fitted the intensity data to the complex part of the susceptibility at various temperatures below the transition temperature T_c to deduce the pressure dependent of frequencies ω_- . He considered the “tunneling model” and the “coupled proton-optic model” to understand the pressure dependence of ω_- at $T < T_c$. He reported that, while the coupled model describe the observed data well the tunneling model does not.

In this study, we deduced the transition temperature, as a function of pressure, by analyzing experimental data [113] of Samara according to Eq. 3.1 that is consistent with the “Ginzburg-Devonshire” phenomenological theory. We compared the T_c values calculated from Eq. (3.1) and $T_c^2 = k(P^* - P)$, as given in Table 3.1. While Eq. (3.1) almost satisfied the expected result the other one did not since the paraelectric-ferroelectric phase transition takes place at 122 K [113]. The pressure dependence of the observed frequencies (normalized) and the calculated one from the mean field theory (inserting Eq. 3.1 into Eq. 2.20) were given in Figs. 3.1 and 3.2. As the pressure increases the coupled mode frequency ω_- increases as expected from the soft mode behavior. We then predicted the Γ_- values as a function of pressure from the P-P model (Eq. 2.16) and the EF model (Eq. 2.19) for constant 80 K (Fig. 3.3) and 90 K (Fig. 3.4) temperatures. The damping constant Γ_- increases as the pressure increases as expected below T_c in KDP. Our calculated pressure dependent Γ_- values can be compared with the observed data when they are available in the literature. Activation energies U have also deduced in terms of Arrhenius plot through Eq. (2.26) for KDAP at temperatures indicated, as given in Table 3.2.

Additionally, we investigated the dynamical properties (Γ_- and U) of KDP at temperatures $T > T_c$. We calculated the temperature dependent Γ_- values through Eqs. (2.16) and (2.19). We then compared the calculated and the observed data of damping constant that was deduced from the experimental relaxation rate data [42], as given in Fig. 3.6. The EF model (Eq. 2.19) describes better the experimental data [42] when compared with the P-P model (Eq. 2.16). Finally, we found the values of U for KDP above T_c at constant pressure, as also given in Table 3.3.

3.2 “Calculation of the damping constant for the soft-optic and acoustic mode in hexagonal barium titanate”

The temperature dependence of the damping constant was calculated below the transition temperature ($T_0 = 222K$) for the hexagonal barium titanate [2]. For this calculation, the order parameter which is related to the bilinear coupling between acoustic and soft-optic modes, was used at various temperatures below T_0 for this ferroelectric material. As indicated in a previous study [21], the bilinear coupling constant A in relation to the order parameter can have a temperature dependence according to Eq. (2.20) in the mean field theory with the critical exponent $\beta = \frac{1}{2}$ below T_C . By considering that the coupling constant varies with the square of the order parameter (P^2) [30] the bilinear coupling constant A studied here can be related to the order parameter (spontaneous polarization) according to

$$A = a_0 + a_1P + a_2P^2 \quad (3.5)$$

where a_0 , a_1 and a_2 are constants. Thus, by fitting P to the experimental data for A [21], the coefficients a_0, a_1 and a_2 were detected, as given in Table 3.4. Fig. 3.7 shows the bilinear coupling constant normalized with respect to the order parameter P for the hexagonal barium titanate. The experimental data for the bilinear coupling constant A [21] are also shown in this figure. Using the calculated order parameter (Fig. 3.7), the damping constant Γ of the soft-optic and acoustic mode was then calculated by Eqs. (2.16) and (2.19) at various temperatures below T_0 in barium titanate, as plotted in Fig.3.8.

Table 3.4 Values of the coefficients obtained by fitting the order parameter P to the bilinear constant A according to Eq. (3.5) ($T < T_0$) for the hexagonal barium titanate [2].

$h - BaTiO_3$	$T_0(K)$	$-a_0$	a_1	$-a_2$
A	222	0.040	1.966	0.531

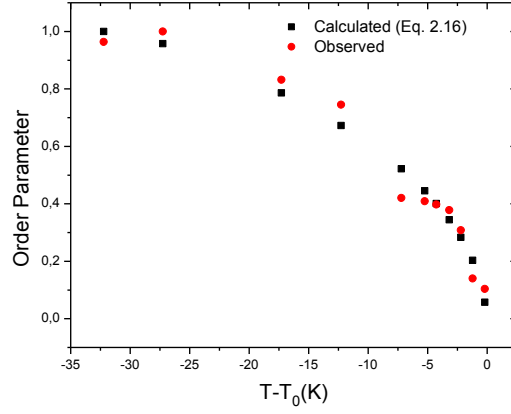


Figure 3.7 Temperature dependent order parameter both observed [21] and calculated [2] (Eq. 2.16) for the hexagonal barium titanate at temperatures $T < T_C$.

From the temperature dependence of the order parameter P (Eq. 2.20) and of the damping constant Γ (Eqs. 2.16 and 2.19), the relaxation time $1/\tau$ or κ of the soft-optic and acoustic mode was then calculated below T_0 in BaTiO₃. This calculation was based on the experimental data [21] for the relaxation time $1/\tau$ of this mode according to the relation

$$\frac{1}{\tau} \cong \frac{\omega_0^2}{\Gamma_0} \quad (3.6)$$

where ω_0 is the soft optic mode frequency and Γ_0 is its damping constant for barium titanate. By assuming that the soft mode frequency ω_0 is accompanied with the order parameter (it goes to zero as $T \rightarrow T_0$) which depends on the temperature below T_0 , the relaxation time $1/\tau$ (Eq. 3.6) or κ was predicted according to

$$\kappa \cong P^2/\Gamma \quad (3.7)$$

Here, Γ_0 in Eq. (3.6) that was used for the analysis of the experimental data [21] for the soft optic mode was replaced by Γ (Eq. 3.7) below T_0 in BaTiO₃.

Table 3.5 Values of the coefficients obtained by fitting κ to the inverse relaxation time τ according to Eq. (3.8) (T/T_0) for the hexagonal barium titanate. The κ values were calculated from Eq. (3.7) through the damping constant Γ (Eqs. 2.16 and 2.19), as indicated.

$T_0(K)$	Γ	$b_0(GHz)$	$b_1(GHz)^2$	$-b_2(GHz)^3$
222	Eq. (2.16)	23.0	37.683	0.712
	Eq. (2.19)	16.5	148.809	28.717

So, in order to calculate κ by Eq. (3.7) we followed the same procedure as $1/\tau$ (Eq. 3.6). As in the case of the order parameter P in relation to the bilinear coupling constant A (Eq. 3.5), it was found that the temperature dependence of the relaxation time κ (Eq. 3.7) was related to $1/\tau$ (Eq. 3.6) according to

$$\frac{1}{\tau} = b_0 + b_1\kappa + b_2\kappa^2 \quad (3.8)$$

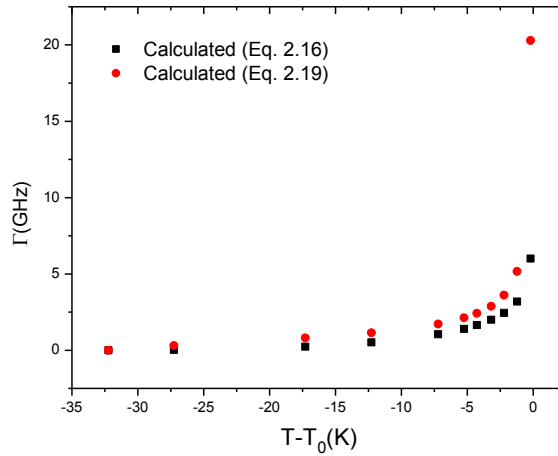


Figure 3.8 The damping constant Γ calculated [2] from Eqs. (2.16) and (2.19) for the hexagonal barium titanate at temperatures $T < T_C$ ($T_0 = 222K$).

with the coefficients b_0, b_1 and b_2 which were determined. So, as for the parameter

P , we also calculated the relaxation time κ based on the experimental data ω_0^2/Γ_0 for the soft-optic and acoustic mode [21] by using Eq. (3.8). Thus, κ (Eq. 3.7) was fitted to $1/\tau$ (Eq. 3.6) by using Eq. (3.8).

Table 3.6 Values of the activation energy U according to Eq. (2.26) where the damping constant Γ calculated from equations indicated, was used in the temperature range ($T < T_0$) for the hexagonal barium titanate. $k_B T_0$ value is also given here.

Damping constant	Temperature range	Activation energy U (eV)	$k_B T_0$ (eV)
Eq. (2.16)	$204.7 < T(K) < 217.7$	0.57	0.02
	$218.8 < T(K) < 221.8$	1.50	
Eq. (2.19)	$204.7 < T(K) < 217.7$	0.32	
	$218.8 < T(K) < 221.8$	2.61	

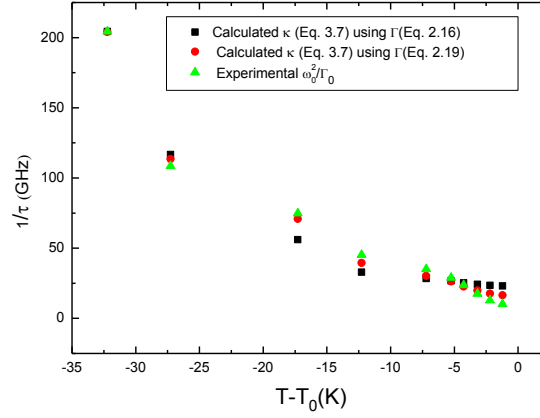


Figure 3.9 Temperature dependent κ values calculated [2] from Eq. (3.7) through the damping constant Γ (Eqs. 2.16 and 2.19) for the hexagonal barium titanate ($T_0 = 222K$). Experimental data [21] for the relaxation time (Eq. 3.6) are also shown here.

For this fitting, we used our calculated Γ values from Eqs. 2.16 and 2.19 (Fig. 3.8) and then we determined the coefficients b_0, b_1 and b_2 , as given in Table 3.5. Comparison of the calculated (Eq. 3.7) and experimental [21] values of the inverse relaxation time was given in Fig. 3.9. Finally, we extracted the U values using our calculated values of the damping constant Γ (Eqs. 2.16 and 2.19) according to Eq. 2.26 for the two different temperature ranges ($T < T_0$) of barium titanate. Table 3.6 gives our extracted values of the activation energy U in the temperature intervals studied.

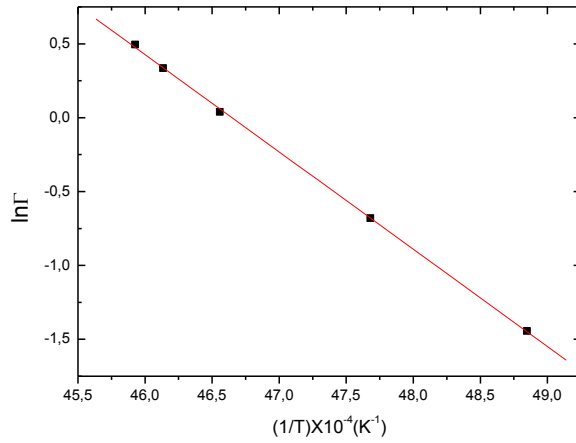


Figure 3.10 Arrhenius plot (Eq. 2.26) by using Eq. (2.16) [2] in the temperature interval of 204.7 to 217K (Table 3.6) for the hexagonal barium titanate. ($T_0 = 222K$).

As examples, we plot $\ln \Gamma$ vs. $\frac{1}{T}$ (Eq. 2.26) using the Γ values given by Eqs. (2.16) and (2.19) in the temperature interval indicated, as shown in Figs. 3.10 and 3.11, respectively. For comparison, the $k_B T_C$ value ($T_C = T_0 = 222K$) is also given for barium titanate in Table 3.6.

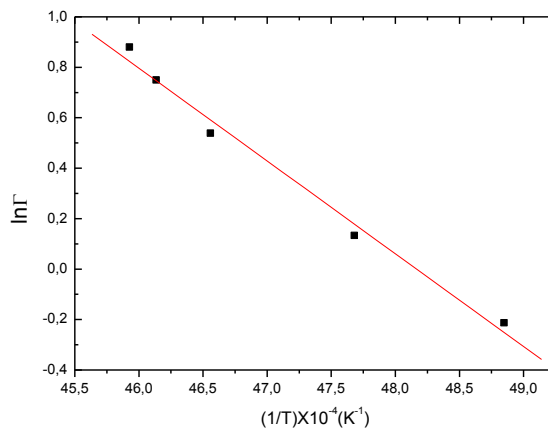


Figure 3.11 Arrhenius plot (Eq. 2.26) by using Eq. (2.19) [2] in the temperature interval of 204.7 to 217K (Table 3.6) for the hexagonal barium titanate. ($T_0 = 222K$).

The damping constant Γ of the soft-optic and acoustic mode was calculated from P-P model (Eq. 2.16) and EF model (Eq. 2.19). We first obtained P values by Eq. (2.20). This power-law formula was also used as

$$A \sim (T - T_0)^{\frac{1}{2}} \quad (T < T_0) \quad (3.9)$$

for the temperature dependence of the bilinear coupling constant A previously [21] to describe the mean field behaviour of the barium titanate below T_0 . Bilinear coupling constant A decreases as the temperature increases towards T_0 (Fig. 3.7), as also pointed out previously [21]. This gives that the soft mode-acoustic mode coupling grows largely at low temperatures, whereas at T_0 it vanishes. It has been observed that below at about $30K$, the coupled mode features disappear completely [21]. As shown in Fig. 3.7, the order parameter (bilinear coupling) exhibits mean-field behaviour with the critical exponent $\beta = \frac{1}{2}$ for the hexagonal barium titanate.

The temperature dependent Γ diverges at T_0 and it decreases with decreasing temperature below T_0 , as shown in Fig. 3.8. In our treatment, we took the non-interacting proton flipping time τ as constant with $A' = k\tau = 1$ (Eq. 2.15). Similarly, $A = 1$ was taken in Eq. (2.19) with the background bandwidths $\Gamma'_0 = 0$ (Eq. 2.16) and $\Gamma_0 = 0$ (Eq. 2.19). Thus, the proton flipping parameters given in the Ising pseudospin-phonon coupled model play no role in the mechanism of the phase transition since no protons are involved in the BaTiO_3 crystal. Instead, the ionic interactions drive the system to the ferroelectric phase with decreasing temperature.

With increasing temperature from the low temperatures, the coupling between acoustic and soft-optic modes becomes much weaker so that the amplitude of the soft-optic mode attains its maximum value at T_0 , as stated above. This is accompanied with the divergence of the damping constant Γ (Fig. 3.8). About $10K$ below T_0 , the Γ values calculated from the energy-fluctuation model get larger than those calculated from the pseudospin-phonon coupled model (Fig. 3.8).

Regarding the temperature dependence of the relaxation time (Fig. 3.9), the κ values calculated from Eq. (3.7) where the Γ values (Eq. 2.16) were used, are in better

agreement with the experimental data. For this calculation of κ or $1/\tau$, we assumed that the soft mode frequency ω_0 and the order parameter P have the same temperature dependence as given by the mean field theory

$$\omega_0 \sim P \sim (T_0 - T)^{\frac{1}{2}} \quad (3.10)$$

down to about 30K below T_0 for the hexagonal barium titanate.

Finally, we extracted the values of the activation energy U by using Γ values (Eqs. 2.16 and 2.19) according to Eq. (2.26), as tabulated in Table 3.6. As shown in Figs. 3.10 and 3.11, $\ln \Gamma$ varies linearly with the inverse temperature, in the temperature interval of 204.7 to 217.7K. However, a linear variation of $\ln \Gamma$ with $1/T$ was not very satisfactory in the temperature interval of 218.8 to 221.8K when the damping constant was calculated from Eqs. (2.16) and (2.19). By taking a linear variation of $\ln \Gamma$ with $1/T$ in both the temperature ranges, the activation energies were deduced (Table 3.6). The U values extracted in the same temperature interval by using Γ values (Eqs. 2.16 and 2.19) are not the same, as might be expected. In the temperature interval of 204.7 to 217.7K, the U value obtained from the pseudospin-phonon coupled model (Eq. 2.16) is almost twice as much the value found by using the energy-fluctuation model (Eq. 2.19), as given in Table 3.6. Also, the U values increase considerably in the temperature interval of 218.8 to 221.8K as the transition temperature T_0 is approached, which is probably not acceptable. Furthermore, in comparison with the $k_B T_0$ value (Table 3.6) which is too small, our approach to deduce the activation energy U from the damping constant Γ should be valid well below T_0 , possibly when $T - T_0 < -15K$ for the hexagonal barium titanate. An Ising pseudospin-phonon coupled model was applied to analyze the experimental data for the soft-optic acoustic mode of barium titanate in the ferroelectric phase ($T < T_0$) in this study, as stated above. Since the phase transition at $T_0 = 222 K$ is of the second order from hexagonal (phase I) to the orthorhombic (phase II) in barium titanate [21,114], the order-disorder transition can be studied within the framework of an Ising model. As the temperature decreases below T_0 , the titanium and oxygen atoms begin to move relative to the barium atoms. A soft mode occurs in BaTiO₃ due to the vibration of Ti ions against oxygen, which are polarizable and can be considered as

“soft” ions [115]. A bilinear [116] or quadrupolar [30,117,118] coupling between the soft mode and the transverse acoustic mode as allowed by the symmetry below T_0 , which is directly related to the order parameter can be regarded as the driving mechanism to explain the order-disorder transition in BaTiO₃.

Regarding the order-disorder transitions in ammonium halides (NH₄Br and NH₄Cl), the temperature dependences of the order parameter and the damping constant for the hard (nonsoft) modes in these compounds were predicted qualitatively by Matsushita [102], as stated above. For the temperature dependence of the internal mode linewidths of KH₂PO₄ (KDP) type crystals, by treating the pseudospin-phonon interactions in an Ising model, it was found that the order-disorder phase transition in this system is not related to the ionic relations, but rather to the proton jumps along the O-H....O bonds [103,104]. So, the protonic motion generates unstable pseudospin waves [41] which interact with all the phonons in the crystal and shorten their lifetime or broadens their spectra [1,103,104]. However, for some other crystals the linewidth changes at the phase transition were attributed to the rotational jumps of the ions [119]. For example, a drastic decrease of the linewidths for the asymmetric stretching and the libration [120] modes of the NO₂⁻ ion in NaNO₂, and also for the various internal modes of CsNO₃ and RbNO₃ [119] should be related to the ionic relations. Additionally, it was pointed out previously [104] that in another ferroelectric material of triglycine selenate (TGSe), a hard (nonsoft) mode linewidth behaves as expected from the Ising pseudospin-phonon coupled model of Matsushita. In the case of BaTiO₃ studied here, there occur a drastic decrease in the damping constant Γ (Fig. 3.8) and an increase in the relaxation time (Fig. 3.9) below T_0 , as also expected from the Ising pseudospin-phonon coupled system. This is due to the fact that the lattice displacements become unstable and that the crystal distorts to the ferroelectric phase.

3.3 “Temperature dependence of the Raman frequency, damping constant and the activation energy of a soft-optic mode in ferroelectric barium titanate”

The temperature dependent frequency ω_0 was calculated [3] by using a power-law formula above the transition temperature T_0

$$\omega_0^2 \sim (T - T_0) \quad (3.11)$$

within the mean field theory for hexagonal barium titanate, as also used in the previous work [114]. Since the Raman frequency of the silent soft E_{2u} mode increased with increasing temperature above T_0 , as observed experimentally [114], it was assumed that this mode can be associated with the order parameter (spontaneous polarization) P for $BaTiO_3$, as stated above. On this basis, the temperature dependence of the order parameter P was fitted to the observed ω_0 data [114] according to the relation

$$\omega_0 / \omega_{\max} = a + bP \quad (3.12)$$

Here, the Raman frequency ω_0 was normalized since the order parameter P varies between 0 and 1. In Eq. (3.12) ω_{\max} represents the maximum observed value of ω_0 , a and b (Table 3.7) are parameters which characterize the ordering effect above T_0 of barium titanate.

Table 3.7 Values of the coefficients a and b according to Eq. (3.12) in the phase above the transition temperature ($T_0 = 221.5K$) of the hexagonal $BaTiO_3$

$h - BaTiO_3$	$T_0 (K)$	a	b
Eq.(3.9)	221.5	0.024	1.003

Fig. 3.12 gives the Raman frequency ω_0 calculated (Eq. 3.11) as normalized with respect to ω_{\max} at various temperatures above T_0 of $BaTiO_3$. The observed data [114] are also given in this figure.

Since the temperature dependent ω_0 was calculated through Eq. (3.11), one can compute the damping constant values of this mode above T_0 for barium titanate. By using the Eqs. (2.16) and (2.19) for the damping constant where the temperature dependence of the order parameter P (Eq. 3.12) was inserted, the Γ_{sp} values were obtained as plotted in Fig. 3.13. The Γ_{sp} values were predicted here for both the soft mode coupled model (Eq. 2.16) and the energy fluctuation model (Eq. 2.19), as

stated above. We also plot the measured Γ values [114] above T_0 for $BaTiO_3$ in Fig. 3.13.

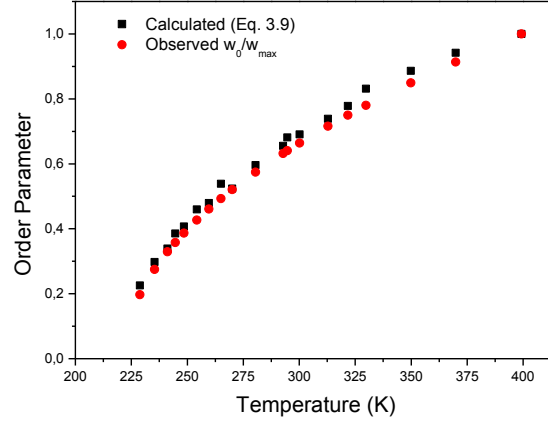


Figure 3.12 The order parameter P fitted to the experimental data [114] for the frequency ratio ω_0/ω_{\max} of the soft phonon according to Eq. (3.11) at various temperatures above the transition temperature ($T_0 = 222K$) of the hexagonal $BaTiO_3$ [3].

Table 3.8 Values of the activation energy extracted from Eq. (2.26) where the calculated Γ_{sp} (Eqs. 2.16 and 2.19) were used in the temperature intervals indicated in the phase above the transition temperature T_c ($T_0 = 222K$) of the hexagonal $BaTiO_3$. $k_B T_c$ value is also given here.

T_c (K)	T (K)	U (eV) from Eq.(2.16)	U (eV) from Eq.(2.19)	$k_B T_c$ (eV)
222	228< T <280	0.035	0.03	0.02
	280< T <329	0.01	0.01	
	329< T <399	0	0.01	

As an extension of this work, the U values was extracted above T_0 of barium titanate using the Γ_{sp} values calculated from P-P model (Eq. 2.16) and the EF model (Eq. 2.19) according to Eq. (2.26).

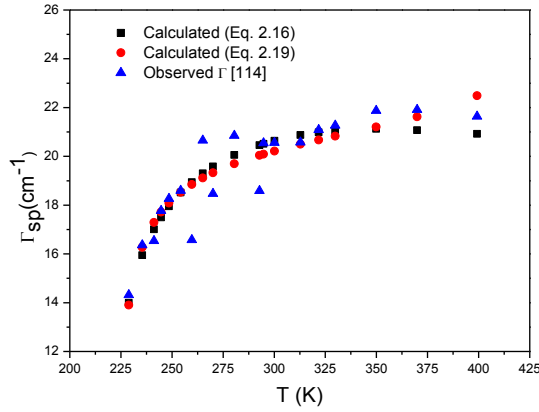


Figure 3.13 The damping constant Γ_{sp} calculated [3] from Eqs. (2.16) and (2.19) of the hexagonal $BaTiO_3$ at temperatures $T > T_C$ ($T_0 = 222K$). The observed Γ data [114] are also given here.

Since in the logarithmic scale, Eq. (2.26) gives a linear dependence of the damping constant Γ_{sp} on the temperature, the U values were deduced in the different temperature intervals above T_0 to get this linear dependence, as given in Table 3.8. In this table, we also give the $k_B T_C (= k_B T_0)$ value for $BaTiO_3$ for comparison.

Previously, the experimental hyper-Raman spectrum was analyzed to get the temperature dependence of the observed Raman frequency and the damping constant by Inoue et al. [114]. Here [3], the frequency was calculated according to Eq. (3.11) which also holds in the framework of the soft mode theory by Landau and Cochran. A linear dependence of ω^2 on T is an indication of the stabilization of the phase above T_0 for $h-BaTiO_3$. Since the frequency of this mode increases sharply above T_0 , as observed experimentally and also it was calculated here (Fig. 3.12) according to Eq. (3.11), this strongly overdamped mode can be attributed to the mechanism of an order-disorder transition instead of a displacive behaviour as shown by an underdamped soft mode for $h-BaTiO_3$, which was discussed in a recent study [30]. The anomalous behaviour of Γ_{sp} just above T_0 in $h-BaTiO_3$ is a supporting evidence, as calculated here (Fig. 3.13). An abrupt increase of the damping constant on heating above T_0 also indicates a kind of ordering accompanied by the soft mode

in $h-BaTiO_3$. Our calculated values of the damping constant Γ_{sp} show clearly this critical behaviour in comparison with the experimental data as given in Fig. 3.13, which is scattered, in particular, above T_0 up to the room temperature. An order-disorder transition has also been considered for the tetragonal-cubic transition in $PbTiO_3$ [121] which has been treated previously as the classic displacive transition. Experimental studies by X-ray analysis [20], dielectrics [23], elastic [31] and optical [122] measurements have shown a second order phase transition at $T_0 = 222K$ for $h-BaTiO_3$, as also pointed out previously [114]. As observed by hyper-Raman scattering [114], a rapid increase in the frequency of the soft mode associated with the ordering above T_0 can be due to the disorder effects since the soft mode (E_{2u}) is located at the zone center

(Γ point) of the Brillouin zone and it is Raman forbidden in this phase. Thus, the disorder-induced Raman scattering occurs above T_0 in $h-BaTiO_3$, as considered previously for the ammonium halides [123]. Due to the reorientations of the molecules coupled with the soft optic mode, the damping constant Γ_{sp} increases above T_0 in $h-BaTiO_3$ (Fig. 3.13), as predicted from the pseudospin phonon coupled model studied here. The temperature dependent Γ_{sp} was calculated for the soft mode using the P-P model (Eq. 2.16) and the EF model (Eq. 2.19), which were both originated from the Ising pseudospin-phonon coupled model [101] and in an extended form [102].

From the Eqs. 2.16 and 2.19, the activation energy U was deduced using Eq. (2.26), which is very close to the $k_B T_C$ value for $h-BaTiO_3$ (Table 3.8). We extracted the U values in different temperature ranges, varying from 0.01 to 0.03eV which also covers the $k_B T_C$ value of 0.02eV. In particular, in the temperature range of 329 to 399K a negative activation energy of nearly zero, was extracted using Eq. (2.16). In this temperature region, the EF model (Eq. 2.19) seems to describe the experimental data better than the pseudospin-phonon coupled model. But, some precise experimental data are needed above T_0 in $h-BaTiO_3$ to make a firm conclusion about the models studied here.

3.4 “Damping constant calculated as a function of temperature for the tetragonal Raman mode close to the paraelectric-ferroelectric transition in BaTiO₃”

The temperature dependent Γ values were calculated using the P-P model (Eq. 2.16) and the EF model (Eq. 2.19) for the “paraelectric-ferroelectric phase transition” in BaTiO₃ [4]. The damping constant Γ was calculated for the tetragonal mode at 308 cm⁻¹ using its observed Raman integrated intensities [124] since the Raman intensity I is proportional to the order parameter P as

$$P^2 \propto I \text{ for } T < T_C \quad (3.13)$$

in the ferroelectric phase, whereas for the paraelectric phase

$$P^2 \propto 1 - I \text{ for } T > T_C \quad (3.14)$$

as the disorder parameter.

Table 3.9 The values of the background bandwidth Γ'_0 (Γ_0) and the amplitude A' (A) for the Raman mode indicated for BaTiO₃ according Eqs. 2.16 and 2.19 [4].

Raman mode	$\Gamma'_0(cm^{-1})$	$A'(cm^{-1})$	$\Gamma_0(cm^{-1})$	$A(cm^{-1})$
308 cm ⁻¹	11.57	46.62	16.08	7.73

Thus, Eqs. (2.16) and (2.19) were fitted to the observed Raman integrated intensities and the bandwidths of the 308 cm⁻¹ mode [124] below (Eq. 3.13) and above (Eq. 3.14) T_c (\approx 450 K) for the ferroelectric-paraelectric transition in BaTiO₃ and the fitted parameters of Γ'_0 and A' (Eq. 2.16) and Γ_0 and A (Eq. 2.19) were determined, as given in Table 3.9. We plot in Fig. 3.14 the bandwidths calculated from Eqs. (2.16) and (2.19) with the observed data for epitaxial thin

film [124] of 308 cm^{-1} mode for the ferroelectric-paraelectric transition ($T_c \sim 450\text{ K}$) in BaTiO_3 . We show in Fig. 3.14 the experimental data for thin films of 60 nm and 200 nm [125] of this Raman mode for comparison. We also show in this figure the experimental data for the Raman bandwidths of the soft-optic mode [114] in the hexagonal BaTiO_3 for comparison.

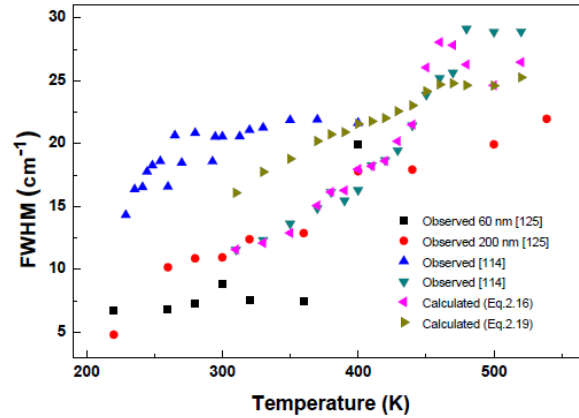


Figure 3.14 Temperature dependence of the full width at half maximum (FWHM) of the 308 cm^{-1} line [4]. The observed data for thin films of 60 nm and 200 nm [125] of this mode are shown, respectively. The observed [114] Raman bandwidths of the soft-optic mode in the hexagonal BaTiO_3 are also shown for comparison.

Marssi et al. [124] have corrected the experimental Raman intensity by the Bose-Einstein factor to get the integrated Raman intensity I . They then used the Lorentzian fitting to determine the FWHM (damping constant) of the central peak at various temperature, as also given in this study .

The Raman integrated intensity I which is related to the square of the order parameter P according to Eqs. (3.13) and (3.14) for the ferroelectric (tetragonal) and paraelectric (cubic) phases, respectively, decreases with increasing the temperature, as observed experimentally [124]. For the barium titanate epitaxial thin film studied here, there is no any abrupt decrease of the Raman intensity for the 308 cm^{-1} mode, whereas for the bulk case a sudden decrease in the Raman intensity of this mode was observed [28,126]. As also pointed out previously [124], the Raman intensity of the 308 cm^{-1} mode for the barium titanate epitaxial thin film decreases gradually near 425 K and it is almost independent of the temperature above 450 K. With this minimal Raman intensity of this mode, the paraelectric phase of BaTiO_3 can be identified.

This decrease in the Raman intensity of the 308 cm^{-1} mode corresponds to the increase in the linewidth of that mode with increasing the temperature in the paraelectric phase, as observed experimentally [124] (Fig. 3.14). Thus, we expressed the increase in the Raman intensity of the 308 cm^{-1} mode with decreasing temperature (ferroelectric phase) by Eq. (3.13) and decrease in the Raman intensity with increasing temperature (paraelectric phase) by Eq. (3.14) as the order parameter for calculating the temperature dependent Raman linewidth according to Eqs. (2.16) and (2.19). As shown in Fig. (3.14), the pseudospin-phonon coupled model (Eq. 2.16) agrees much better with the observed Raman linewidth [124] than the energy fluctuation model (Eq. 2.19). Above the transition temperature ($T_C \approx 450 \text{ K}$) in the paraelectric phase, our predicted Γ values are smaller of about 4 cm^{-1} than the observed ones (Fig. 3.14). In this figure, we show the experimental data for thin films of 60 nm and 200 nm [125] of the 308 cm^{-1} mode, also the observed data for the soft-optic mode [114] in the hexagonal BaTiO_3 for comparison purposes, as stated above. It looks that the observed data for the thin film of 200 nm [125] for the Raman bandwidths of the 308 cm^{-1} mode follow the same trend as our calculated values (Eq. 2.16) due to the pseudospin-phonon coupled model, as well as the observed ones [124]. The experimental data for the thin film of 60 nm [125] are much lower (about 5 cm^{-1}) than those calculated and the observed values when extrapolated down to about 200 K. On the other hand, the observed data for the Raman bandwidths of the soft-optic mode [114] show rather different critical behavior above the transition temperature ($T_0 = 221 \text{ K}$) in the hexagonal BaTiO_3 . It increases rapidly above T_0 up to around 275 K and then it does not vary with the temperature to 400 K (Fig. 3.14). These observed data [114] do not describe the tetragonal-cubic transition ($T_C \sim 400 \text{ K}$) as studied here, instead it is for the transition ($T_0 = 221 \text{ K}$) in the hexagonal BaTiO_3 , as stated above. But, it can be taken to be a representative behavior of the bandwidths of a Raman mode, which increases with increasing temperature, as that of the observed data [124] and our calculated values (Eqs. 2.16 and 2.19) (See Figure 3.14).

Since the pseudospin-phonon coupling leads to the pseudo-spin waves [41] interacting with all the phonons in the crystal, their lifetime is shortened and the Raman linewidth is broadened. ($\Gamma \propto 1/\tau$, τ is the spin-lattice relaxation time).

The broadening of the tetragonal mode (308 cm^{-1}) occurs rather rapidly with the greater slope of $d\Gamma/dT$ for the P-P coupled model in comparison with the EF model (Fig. 3.14). Decrease in the linewidth of this mode in the ferroelectric phase is more apparent for the pseudospin-phonon coupled model, as also observed experimentally and the bandwidth value is about 4 cm^{-1} smaller at room temperature than the energy fluctuation model. The linewidth of the 308 cm^{-1} mode increases gradually with increasing temperature above 450 K (around 475 K) according to the energy fluctuation model (Fig. 3.14). This gradual change of $d\Gamma/dT$ makes it difficult to distinguish transition from the ferroelectric to the paraelectric phase, as obtained by the energy fluctuation model. The pseudospin-phonon coupled model provides a better picture to see the phases, which agrees with the experimental data (Fig. 3.14).

3.5 “Temperature dependence of the polarization and the dielectric constant near the paraelectric- ferroelectric transitions in BaTiO_3 ”

The expansion of the P dependent of the free energy F was given by Landau’s theory, as follows:

$$F = a_0 + a_2P^2 + a_4P^4 + a_6P^6 \quad (3.15)$$

In Eq. (3.15) the coefficient a_2 can be taken to be the temperature dependent,

$$a_2 = \alpha(T - T_C) \quad (3.16)$$

where α is a positive constant, and all the other coefficients (a_0, a_4 and a_6) are assumed to be constant.

From the minimization ($\partial F/\partial P = 0$), one gets

$$a_2 + 2a_4P^2 + 3a_6P^4 = 0 \quad (3.17)$$

the roots of Eq. (3.17) are

$$P^2 = -\frac{a_4}{3a_6} \pm \frac{1}{3a_6} \sqrt{a_4^2 - 3a_2a_6} \quad (3.18)$$

By taking $a_4 < 0$ and $a_6 > 0$, a positive P solution of Eq. (3.18) defines the ferroelectric phase ($T < T_C$) whereas $P = 0$ corresponds to the paraelectric phase $T > T_C$ in BaTiO_3 .

The definition of the susceptibility χ given by,

$$\chi^{-1} = \left(\partial^2 F / \partial P^2 \right) \quad (3.19)$$

which gives

$$\chi^{-1} = 2a_2 + 12a_4 P^2 + 30a_6 P^4 \quad (3.20)$$

In the paraelectric phase ($P = 0$), the reciprocal dielectric susceptibility χ^{-1} or the dielectric constant ε becomes

$$\chi^{-1} = (\varepsilon - 1)^{-1} = 2a_2 \quad (3.21)$$

In the ferroelectric phase ($P \neq 0$), using Eq. (3.18) in Eq. (3.20) χ^{-1} can be expressed in terms of the coefficients a_2, a_4 and a_6 . By Eq. (3.16), the temperature dependence of χ^{-1} can be obtained. Since the functional form of P^2 Eq. (3.18) is rather long, the temperature dependent values of the P and χ can be obtained approximately by making an ansatz,

$$\frac{a_2 a_6}{a_4^2} \ll 1 \quad (3.22)$$

which gives the root square in the P^2 expression (Eq. 3.18) as

$$\left(a_4^2 - 3a_2 a_6 \right)^{1/2} = a_4 - \frac{3}{2} \frac{a_2 a_6}{a_4} \quad (3.23)$$

By considering the minus solution in the root square of Eq. (3.18), the spontaneous polarization P can be obtained as

$$P^2 = -\frac{2a_4}{3a_6} + \frac{a_2}{2a_4} \quad (3.24)$$

With this ansatz, we get the spontaneous polarization in the simplified form (Eq. 3.24) in comparison with Eq. (3.18).

Similarly, using Eq. (3.24) in Eq. (3.20) through the ansatz (Eq. 3.22) the expression for χ^{-1} can be written in the simplified form as

$$\chi^{-1} = (\varepsilon - 1)^{-1} = -12a_2 + \frac{16}{3} \frac{a_4^2}{a_6} \quad (3.25)$$

in the ferroelectric phase. Using the simplified forms of the spontaneous polarization P (Eq. 3.24) and the reciprocal dielectric susceptibility χ^{-1} (Eq. 3.25), their temperature dependence in the ferroelectric phase can then be obtained according to Eq. (3.16), which gives, respectively,

$$P^2 = \frac{\alpha(T - T_C)}{2a_4} - \frac{2a_4}{3a_6} \quad (3.26)$$

$$\chi^{-1} = -12\alpha(T - T_C) + \frac{16 a_4^2}{3 a_6} \quad (3.27)$$

In the paraelectric phase ($P = 0$), χ^{-1} will be obtained as

$$\chi^{-1} = 2\alpha(T - T_C) \quad (3.28)$$

according to Eq. (3.21) through Eq. (3.16).

The temperature dependence of the spontaneous polarization P was calculated using the experimental data [125] for the peak positions (frequency) of the lattice phonon ($\sim 310 \text{ cm}^{-1}$) from the Raman spectroscopic measurements of BaTiO_3 by using the following power-law formula

$$\omega^2 \propto (T - T_C) \quad (3.29)$$

Since the peak position of the 310 cm^{-1} mode decreased considerably as observed experimentally [125], this phonon frequency was related with P (spontaneous polarization) in this crystal. Thus, in our analysis the temperature dependence of the Raman peak position of the 310 cm^{-1} mode (Eq.3.29) was correlated to the spontaneous polarization P (Eq. 3.26) which gives

$$\left(\frac{\omega}{\omega_{\max}}\right)^2 = \frac{\alpha(T - T_C)}{2a_4} - \frac{2a_4}{3a_6} \quad (3.30)$$

We analyzed the temperature dependence of the observed [125] Raman frequencies for the 310 cm^{-1} mode for thin films of 60 nm and 200 nm in BaTiO_3 . By fitting Eq. (3.30) to the observed Raman frequency data [125], the fitted parameters were determined, as given in Table 3.10. For this determination of α and a_4 , we took $a_6 = 1$ regarding both thin films (Table 3.10). We plot square of the frequency ratio ω/ω_{\max} as a function of temperature close to the ferroelectric-paraelectric transition in BaTiO_3 for the thin films of 60 nm and 200 nm in Figs. 3.15 and 3.16, respectively.

Table 3.10 Values of the temperature T_C , the parameters α and a_4 (Eq. 3.26) for the ferroelectric-paraelectric transition for the thin films indicated in BaTiO_3 [5].

Thin Films (nm)	T_C (K)	$\alpha \times 10^{-5}$ (1/K)	a_4
60	360	9.759	-0.488
200	440	9.490	-0.484

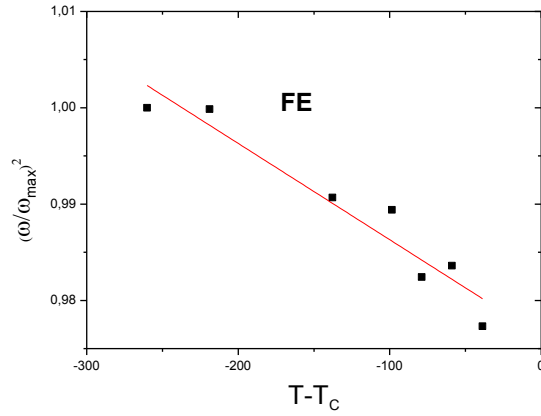


Figure 3.15 Temperature dependent $(\omega/\omega_{\max})^2$ values of the 310 cm^{-1} Raman mode (correlated to the spontaneous polarization P) for the ferroelectric (FE) – paraelectric (PE) transition using the thin film of 60 nm according to Eq. (3.30) in BaTiO_3 [5]. The observed data [125] are also shown here.

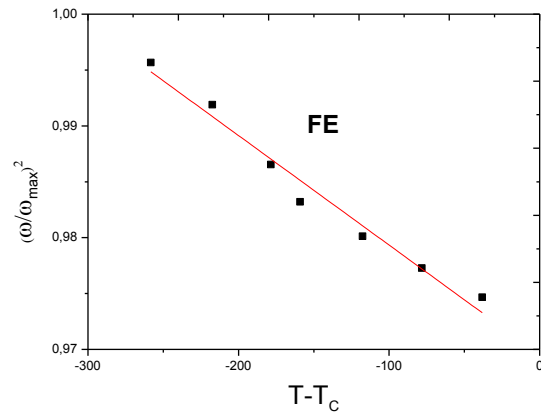


Figure 3.16 Temperature dependent $(\omega/\omega_{\max})^2$ values of the 310 cm^{-1} Raman mode (correlated to the spontaneous polarization P) for the ferroelectric (FE) – paraelectric (PE) transition using the thin film of 200 nm according to Eq. (3.30) in BaTiO_3 [5]. The observed data [125] are also shown here.

Using the fitting parameters α and a_4 ($a_6 = 1$), we calculated the χ^{-1} values from Eq. (3.27). We also calculated χ^{-1} values for the paraelectric phase using Eq. (3.28) for both thin films (60 nm and 200 nm), as plotted in Fig.3.17 and Fig.3.18 respectively.

compare our calculated values of $(\omega/\omega_{\max})^2$ with the observed P_S^2 data since there are no experimental data available in the literature for thin films of 60 and 200 nm in BaTiO₃. In order to see the behavior of $(\omega/\omega_{\max})^2$ for thin films of 60 and 200 nm (Figs. 3.15 and 3.16), we compared our calculated values of $(\omega/\omega_{\max})^2$ observed [127] spontaneous polarization (P_S^2) of single-crystal BaTiO₃, as plotted in Fig. 3.19. These experimental data [127] were obtained for the temperature range of $-80\text{K} < T - T_C < 0\text{K}$ for constant pressures of 1, 4, 8 and 12 kbar in this crystal. When plotted the spontaneous polarization P_S as a function of the temperature difference, $T - T_C$, all the experimental data points are almost at the same positions, which decrease continuously as $T - T_C$ decreases. This then gives rise to a linear variation of P_S^2 with the $T - T_C$, as plotted in Fig. 3.19. Thus, a linear variation of the observed spontaneous polarization P_S^2 [127] with the temperature $T - T_C$ within the temperature range of $-80\text{K} < T - T_C < -20\text{K}$ (Fig. 3.19) is the same as the calculated $(\omega/\omega_{\max})^2$ for thin films of 60 and 200 nm within the temperature range of $-250\text{K} < T - T_C < -50\text{K}$ for BaTiO₃.

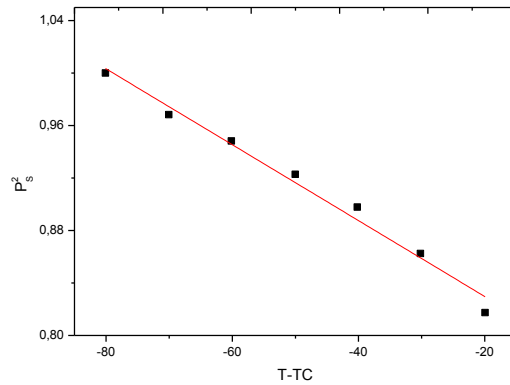


Figure 3.19 The observed spontaneous polarization P_S^2 of single-crystal BaTiO₃ [127]. P_S^2 was normalized with respect to its maximum value.

The inverse susceptibility χ^{-1} or the dielectric constant ($\epsilon = \chi + 1$), which was calculated using the parameters of the spontaneous polarization (Eq. 3.26), shows a linear variation with the temperature, as plotted in Figs. 3.17 and 3.18 according to Eqs. (3.27) and (3.28) in the ferroelectric and paraelectric phases, for both thin films (60 and 200 nm) in BaTiO₃ respectively. This is also expected from the mean field theory according to a power-law formula $\chi \propto (T - T_C)^{-\gamma}$ with the $\gamma = 1$ value for both phases above and below T_C . Since there are no experimental data in the literature for

the dielectric constant for thin films of 60 and 200 nm in BaTiO₃, the closest experimental data available were the dielectric constant at various temperatures near the ferroelectric-paraelectric transition for barium titanate ceramics with different porosities and pore sizes [128]. In the case of small and large pores (5 %) for the observed dielectric constant ϵ , we plot the inverse susceptibility χ^{-1} against T-T_C in Fig. 3.20 for the ferroelectric (FE) and paraelectric (PE) phases in BaTiO₃ ceramics which can be compared with our calculated values of χ^{-1} in Figs. 3.17 and 3.18 for thin films of 60 and 200 nm respectively, in this crystal. For those plots (Figs. 3.17, 3.18 and 3.20), we see that the inverse susceptibility (χ^{-1}) decreases as the T_C is approached in both ferroelectric (FE) and paraelectric (PE) phases in this crystalline system. Also, for comparison purposes, we analyzed recent experimental data [129] of Ba_{1-x}Ce_xTiO₃ compounds for x=0 (BaTiO₃), as given Fig. 3.21. We also see similar behavior of χ^{-1} as our calculated χ^{-1} (Figs. 3.17 and 3.18) and also the observed χ^{-1} (Fig. 3.20).

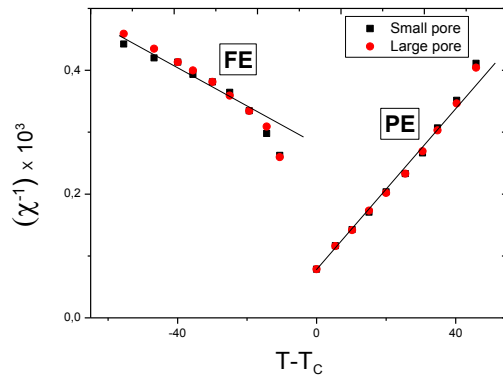


Figure 3.20 Inverse susceptibility (χ^{-1}) obtained from the observed dielectric constant (ϵ) [128] as a function of the temperature for barium titanate ceramics with different porosities and pore size (5%) [5].

As given in our calculated values of χ^{-1} (Figs. 3.17 and 3.18), the temperature range (-300K < T-T_C < 300K) is much wider than the experimentally obtained temperature range (-40K < T-T_C < 40K in Fig. 3.20) and (-80K < T-T_C < 80K in Fig. 3.21). Our results show that the temperature dependent behaviour of the BaTiO₃ film is qualitatively similar to that observed for single crystal BaTiO₃ and barium titanate ceramic.

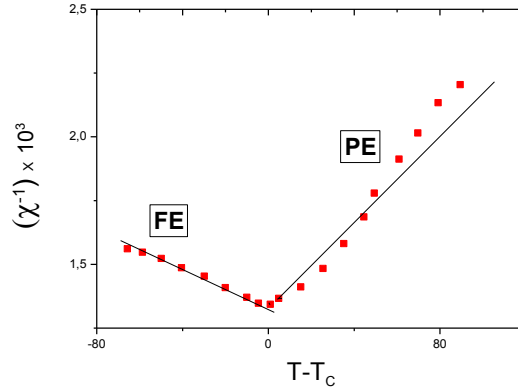


Figure 3.21 Variation of the inverse susceptibility (χ^{-1}) obtained from the experimental dielectric constant (ϵ) [129] with the temperature at three frequencies (10, 100 and 100 kHz) of $\text{Ba}_{1-x}\text{Ce}_x\text{TiO}_3$ for $x=0$ (BaTiO_3) [5].

The spontaneous polarization P was calculated by analyzing the temperature dependence of the Raman frequency of the 310 cm^{-1} lattice mode according to Eq. (3.29) for BaTiO_3 . This temperature dependent frequency was also studied previously for the translational optic (TO) mode in the cubic paraelectric phase of BaTiO_3 [19]. The soft mode damping was studied experimentally [115] and it was discussed in the framework of the soft-mode theory of Landau and Cochran. By relating the temperature dependence of a bilinear coupling constant A between acoustic and soft-optic modes to the order parameter Q_3 according to the power-law formula given by Eq. 3.9, the hexagonal- BaTiO_3 was studied above the transition temperature ($T_0=222 \text{ K}$) in the paraelectric phase [21]. Eq. (3.9) was also used to analyze the experimental data [21] to calculate the damping constant and the relaxation time for the soft-optic and acoustic mode in hexagonal- BaTiO_3 in our recent study [2].

For the tetragonal phase of BaTiO_3 , the quadrupole coupling constant C_Q which can be measured in this phase, has been related to the spontaneous ferroelectric polarization for a first order transition according to a power-law expression

$$C_Q \propto (T_f - T)^\beta \quad (3.31)$$

where T_f is the upper stability limit ($T_f=403.5 \text{ K}$) of the ferroelectric phase and it was found that the β value was less than $1/2$. Since the quadrupole coupling constant C_Q describes the square of the frequency (ω^2) for the Raman mode (310 cm^{-1}), the

frequency (squared) is directly proportional to the square of the order parameter (spontaneous polarization). So, the variation of the Raman frequency and width of this mode with the temperature can be considered as the order parameter (spontaneous polarization) in the ferroelectric (FE) phase of BaTiO₃ and the polarization is along the c- axis, as also studied previously [125]. A linear relationship between $(\omega/\omega_{\max})^2$ of the internal ammonium mode (ν_3) and P_S^2 (spontaneous polarization) has also been obtained in the ferroelectric phase of (NH₄)₂SO₄, as reported in our earlier study [116]. For BaTiO₃, we have assumed the same temperature dependent frequency given by the mean field theory (Eq. 2.20) and the order parameter P (spontaneous polarization) [3], and a linear variation of ω/ω_0 was obtained with the P in the ferroelectric phase [2]. As observed experimentally [127], before the dielectric constant ϵ attains its maximum value at the Curie point, a permanent polarization P develops in the BaTiO₃ crystallites ($T_C=110$ °C) [130]. On the other hand, it was suggested that for the hexagonal BaTiO₃ below T_0 (=220 K) the temperature dependence of the Raman frequency of the soft mode can be expressed as

$$\omega_0^2 \propto (T - T_0)^{2/3} \quad (3.32)$$

down to 100 K [21]. On the basis of the hard-soft mode coupling model [103-106], the frequency of a coupled mode ω_{sh} can be written [104] as

$$\omega_{sh} \propto (T_C - T)^{1/2} \quad (3.33)$$

similar to Eq. (3.29) or in general,

$$\omega_{sh} \propto (T_C - T)^\beta \quad (3.34)$$

as applied to several ferroelectric crystals such as triglycine sulphate (TGS) [131,132], triammonium hydrogen disulphate, (NH₄)₃ H (SO₄)₂ [133] and lithium ammonium sulphate, LiNH₄SO₄ [134]. In those studies, the experimentally measured Raman frequencies were analyzed according to Eq. (3.34). We have also used hard-soft mode coupling model for various ferroelectric materials such as BaTiO₃, KH₂PO₄ (KDP) and (NH₄)₂SO₄ in our recent studies [1,2,3,116].

3.6 “Calculation of the damping constant and the order parameter for the lattice mode in ferroelectric PbTiO₃”

The order parameter of the ferroelectric-paraelectric transition as an order-disorder transition of this ferroelectric material, can be predicted from the molecular field theory [107] as given by Eq. 2.20. In this study [6], we associated the order parameter with the temperature dependent frequency of the soft mode E (1TO), as observed experimentally for single crystals [33] and thin films of [36] PbTiO₃. On that basis, we analyzed the experimental data [33] for the temperature dependence of the soft mode frequencies for a single crystal of PbTiO₃ using a polynomial function

$$v = a_0 + a_1T + a_2T^2 \quad (3.36)$$

where a_0 , a_1 and a_2 are constants (Table 3.11). Those frequencies of the E (1TO) mode were then fitted to the values of the order parameter calculated from the molecular field theory (Eq. 2.20) at various temperatures below the transition temperature ($T_C=493$ °C) according to the relation

$$v(P) = b_0 + b_1P + b_2P^2 \quad (3.37)$$

where b_0 , b_1 and b_2 are constants. Table 3.12 gives the values of b_0 , b_1 and b_2 for the E (1TO) soft mode of PbTiO₃. In Fig.3.22 we give the temperature dependent of the frequency for the E (1TO) mode of PbTiO₃ ($T_C=493$ °C). The observed data [33] are also plotted in this figure.

Table 3.11 Values of the coefficients a_0 , a_1 and a_2 determined for the soft mode of E (1TO) within the temperature interval indicated in the ferroelectric phase of PbTiO₃ according to Eq. (3.36).

Raman Mode	$a_0(\text{cm}^{-1})$	$a_1(\text{cm}^{-1}/^\circ\text{C})$	$a_2(\text{cm}^{-1}/^\circ\text{C}^2)$	Temperature Interval ($^\circ\text{C}$)
E(1TO)	105.88	0.025	-1.92×10^{-4}	400-492

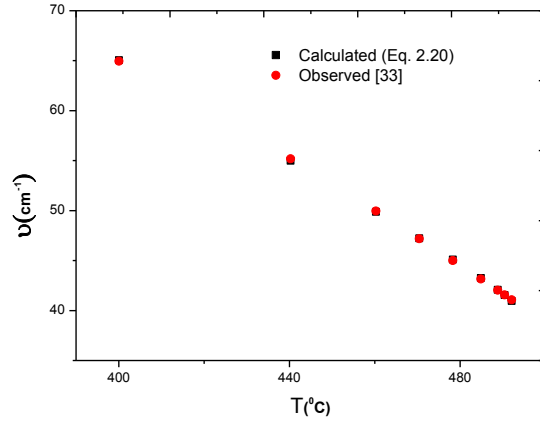


Figure 3.22 Raman frequencies of the soft mode E (1TO) which were calculated as a function of temperature using the molecular field theory (Eq. 2. 20) by fitting to the experimental data [33] in the ferroelectric phase of PbTiO₃ ($T_C = 493^{\circ}\text{C}$) [6].

Table 3.12 Values of the coefficients b_0 , b_1 and b_2 determined for the soft mode of E (1TO) within the temperature interval indicated in the ferroelectric phase of PbTiO₃ according to Eq. (3.37).

Raman Mode	b_0 (cm^{-1})	b_1 (cm^{-1})	b_2 (cm^{-1})	Temperature Interval ($^{\circ}\text{C}$)
E(1TO)	40.42	4.34	37.77	400-492

In order to predict the temperature dependence of the damping constant on the basis of the pseudospin-phonon coupled model (Eq. 2.16) and the fluctuation model (Eq. 2.19), we used in these equations the values of the ratio ν/ν_{\max} for the E (1TO) soft mode as the values of the order parameter. This is due to the fact that in the ferroelectric phase ($T < T_C$) the order parameter varies from 0 to 1 so that the damping constant of this mode was predicted at various temperatures, as plotted in Fig. 3.23 for both models. Eqs. (2.16) and (2.19) were fitted to the experimental data [33] for the damping constant of E (1TO) mode and the fitted parameters were determined within the temperature intervals, as given in Table 3.13.

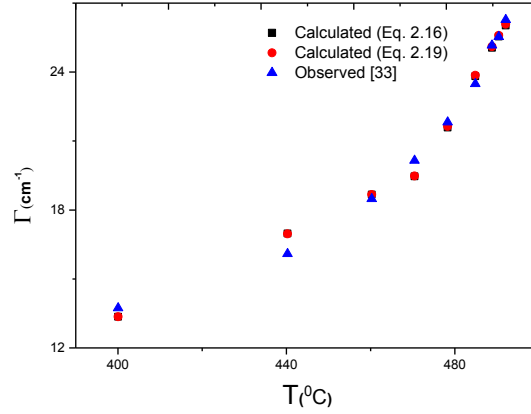


Figure 3.23 Damping constant Γ calculated [6] using both the pseudospin-phonon coupled model (Eq. 2.16) and the energy fluctuation model (Eq. 2.19) for the soft mode of E (1TO) in the ferroelectric phase of PbTiO_3 ($T_C=493$ °C). Observed data are also given here.

Table 3.13 Values of the background damping constant (Γ'_0, Γ_0) and the coefficient (A', A) for the soft mode E (1TO) in the temperature intervals indicated according to the pseudospin-phonon coupled model (Eq. 2.16) and the energy fluctuation model (Eq. 2.19) for the ferroelectric phase of PbTiO_3 .

Raman Mode	Γ'_0 (cm ⁻¹)	A' (cm ⁻¹)	Γ_0 (cm ⁻¹)	A (cm ⁻¹)	Temperature Interval (°C)
E (1TO)	-2.00	13.77	-4.90	10.59	400-470
	-92.41	71.29	-102.91	52.83	478-492

The analysis of the damping constant was done by Burns and Scott [33] using the damped harmonic oscillations model and the Devonshire formulation. In this study, the damping constant was calculated for the E (1TO) mode as a function of temperature using P-P model (Eq. 2.16) and the EF model (Eq. 2.19), as given in Fig. 3.22. Our predictions from both models for the E (1TO) mode (Fig. 2.19) agree with the experimental data [33] according to the fitted parameters (Table 3.13). As seen in Fig. 3.23, the damping constant increases sharply close to the transition temperature. Since we associate the temperature dependence of the Raman frequency for this soft mode (Eq. 3.37) on the basis of the P-P model (Eq. 2.16) and the EF model (Eq. 2.19), the soft behaviour occurs for the E (1TO) mode according to the Eq. 3.11. Thus, the Raman frequency of the E (1TO) mode drops to a smaller value (ultimately to zero for a soft mode according to Eq. 3.11) from considerably higher values, as

also observed for both single crystal [33] and thin films [36]. This indicates that, the “order-disorder” transition in PbTiO_3 can be correlated with the E (1TO) mode.

3.7 “Calculation of the infrared frequencies as a function of temperature using the volume data in the ferroelectric phase of NaNO_2 ”

Longitudinal optic (LO) and transverse optic (TO) frequencies of A_1 , B_1 and B_2 modes of NaNO_2 have been studied as a function of temperature according to the “Grüneisen parameter” γ_P given by Eq.(2.24) [7]. The temperature dependent $A(T)$ term in Eq. 2.24 can be assumed as

$$A(T) = a_0 + a_1T + a_2T^2 \quad (3.38)$$

with the constants a_0 , a_1 and a_2 . Fig. 3.24 gives the temperature dependence of the observed volume data for bulk NaNO_2 [135].

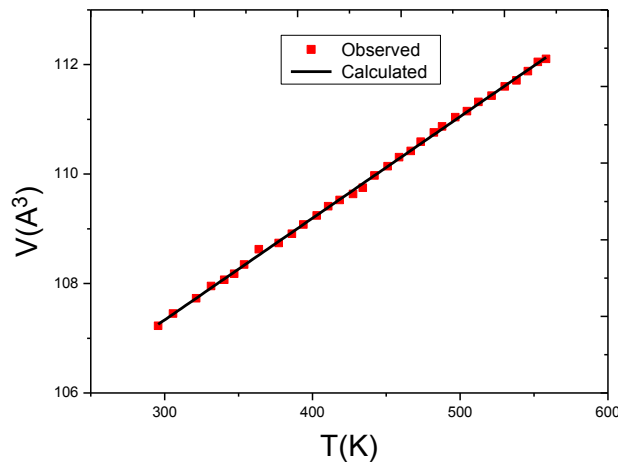


Figure 3.24 Temperature dependence of the observed volume [135] for bulk NaNO_2 . [7] The best line is shown by a solid line.

The linearity of the bulk volume of NaNO_2 with temperature can be given as

$$V = a + bT \quad (3.39)$$

the fitted parameters a and b were tabulated in Table 3.14. by using Eq. (3.39), we calculated the V_1 values for those modes in NaNO_2 at around 500 K.

Table 3.14 Values of the fitting parameters of Eq. (3.39) for the observed volume data [135] .

$V(\text{\AA}^3)$	$a(\text{\AA}^3)$	$b(\text{\AA}^3)$
Eq. (3.39)	101.76	1.86×10^{-2}

Table 3.15 Constant volume V_1 , constant frequencies ν_1 values of lattice modes in NaNO_2 . Values of the constant “Grüneisen parameter” γ_P is also given here [60].

Lattice modes	$V_1(\text{\AA}^3)$	$\nu_1(\text{cm}^{-1})$	γ_P
$A_1\text{LO}$	110.86	275.59	0.2
$A_1\text{TO}$	110.93	171.93	1.8
$B_1\text{LO}_1$	111.00	147.47	2.3
$B_1\text{TO}_1$	111.00	144.92	1.5
$B_1\text{LO}_2$	110.98	238.15	2.5
$B_1\text{TO}_2$	110.98	175.44	2.0
$B_2\text{LO}_1$	111.11	181.64	1.5
$B_2\text{TO}_1$	111.14	148.30	1.1
$B_2\text{LO}_2$	111.14	251.72	1.2
$B_2\text{TO}_2$	111.12	220.96	1.4

we also get ν_1 values (at zero pressure) and the “Grüneisen parameter” values γ_P from the observed data of those Raman lattice modes of NaNO_2 studied here [60].

Table 3.16 Coefficients of Eq. (3.38), whose values detected from the fitting procedure of Eq. (2.24) and observed frequency data [60] in bulk NaNO_2 .

Lattice modes	$a_0(\text{cm}^{-1})$	$a_1(\text{cm}^{-1}/\text{K})$	$a_2(\text{cm}^{-1}/\text{K}^2)$
$A_1\text{LO}$	125053	-900.25	1.6237
$A_1\text{TO}$	-1408	16.23	-0.0041
$B_1\text{LO}_1$	-581	8.25	-0.0023
$B_1\text{TO}_1$	-769	10.99	-0.0323
$B_1\text{LO}_2$	290	-0.88	0.0027
$B_1\text{TO}_2$	-375	5.02	-0.0108
$B_2\text{LO}_1$	-869	9.90	-0.0227
$B_2\text{TO}_1$	290	-2.50	0.0103
$B_2\text{LO}_2$	1231	-8.27	0.0174
$B_2\text{TO}_2$	1800	-14.08	0.0314

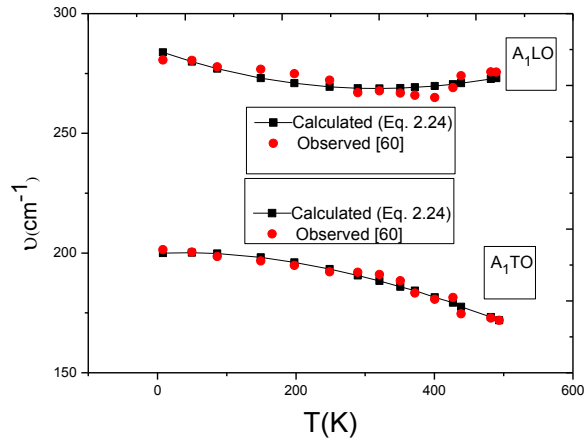


Figure 3.25 Temperature dependence of the calculated Eq. (2.24) and observed [60] longitudinal optic and transverse optic frequencies of A_1 mode in NaNO_2 [7].

We then calculated the frequencies of the lattice modes of A_1 , B_1 and B_2 through Eq. (2.24) by using the values of V_1 , v_1 and γ_p (Table 3.15) at constant temperature of $T= 500$ K. Finally, the temperature dependence of the calculated Eq. (2.24) and observed [60] longitudinal optic (LO) and transverse optic (TO) frequencies of A_1 , B_1 and B_2 modes of NaNO_2 have shown in Figs. (3.25-3.27), respectively.

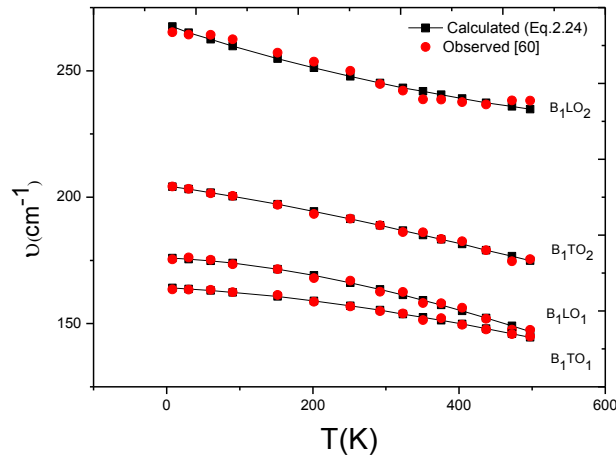


Figure 3.26 Temperature dependence of the calculated Eq. (2.24) and observed [60] longitudinal optic and transverse optic frequencies of B_1 mode in NaNO_2 [7].

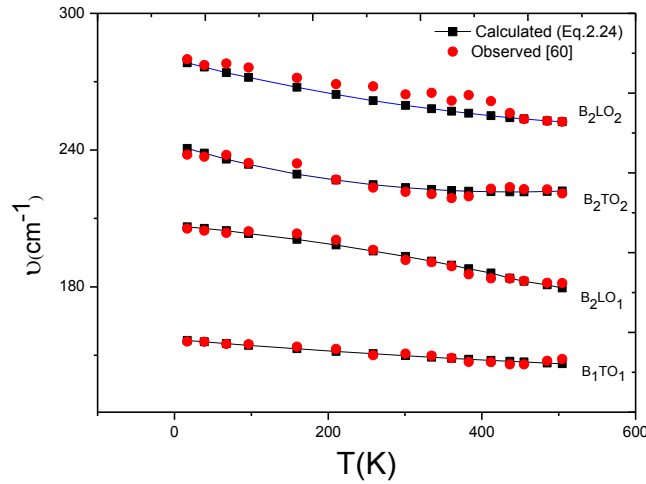


Figure 3.27 Temperature dependence of the calculated Eq. (2.24) and observed [60] longitudinal optic and transverse optic frequencies of B₂ mode in NaNO₂ [7].

In their study, Brehat and Wyncke [60] have fitted the far-infrared reflectivity spectra to the dielectric constant through “dielectric dunction model” to extract the behavior of lattice mode frequencies (A₁, B₁ and B₂) for NaNO₂. Analysis of these frequencies have also studied by Ema et. al. [57] by using the thermal expansion data through the “quasi-harmonic oscillator model”.

In this study, we predicted the values of the infrared frequencies of lattice modes in NaNO₂ by considering the isobaric “Grüneisen parameter” (Eq. 2.24). Initially, we fitted the observed volume data [135] of bulk sodium nitrite according to Eq. (3.39), as given in Fig. 3.24. Fitting parameters of this aquation was given in Table 3.14. Then, we used Eq. (3. 39) to calculate tha values of V_1 at around 500 K fort he lattice modes of sodium nitrite. We also used the constant ν_1 and γ_P values from the literature as given in Table 3.15. By using the values of the constant parameters given in Table 3. 15 (V_1 , ν_1 and γ_P), we investigated the temperature dependent frequencies for the A₁, B₁ and B₂ modes of NaNO₂ through Eq. (2.24). those calculated values of frequencies were then fitted to the observed data [60] to deduce the coefficients of Eq. (3.38) ,as we given in Table 3. 16. Figs. (3.25-3.27) show the calculated and observed [60] frequencies of longitudinal optic and transverse optic modes of A₁, B₁ and B₂, respectively. As the temperature increases the frequency decreases, as expected. This result is in good agreement with the observed [60] and calculated ones [57,60]. As the temperature increases, the volume of the bulk sodium

nitrite increases due to the thermal expansion which is inversely proportional with force constant results in decreasing frequency.

3.8 “Temperature dependence of the Brillouin frequency shift and the linewidth of the LA mode in the ferroelectric phase of PZT-x (PbZr_{1-x}Ti_xO₃)”

In this study, we analyzed the temperature dependence of the damping constant (Eqs. 2. 16 and 2.19) using the experimental data [70] for the bandwidth (FWHM) of the LA mode for the concentration of x=0.45 of PbZr_{1-x}Ti_xO₃. We used the observed [70] Brillouin frequencies of the LA mode as an order parameter P in Eqs. (2. 16) and (2.19) at various temperatures in the ferroelectric phase of this mixture. We plot in Fig. 3.28 the square of the observed [70] Brillouin frequency with respect to the maximum frequency, $(\omega/\omega_{max})^2$, for PbZr_{1-x}Ti_xO₃ single crystals ($T_C=657$ K). Since the order parameter varies from 0 to 1, we normalized the observed frequency (ω) values with respect to the maximum frequency (ω_{max}). Thus, on the basis of the Brillouin frequency being proportional to the order parameter ($\omega \propto P$), the damping constant Γ_{sp} was calculated using both models (pseudospin-phonon coupling and energy fluctuation models) according to Eqs. (2.16) and (2.19) at temperatures $T < T_C$ for x=0.45 of PbZr_{1-x}Ti_xO₃.

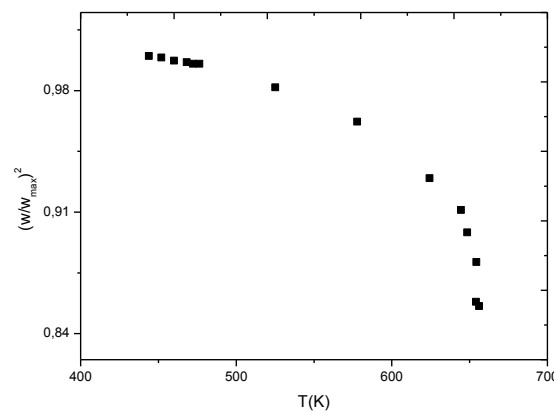


Figure 3.28 Temperature dependence of the observed Brillouin frequencies of the LA mode in the ferroelectric ($T < T_C$) of PbZr_{1-x}Ti_xO₃ [70] ($T_C= 657$ K).

Table 3.17 Values of the fitted parameters for the damping constant Γ_{sp} (Eqs. 2.16 and 2.19) using the observed data [70] in the ferroelectric phase ($T < T_C$) of $\text{PbZr}_{1-x}\text{Ti}_x\text{O}_3$ ($x=0.45$).

Temperature Range (K)	$\Gamma_0(\text{cm}^{-1})$	$A(\text{cm}^{-1})$	$\Gamma'_0(\text{cm}^{-1})$	$A'(\text{cm}^{-1})$
443-476	0.72	0.50	0.72	0.01
525-656	-0.02	185.80	-1.44	12.46

In order to compare our calculated damping constant (Γ_{sp}) from both models with the observed data, we then fitted Eqs. (2.16) and (2.19) to the observed linewidths [70] of the LA Brillouin mode ($x=0.45$) of $\text{PbZr}_{1-x}\text{Ti}_x\text{O}_3$. Table 3.17 gives our fitted parameters (Γ'_0, A', Γ_0 and A). We plot in Fig. 3.29 our calculated values of the damping constant Γ_{sp} using the P-P model (Eq. 2.16) and the EF model (Eq. 2.19) at various temperatures for $x=0.45$ of $\text{PbZr}_{1-x}\text{Ti}_x\text{O}_3$. The observed FWHM data for the Brillouin LA mode [70] are also shown in this figure.

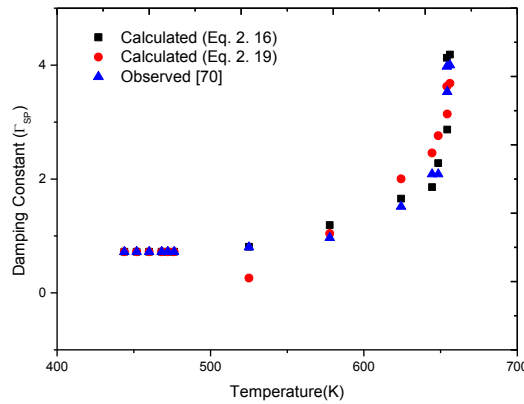


Figure 3.29 Temperature dependent Γ_{sp} values calculated (Eqs. 2.16 and 2.19) using the observed Brillouin frequency data [70] for the ferroelectric phase ($T < T_C$) of $\text{PbZr}_{1-x}\text{Ti}_x\text{O}_3$ ($x=0.45$). Observed FWHM [70] are also shown here ($T_C=657$ K).

Using the temperature dependent Γ_{sp} values, we extracted the U values (Eq. 2.26) for the $\text{PbZr}_{1-x}\text{Ti}_x\text{O}_3$ (Table 3.18). For comparison, we give in Table 3.18 the $k_B T_C$ values of this mixture at the transition temperature ($T_C=657$ K).

Table 3.18 Values of the activation energy (U) which were calculated using the models within the temperature range indicated for the ferroelectric phase ($T < T_C$) of $\text{PbZr}_{1-x}\text{Ti}_x\text{O}_3$ ($x=0.45$). $k_B T_C$ value at $T_C = 657$ K is also given here.

Damping Constant	Activation Energy (eV)	Temperature Range (K)	$k_B T_C$ (eV)
Pseudospin-phonon Coupled Model (Eq. 2.16)	2.467	644-656	0.056
Energy fluctuation Model (Eq. 2.19)	1.234		

We calculated the temperature dependent Γ_{sp} values through the P-P model (Eq. 2.16) and the EF model (Eq. 2.19) for $\text{PbZr}_{1-x}\text{Ti}_x\text{O}_3$ ($x=0.45$) as shown in Fig. 3.29. The observed data of the damping constant were extracted through the fitting procedure of the Brillouin spectra to the damped harmonic oscillator response function and to a single Debye relaxation model for the central peak of PZT in the ferroelectric phase [70]. Our calculated Γ_{sp} values from both models are in good agreement in the ferroelectric phase ($T < T_C$) of $\text{PbZr}_{1-x}\text{Ti}_x\text{O}_3$ for the concentration $x=0.45$. This agreement is much better as T_C is approached in this mixture (Fig. 3.29). This shows that the P-P model and the EF model describe adequately the observed behavior of the linewidths of the Brillouin LA mode associated with the ferroelectric-paraelectric transition in $\text{PbZr}_{1-x}\text{Ti}_x\text{O}_3$.

When we calculated the damping constant Γ_{sp} , we used observed Brillouin frequencies of the LA mode [70] in the ferroelectric phase ($T < T_C$) as the order parameter (spontaneous polarization) in this mixture, as we stated above. Since the Brillouin frequency (ω) of this mode decreases rapidly as T_C is approached from the ferroelectric phase as observed experimentally (Fig. 3.28), this can be considered as a soft mode behavior according to

$$\omega \sim (T - T_C)^{\frac{1}{2}} \quad (3.40)$$

Thus we assumed that the Brillouin frequency of the LA mode is directly related to the order parameter of $\text{PbZr}_{1-x}\text{Ti}_x\text{O}_3$. Brillouin frequency of this phonon mode can then be used to describe its spontaneous polarization (order parameter) as we used in Eqs. (2.16) and (2.19) for the damping constant (linewidth) of $\text{PbZr}_{1-x}\text{Ti}_x\text{O}_3$. The U

values were deduced through Eq. 2.26, as given in Table 3.18. Our U values are about 2.5 eV for the pseudospin-phonon coupled model and 1.2 eV for the energy fluctuation model within the temperature range of nearly 10 K (between 644 and 656 K) for $\text{PbZr}_{1-x}\text{Ti}_x\text{O}_3$. Our U values extracted from both models are much larger than the value of $k_B T_C = 0.056 \text{ eV}$ as calculated at T_C ($x=0.45$). Similar calculation for the damping constant and determination of the activation energy from both models (P-P model and the EF model), can be conducted for $x=0.42$ of $\text{PbZr}_{1-x}\text{Ti}_x\text{O}_3$ by using the Brillouin frequency data for the LA mode [70] according to Eqs. (2.16) and (2.19) in this mixture. More generally, for various concentrations x in the T-x phase diagram of $\text{PbZr}_{1-x}\text{Ti}_x\text{O}_3$ temperature dependent Γ_{sp} values might be calculated using the Brillouin frequencies of different modes and the activation energy U as a function of x can be extracted.

3.9 “Calculation of the damping constant, relaxation time and the activation energy for lead titanate zirconate in the paraelectric phase”

We calculated the damping constant, relaxation time and the activation energy as a function of temperature for the concentration of $x=0.45$ in the lead titanate zirconate $\text{Pb}(\text{Zr}_{1-x}\text{Ti}_x\text{O}_3)$ (PZT) ceramics above the transition temperature ($T_C=657 \text{ K}$), in the paraelectric phase by using the frequency data from the literature. We assumed that Brillouin shift of the LA mode can be associated with the order parameter P for PZT as $(\frac{\omega}{\omega_{max}}) = P$. Here the Brillouin frequency shift ω is normalized since the order parameter P varies from 0 to 1. ω_{max} is the maximum observed value of ω and it is 50.24 cm^{-1} in the paraelectric phase of PZT. Fig. 3.30 shows the squared Brillouin frequency shift as normalized with respect to ω_{max} at various temperatures above T_C of the LA mode for PZT-0.45. By $P = \frac{\omega}{\omega_{max}}$ into the Eqs. 2.16 and 2.19, Γ_{sp} values of this LA mode were calculated above T_C of PZT-0.45.

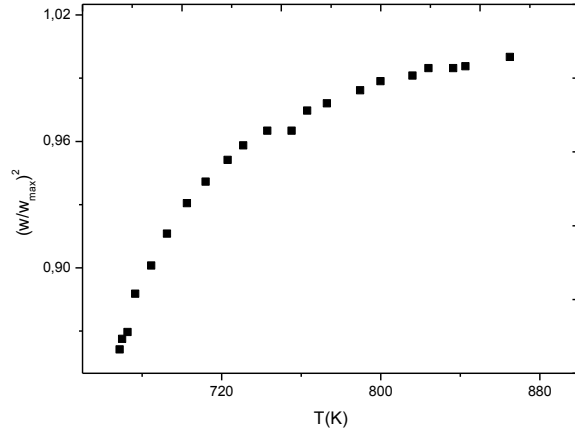


Figure 3.30 Temperature dependence of the observed Brillouin frequencies of the LA mode in the paraelectric ($T > T_C$) of $\text{PbZr}_{1-x}\text{Ti}_x\text{O}_3$ [70] ($T_C = 657$ K).

Table 3.19 Coefficients of Eqs. 2.16 and 2.19 using the observed data [70] in the paraelectric phase ($T > T_C$) of $\text{PbZr}_{1-x}\text{Ti}_x\text{O}_3$ ($x=0.45$).

Temperature Range(K)	$\Gamma_0(\text{cm}^{-1})$	$A(\text{cm}^{-1})$	$\Gamma'_0(\text{cm}^{-1})$	$A'(\text{cm}^{-1})$
668-755	1.07	97.67	-1.37	9.84
763-865	0.50	-29.93	0.50	0.64

Damping constant values were predicted for both the P-P model (Eq. 2.16) and the EF model Eq. (2.19) as we give in Figure 3.31. We also plot the measured damping constants [70] of this LA mode above T_C for PZT-x in Figure 3.31. Table 3.19 gives our fitted parameters (Γ'_0, A', Γ_0 and A) extracted through Eqs. 2.16 and 2.19 for the different temperature ranges indicated here. From the temperature dependence of the damping constant (Eqs. 2.16 and 2.19) and of the order parameter P , the inverse relaxation time τ^{-1} or κ of the LA mode was then calculated above T_C in PZT ceramics. So, τ^{-1} or κ was predicted according to

$$\kappa = \left(\frac{\omega}{\omega_{max}}\right)^2 / \Gamma \quad (3.41)$$

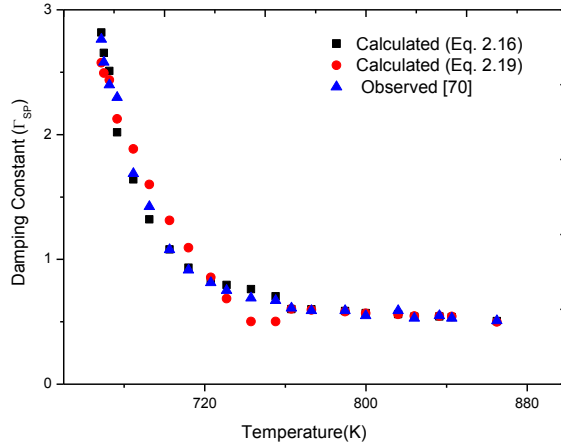


Figure 3.31 Temperature dependent Γ_{SP} values calculated (Eqs. 2. 16 and 2. 19) using the observed Brillouin frequency data [70] for the paraelectric phase ($T > T_C$) of $PbZr_{1-x}Ti_xO_3$ ($x=0.45$). Observed FWHM [70] are also shown here.

We then calculated the κ values according to Eq. 3.41 by using Γ_{SP} values from both models (P-P model and EF model). By fitting the calculated κ values and the observed ones (τ^{-1}), we found a linear relation according to

$$\tau^{-1} = a + b\kappa \quad (3.42)$$

The coefficients a and b were determined for the two different ranges as given in Table 3.20. We plot our calculated values of the inverse relaxation time (Eq. 3.41) as a function of temperature with the experimental data [70] above the transition temperature in Fig. 3.32.

Table 3.20 Coefficients of Eq. (3.42) for the inverse relaxation time τ^{-1} using the observed data [70] in the paraelectric phase ($T > T_C$) of $PbZr_{1-x}Ti_xO_3$ ($x=0.45$).

Damping constant	Temperature Range (K)	$a \times 10^{-4} (ps)^{-1}$	b
Eq. 2.16	670-697	8.7	-0.1498
	702-773	4.6	0.7238
Eq. 2.19	670-697	8.7	-0.1399
	702-773	4.4	0.7624

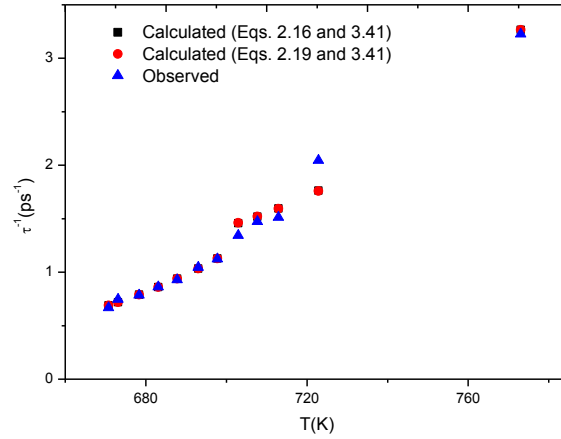


Figure 3.32 Temperature dependence of the relaxation time calculated (Eq. 3.41) using the observed Brillouin frequency data [70] for the paraelectric phase ($T > T_C$) of $\text{PbZr}_{1-x}\text{Ti}_x\text{O}_3$ ($x=0.45$). Observed relaxation time [70] also shown here.

Table 3.21 Values of the activation energy (U) which were calculated using the models within the temperature range indicated for the paraelectric phase ($T > T_C$) of $\text{PbZr}_{1-x}\text{Ti}_x\text{O}_3$ ($x=0.45$). $k_B T_C$ value at $T_C = 657$ K is also given here.

Damping Constant	Temperature Range(K)	Activation Energy (eV)	$k_B T_C$ (eV)
Pseudospin-phonon (Eq. 2.16)	668-702	-1.17	0.056
Energy Fluctuation (Eq. 219)	668-702	-0.8	

Finally, we extracted the activation energy values using our calculated damping constant Γ (Eqs. 2.16 and 2.19) from the Arrhenius plot according to Eq. 2.26. Our calculated values of activation energies U and the $k_B T_C$ value (for comparison) are given in Table 3.21 in the temperature interval studied here.

The Brillouin frequency shift of the LA mode for PZT-0.45 increases with increasing temperature in the paraelectric phase as observed experimentally [70]. So, we associated this observed Brillouin frequency shift (normalized) with the order parameter as given in Fig. 3.30. By using those calculated values of order parameter, the temperature dependent Γ_{sp} values were calculated according to the P-P model

(Eq. 2.16) and EF model (2.19) for the concentration of $x=0.45$ in the PZT ceramic above the transition temperature ($T_C=657$ K). We showed in Fig. 3.31 our calculated values of damping constants from both models and the observed data [70] for this LA mode of PZT-0.45. Kim et al. [70] deduced the temperature dependence of the damping constant for the LA mode for PZT-0.45 above the transition temperature. This was done by fitting the Brillouin spectra to a superposition of the damped harmonic oscillator model and the Debye relaxation model. Our results are in good agreement with the observed data and the damping constant decreases as the temperature increases above the transition temperature as we expected. We also determined the fitting parameters of Eqs. 2.16 and 2.19 for this LA mode of PZT-0.45 as given in Table 3.19. The observed relaxation time in the paraelectric phase of PZT-0.45 was extracted by fitting procedure of the Brillouin spectra to a single Debye relaxator [70]. Calculation of the temperature dependence of relaxation time was then performed according to Eq. 3.41 using the values of the damping constant of both pseudospin-phonon coupled and the energy fluctuation models, and the order parameter above the transition temperature of the LA mode of PZT-0.45. We extracted the fitting parameters of Eq. 3.42 in the temperature ranges of $670 \text{ K} < T < 697 \text{ K}$ and $702 \text{ K} < T < 773 \text{ K}$ above the transition temperature by using the observed data for the relaxation time [70] and the values of the relaxation time calculated through Eq. 3.41 of this LA mode of PZT-0.45 ceramic. These fitting parameters of Eq. 3.42 were given in Table 3.20. In Fig. 3.32 we plotted the calculated inverse relaxation time for PZT-0.45 in the temperature range indicated. We also gave the observed inverse relaxation time in this figure. As the temperature increases the inverse relaxation time increases as expected. Finally, we used the calculated Γ_{sp} values from both P-P model and the EF model to extract the activation energy values of PZT-0.45 according to Eq. 2.26 in the paraelectric phase of this LA mode. Table 3.21 gives the values of the activation energies for the temperature range of $668 \text{ K} < T < 702 \text{ K}$ for the LA mode of PZT-0.45 which are much greater than the $k_B T_C$ value of 0.056 eV.

3.10 “Temperature dependence of the Raman frequency, damping constant and the activation energy of a soft mode in Cd₂Nb₂O₇”

The temperature dependent spontaneous polarization values P was calculated by using the mean field theory (Eq. 2. 20) for the Raman soft mode of cadmium pyroniobate (Cd₂Nb₂O₇: CNO) below the transition temperature $T_C=196$ K. Calculated values of the order parameter was then fitted to the observed frequency data ω [91] according to the relation

$$\omega = a + bP \quad (3.43)$$

where a and b are the fitting parameters and their values are given in Table 3.22.

Table 3.22 Values of the coefficients a and b according to Eq. (3.43) below the transition temperature ($T_C= 196$ K) of Cd₂Nb₂O₇.

Raman frequency	Temperature Range (K)	$a(cm^{-1})$	$b(cm^{-1})$
Eq. 3.43	102-147	-38.96	73.96
	151-179	-2.83	31.28

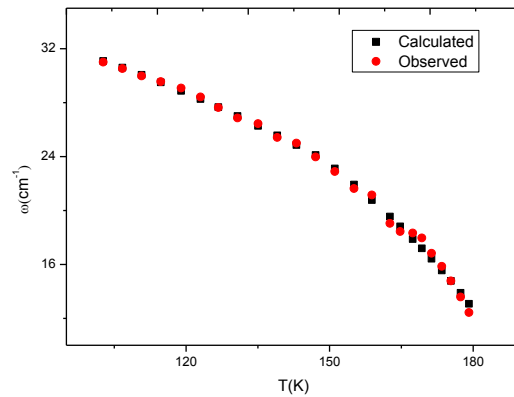


Figure 3.33 Calculated (Eq. 3.37) and observed [91] values of the soft mode frequency at temperatures $T < T_C$ for CNO.

Fig. 3.33 shows the calculated values of the Raman frequency in the ferroelectric phase of CNO. The observed frequency data [91] of this Raman mode are also shown in this figure. By using the calculated values of the order parameter from mean field theory (Eq. 2.20), we calculated the temperature dependent Γ values in the

ferroelectric phase of CNO for this Raman mode. This calculation was performed by using both P-P model (Eq. 2.16) and the EF model (Eq. 2.19). Fig. 3.34 gives the calculated values of the damping constant from both models below T_C for this Raman soft mode of CNO. The observed damping constant data [91] are also plotted in this figure. The fitting parameters of Eqs. 2.16 and 2.19 are given in Table 3.23.

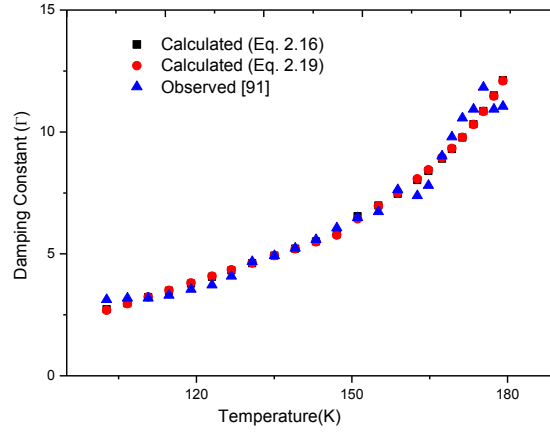


Figure 3.34 Comparison of the calculated (Eqs. 2.16 and 2.19) and observed Γ [91] values at temperatures $T < T_C$ for CNO.

Table 3.23 Values of the fitted parameters for the damping constant Γ (Eqs. 2.16 and 2.19) using the observed data [91] in the ferroelectric phase ($T < T_C$) of the $\text{Cd}_2\text{Nb}_2\text{O}_7$.

Temperature Range(K)	$\Gamma_0(\text{cm}^{-1})$	$A(\text{cm}^{-1})$	$\Gamma'_0(\text{cm}^{-1})$	$A'(\text{cm}^{-1})$
102-147	0.79	27.27	-0.51	9.98
151-179	5.26	5.26	3.17	4.50

Finally, we deduced the U values of this Raman mode of CNO by means of the Arrhenius plot, $\ln\Gamma$ vs. $1/T$. This calculation was done by inserting the calculated values of the damping constant from both models studied here into the Eq. 2.26. Table 3.24 gives our calculated U values from both P-P model and the EF model for this Raman mode of CNO. The $k_B T_C$ value of this structure is also given in this table for comparison.

Table 3.24 Values of the activation energy (U), which were calculated using the models within the temperature ranges indicated for the ferroelectric phase ($T < T_c$) of cadmium pyroniobate. $k_B T_c$ value at $T_c = 196$ K is also given here.

Damping Constant	Temperature Range(K)	Activation Energy (meV)	$k_B T_c$ (meV)
Pseudospin-phonon (Eq. 2.16)	102-147	22	17
	151-179	51	
Energy Fluctuation (Eq. 2.19)	102-147	22	
	151-179	52	

The Raman frequency (ω) data were observed to decrease with increasing temperature in the ferroelectric phase of CNO [91]. The same behaviour is also valid for the spontaneous polarization (order parameter) P in the ferroelectric phase of CNO as reported in the literature. So, we related the order parameter P with the observed Raman frequency (ω) data by using a linear relation given by Eq. 3. 43 for this Raman mode of $\text{Cd}_2\text{Nb}_2\text{O}_7$ below the transition temperature. We gave the values of the fitted parameters a and b for the temperature ranges of $102 \text{ K} < T < 147 \text{ K}$ and $151 \text{ K} < T < 179 \text{ K}$ in Table 3. 22. Figure 3.33 shows the calculated values of the Raman frequency and the observed data [91] for this Raman soft mode of CNO below T_c . In their study, Taniguchi et al. [91] have used the Cochran's law to investigate the temperature dependent ω values according to $\omega_s = 3.3|T - 196|^{0.5}$. Our calculated values of the Raman frequency ω are in good agreement with the observed data and also with those calculated from the Cochran's law. Since we calculated the order parameter from the mean field theory (Eq. 2.20), we were able to calculate the temperature dependent Γ values from both P-P model (Eq. 2.16) and the EF model (Eq. 2.19). By fitting procedure of the calculated Γ values (Eqs. 2.16 and 2.19) and the observed data [91] of this Raman mode in CNO, we determined the fitting parameters of Eqs. 2.16 and 2.19 as we gave in Table 3.23. Taniguchi et al [91] have analyzed the temperature dependent Γ values through the equation $\Gamma = 110|T - 196|^{-0.76}$, which is given by Cochran's theory. Their results describe the observed data of the damping constant very well as our calculated values from the two models studied here. Fig. 3.34 shows our calculated values of the damping

constant from both models and the observed data for this Raman mode of CNO below the transition temperature T_C . The damping constant increases very abruptly close to the phase transition temperature of $T_C=196$ K as expected (Fig. 3.34). As an extension of this work, we evaluated values of the activation energy of the Raman mode of CNO, as given in Table 3.24. The values of the activation energies are much greater than the $k_B T_C$ value of 17 meV very close to the transition temperature.

3.11 “Calculation of the damping constant and the activation energy of the E_g soft phonon mode in ferroelectric $SrZrO_3$ ”

The temperature dependence of the damping constant and of the activation energy was calculated by using the frequency data [81] of the E_g soft phonon mode below the transition temperature $T_C= 1443$ K. We related the normalized frequency ($\frac{\omega}{\omega_{max}}$) with the order parameter P (spontaneous polarization) as $\frac{\omega}{\omega_{max}} = P$. Fig. 3.35 gives the temperature dependence of the squared frequency ratio (P^2) below the transition temperature for this E_g soft mode in $SrZrO_3$.

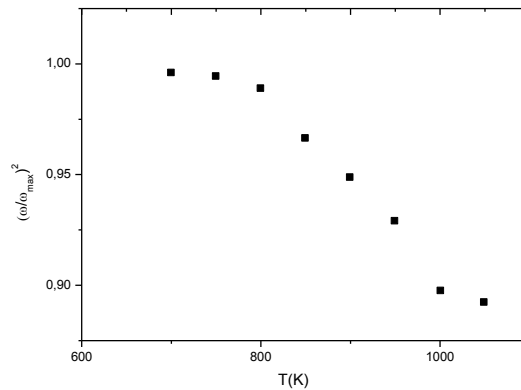


Figure 3.35 The temperature dependent frequency ratio squared $(\omega/\omega_{max})^2$ values of the E_g mode of $SrZrO_3$ at temperatures $T < T_C$. ($T_C= 1443$ K).

We then calculated the temperature dependent damping constant values by using the normalized observed frequency data (order parameter) for E_g soft mode of $SrZrO_3$. This calculation was performed by using the P-P model (Eq. 2.16) and the EF model

(Eq. 2.19). The fitting parameters (Γ'_0 , A' , Γ_0 and A) were then obtained by using the calculated values of the damping constant from both models (Eqs. 2.16 and 2.19) and the observed damping constant data [81]. We give these fitting parameters in Table 3.25 in the ferroelectric phase of SrZrO₃ for the E_g mode. Then, with help of the fitting parameters (Table 3.25), we plot the temperature dependence of the damping constant calculated from both models studied here in Fig. 3.36. The observed damping constant data [81] are also given in this figure.

Table 3.25 Values of the fitted parameters for the damping constant Γ (Eqs. 2.16 and 2.19) using the observed data [81] in the ferroelectric phase ($T < T_C$) of the SrZrO₃.

Temperature Range (K)	$\Gamma_0(cm^{-1})$	$A(cm^{-1})$	$\Gamma'_0(cm^{-1})$	$A'(cm^{-1})$
972-1072	14.24	384.52	13.75	17.02
1122-1321	10.46	461.85	6.81	43.13

Finally, we extracted the values of the activation energy of the E_g soft phonon mode from Eq. 2.26 in the ferroelectric phase of SrZrO₃. This calculation was performed by using the evaluated damping constant values from both models (Eqs. 2.16 and 2.19) studied here. Table 3.26 gives these calculated values of the activation energy of the SrZrO₃ crystal for temperature ranges indicated.

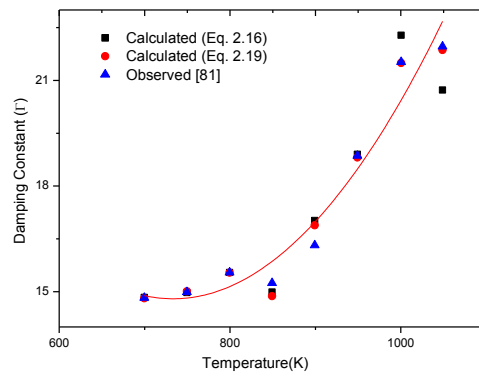


Figure 3.36 The calculated Γ values using both the P-P model (Eq. 2.16) and the EF model (Eq. 2.19) for the Raman mode of SrZrO₃ in the ferroelectric phase. Observed damping constant [81] is also shown here. Solid curve is a guide to eye.

Table 3.26 Values of the activation energy (U), which were calculated using the models within the temperature range indicated for the ferroelectric phase ($T < T_C$) of SrZrO₃. $k_B T_C$ value at $T_C = 1443$ K is also given here.

Damping Constant	Activation Energy (eV)	Temperature Range (K)	$k_B T_C$ (eV)
Pseudospin-phonon Coupled Model (Eq. 2.16)	0.13	972-1321	0.12
Energy fluctuation Model (Eq. 2.19)	0.13		

The frequency of the E_g mode in SrZrO₃ softens (decreases) as the transition temperature is approached as observed experimentally [81]. This behaviour is similar to the order parameter (spontaneous polarization) in the ferroelectric materials below T_C . So, we associated the normalized frequency (ω/ω_{max}) with the order parameter P for this E_g mode. We used the normalized frequency since the order parameter can take only the values between 0 and 1. In Fig. 3.35, we gave the temperature dependence of the order parameter (squared) $(\omega/\omega_{max})^2$, of the E_g mode of SrZrO₃. The temperature dependence of the frequency (squared) for the E_g mode of SrZrO₃ has also been analyzed by Fujimori et al. [81] according to the linear relation $\omega^2 = \omega_{T_C}^2 + \alpha(T - T_C)$ in the temperature range of 1123 K and 1323 K. Here $\omega_{T_C}^2$ and α are $1.29 \times 10^4 \text{ cm}^{-2}$ and $6.36 \text{ cm}^{-2}/\text{K}$, respectively. Their result are in good agreement with the observed data of frequency. They also considered the universal scaling law to investigate the temperature dependence of the damping constant for the E_g mode of SrZrO₃.

From the calculation of the order parameter P , we were able to calculate the damping constant Γ as a function of temperature by using the pseudospin-phonon coupled model (Eq. 2.16) and the energy fluctuation model (Eq. 2.19) for the E_g mode in SrZrO₃ in the ferroelectric phase. Since we have the experimental data for the damping constant of this mode, we performed the fitting procedure to find the fitting parameters of Eqs. 2.16 and 2.19. This calculation was carried out in the temperature ranges of $972 \text{ K} < T < 1072 \text{ K}$ and $1122 \text{ K} < T < 1322 \text{ K}$, respectively. In Table 3.25, we gave the values of Γ'_0, A', Γ_0 and A which were obtained through the fitting

procedure in the temperature ranges given above. With help of the fitting parameters (Table 3.25), we plotted the temperature dependence of the damping constant calculated from both models in Fig. 3.36. The energy fluctuation model agrees better than the pseudospin-phonon coupled model when compared with the observed data for the damping constant. As the temperature approaches the transition temperature ($T_C=1443$ K), the damping constant increases rapidly which indicates that this E_g soft phonon mode of $SrZrO_3$ plays an important role for the ferroelectric phase transition from cubic to tetragonal.

Finally, we extracted values of the activation energy of $SrZrO_3$ crystal using the Arrhenius plots (Eq. 2.26) in the temperature range of $972\text{ K} < T < 1321\text{ K}$. Table 3.26 shows those values of activation energy which were extracted through both models studied here. The $k_B T_C$ value was also given for comparison.

3.12 “Temperature dependence of the order parameter, damping constant, relaxation time and the activation energy of the $A_1(TO_1)$ soft phonon mode in ferroelectric $LiNbO_3$ ”

We calculated the order parameter P , damping constant Γ , inverse relaxation time τ^{-1} and the activation energy U of the lowest Raman mode, $A_1(TO_1)$, of lithium niobate (LN) by using the frequency (ω) and the dielectric data (ϵ) below the transition temperature $T_C=1260$ K. We related the squared of the observed frequency data (squared,) $(\frac{\omega}{\omega_{max}})^2$ [92] with the order parameter squared P^2 as follows:

$$(\frac{\omega}{\omega_{max}})^2 \sim = m(T - T_C) + n \quad (3.44)$$

We plot the temperature dependence of the squared frequency (normalized) in Fig. 3.37 and from the linear fitting procedure we determined the values of m and n of Eq. 3.44. These fitted parameters are given in Table 3.27.

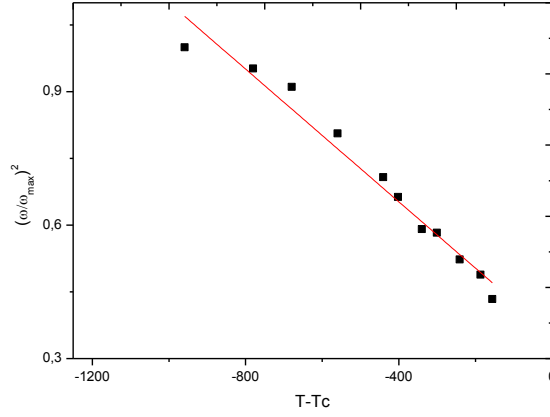


Figure 3.37 The best linear fit for the square of the observed frequency (normalized) data [92] as a function of temperature difference for the lowest Raman mode $A_1(TO_1)$ in the $LiNbO_3$ below the transition temperature ($T_C= 1260$ K).

Table 3.27 Values of the fitted parameters (Eq. 3.44) for the lowest Raman mode $A_1(TO_1)$ in the $LiNbO_3$ below the transition temperature ($T_C= 1260$ K).

Temperature Range (K)	$m \times 10^{-4} (K^{-1})$	n
301-1103	-7.46	0.35

Then, we calculated the inverse dielectric susceptibility χ^{-1} by using the dielectric constant data ϵ of this soft phonon mode of LN [92] according to the relation

$$\chi^{-1} = \frac{1}{\epsilon - 1} \quad (3.45)$$

The inverse dielectric susceptibility χ^{-1} can also be calculated by Eq. (3.20). In this equation a_2 can be taken as the temperature dependent (Eq. 3.16), a_4 and a_6 are assumed to be constant. Replacing P^2 in Eq. (3.20) by $(\omega/\omega_{\max})^2$ in Eq. 3.44, one gets

$$\chi^{-1} = 30a_6m^2(T - T_C)^2 + [2\alpha + 12a_4m + 60a_6mn](T - T_C) + 12a_4n + 30a_6n^2 \quad (3.46)$$

In Fig. 3.38, we plot the calculated values of the inverse dielectric susceptibility χ^{-1} as a function of the temperature difference, $(T - T_C)$, for this lowest Raman mode in LN in the ferroelectric phase. By using the quadratic fitting equation (Fig. 3.38) and the fitting parameters of Eq. 3.44 (Table 3.27), we extracted the values of the α , a_4 and a_6 . Table 3.28 gives those fitting parameters for the lowest Raman mode

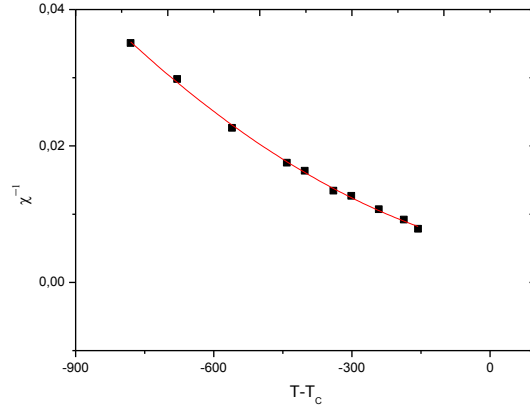


Figure 3.38 The best fit (quadratic) for the inverse dielectric susceptibility χ^{-1} (Eq. 3.46) as a function of the temperature difference for the lowest Raman mode $A_1(TO_1)$ in the LiNbO_3 below the transition temperature ($T_C = 1260$ K).

Table 3.28 Values of the fitted parameters (Eq. 3.46) for the lowest Raman mode $A_1(TO_1)$ in the LiNbO_3 below the transition temperature ($T_C = 1260$ K).

Temperature Range (K)	$\alpha \times 10^{-6} (K^{-1})$	$a_4 \times 10^{-4}$	$a_6 \times 10^{-4}$
301-1103	4.46	-3.82	17.69

$A_1(TO_1)$ in the LiNbO_3 below the transition temperature ($T_C = 1260$ K). Once we calculated the fitted parameters of Eq. 3.46 (Table 3.28), we could calculate the values of the squared order parameter P^2 through Eq. 3.18 (Landau theory). The ratios in Eq. 3.44 can be given as

$$\left(\frac{\omega}{\omega_{max}}\right)^2 = c_0 + c_1 P^2 \quad (3.47)$$

Table 3.29 gives the values of the c_0 and c_1 . The temperature dependence of the P^2 (both observed and calculated) is given in Fig. 3.39 for this soft phonon mode in LN.

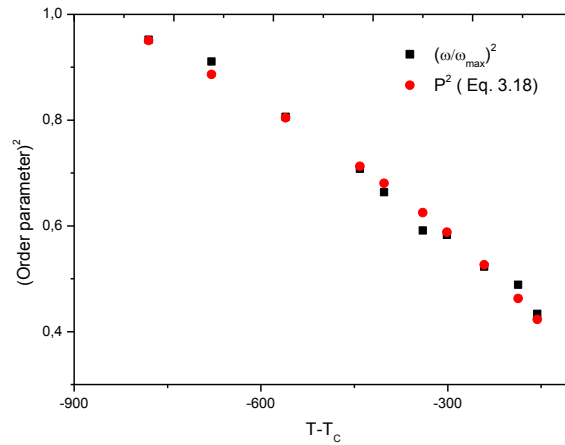


Figure 3.39 Temperature dependence of the normalized observed frequencies (squared) and the calculated values of P^2 (Eq. 3.18) for the lowest Raman mode $A_1(TO_1)$ in the $LiNbO_3$ below the transition temperature ($T_C=1260$ K).

Table 3.29 Values of the fitted parameters (Eq. 3.47) for the lowest Raman mode $A_1(TO_1)$ in the $LiNbO_3$ below the transition temperature ($T_C=1260$ K).

Temperature Range (K)	c_0	c_1
301-1103	-0.10	1.19

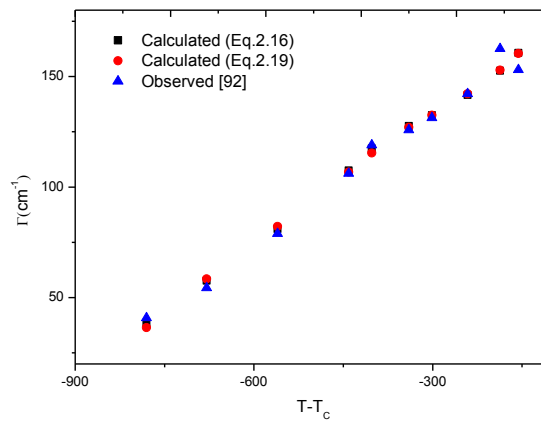


Figure 3.40 Damping constant Γ calculated as a function of temperature using both the pseudospin-phonon coupled model (Eq. 2.16) and the energy fluctuation model (Eq. 2.19) for the Raman mode of $LiNbO_3$ in the ferroelectric phase. Observed damping constant [92] are also shown here.

Table 3.30 Values of the fitted parameters for the damping constant Γ (Eqs. 2.16 and 2.19) using the observed data [92] in the ferroelectric phase ($T < T_C$) of the LiNbO_3 .

Temperature Range (K)	$\Gamma_0(\text{cm}^{-1})$	$A(\text{cm}^{-1})$	$\Gamma'_0(\text{cm}^{-1})$	$A'(\text{cm}^{-1})$
479-857	22.13	291.07	1.50	146.74
920-1103	86.08	107.03	57.71	78.94

Then, we calculated the damping constant from the pseudospin-phonon coupled model (Eq. 2.16) and the energy fluctuation model (Eq. 2.19) by using the order parameter squared (P^2) through Eq. 3.18 for the $A_1(\text{TO}_1)$ mode in the ferroelectric phase of LiNbO_3 . Table 3.30 gives the fitted parameters (Γ'_0, A', Γ_0 and A) which were obtained from the observed damping constant data [92] and those calculated from the both models studied here for the temperature range indicated. We plot the damping constant calculated from both models (Eqs. 2.16 and 2.19) as a function of the temperature in Fig. 3.40. The observed damping constant data are also given in this figure.

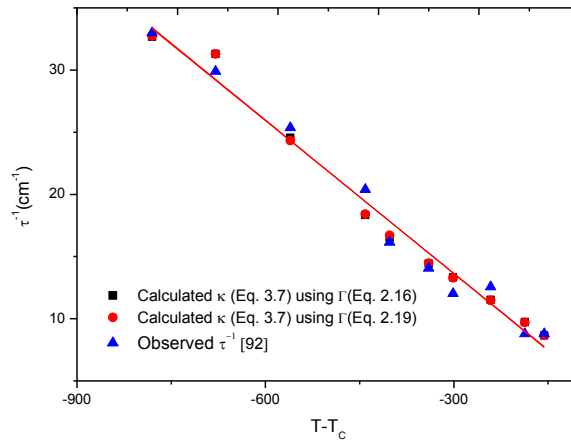


Figure 3.41 Temperature dependence of the relaxation time κ calculated from Eq. (3.7) through the damping constant Γ (Eqs. 2.16 and 2.19) for the LiNbO_3 . Experimental data τ^{-1} [92] for the relaxation time are also shown here. The solid line is a guide to eye.

Table 3.31 Values of the coefficients obtained by fitting κ to the inverse relaxation time τ^{-1} according to Eq. (3.48) ($T < T_c$) for the LiNbO₃. The κ values were calculated from Eq. (3.7) through the damping constant Γ (Eqs. 2.16 and 2.19), as indicated.

Temperature Range (K)	Γ	$d_0(cm^{-1})$	d_1	$d_2(cm)$
479-1103	Eq. (2.16)	0.99	3108.36	-73967.64
	Eq. (2.19)	1.05	3077.68	-71412.89

Then, we calculated the inverse relaxation time τ^{-1} or κ as a function of temperature for the A₁(TO₁) mode in the LiNbO₃ by Eq. 3.7 for both pseudospin-phonon coupled model and the energy fluctuation model. These calculated values of the inverse relaxation time κ from both models were then fitted to the observed inverse relaxation time τ^{-1} [92] by a quadratic equation given as

$$\tau^{-1} = d_0 + d_1\kappa + d_2\kappa^2 \quad (3.48)$$

We give the fitted parameters of Eq. 3.40 in Table 3.31. The inverse relaxation time κ calculated from both pseudospin-phonon coupled model and the energy fluctuation model as a function of temperature is given in Fig. 3.41 for this lowest Raman mode of LN in the ferroelectric phase. The observed data of the inverse relaxation time τ^{-1} are also given in this figure. Finally, we extracted the activation energy values U calculated from Eq. 2.26. This calculation was performed by using the damping constant data calculated from both models studied here below the transition temperature for the A₁(TO₁) Raman mode in lithium niobate. Table 3.32 gives those values of the activation energy U below the transition temperature.

Table 3.32 Values of the activation energy (U) which were calculated using the models within the temperature range indicated for the ferroelectric phase ($T < T_c$) of LiNbO₃. $k_B T_c$ value at $T_c = 1260$ K is also given here.

Damping Constant	Activation Energy (meV)	Temperature Range (K)	$k_B T_c$ (meV)
Pseudospin-phonon Coupled Model (Eq. 2.16)	104	479-1103	109
Energy fluctuation Model (Eq. 2.19)	107		

The imaginary part of the dielectric permittivity can be related to the temperature and the frequency dependence of the Raman-scattered intensity through the Kramer-Kronig relation. Ridah et al. [92] have fitted the observed Raman intensity of the A₁(TO) phonon modes of LN to the dielectric permittivity which are given through the damped harmonic oscillator model (DHO) in order to deduce the temperature dependence of the frequency, damping constant and the oscillator strength below the transition temperature. They also fitted the Raman intensity to the dielectric permittivity which is given through the Debye relaxation model to extract the temperature dependence of the relaxation time and the relaxation strength in the ferroelectric phase of LN. Here, we used the Landau theory to calculate the temperature dependence of the order parameter for the A₁(TO₁) lowest Raman mode in LiNbO₃ below the transition temperature T_C=1260 K. We assumed that the observed frequency (squared) which was normalized, $(\frac{\omega}{\omega_{max}})^2$, is proportional to the order parameter (squared) P^2 through Eq. 3.44. We obtained from the fitting procedure the equation of the $(\omega/\omega_{max})^2$ as a function of the temperature $T - T_C$ (Table 3.27), as plotted in Fig. 3.37. This equation was replaced in Eq. 3.20 instead of P^2 to get Eq. 3.46. Since we have the dielectric constant data [92] for this Raman mode below T_C, we calculated the inverse dielectric susceptibility χ^{-1} from Eq. 3.45. In Fig. 3.38 we plotted χ^{-1} versus $T - T_C$. We then found a quadratic equation of this figure as a function of the temperature. We extracted the fitted parameters of Eq. 3.46 (α , a_4 and a_6) by using the quadratic equation of χ^{-1} from Eq. 3.46. These fitted parameters were given in Table 3.28. We found $\alpha > 0$, $a_4 < 0$ and $a_6 > 0$ which describes a first order phase transition (Landau theory) for this A₁(TO₁) mode in lithium niobate. We then calculated P^2 values of the lowest Raman mode in LiNbO₃ by using Eq. 3.18 (Landau theory) in the ferroelectric phase. The proportionality between $(\omega/\omega_{max})^2$ and P^2 (Eq. 3.44) was given by Eq. 3.47. From the fitting procedure we found the c_0 and c_1 values which were given in Table 3.29. We plotted both observed and calculated values of the order parameter (squared) as a function of $T - T_C$ in Fig. 3.39 for this soft Raman mode in LN. As the temperature increases, values of the order parameters decrease linearly as expected from the mean field theory (Eq. 3.9).

We then calculated the damping constant Γ of this Raman mode as a function of temperature by using the pseudospin-phonon coupled model (Eq. 2.16) and the

energy fluctuation model (Eq. 2.19). This calculation was performed by using P^2 values obtained from the Landau theory (Eq. 3.18). We fitted the observed data for the damping constant [92] and those calculated from the both models (Eqs. 2.16 and 2.19) in the temperature ranges of $479 \text{ K} < T < 857 \text{ K}$ and $920 \text{ K} < T < 1103 \text{ K}$, respectively. Values of the fitted parameters for the damping constant Γ (Eqs. 2.16 and 2.19) were given in Table 3.30 in the temperature ranges indicated for the $A_1(\text{TO}_1)$ mode in LN. The temperature dependence of the damping constant Γ (both observed and calculated) was given in Fig. 3.40. Both models seem to describe very well the observed behavior of the damping constant Γ of $A_1(\text{TO}_1)$ mode in LiNbO_3 . These calculated values of the damping constant Γ from both models and those calculated values of the P^2 from Landau theory were then used to calculate the inverse relaxation time κ through Eq. 3.7. These calculated values of the κ were then fitted to the observed data for the inverse relaxation time (τ^{-1}) according to Eq. 3.48. Values of the coefficients of Eq. 3.48 were given in Table 3.31. We give in Fig. 3.41 the temperature dependence of the relaxation time τ^{-1} (both observed and calculated) for the LiNbO_3 in the ferroelectric phase. Values of the observed dynamical quantities (frequency, damping constant and relaxation time) were compared to those which we calculated from the Landau theory (frequency), the pseudospin-phonon coupled model and the energy fluctuation model (damping constant and relaxation time). Finally, we extracted the activation energy U through Eq. 2.26 for the ferroelectric phase of LN. Damping constant Γ calculated from both models was used in Eq. 2.26. These U values were given in Table 3.32.

3.13 Summary

The temperature and/or pressure dependence of the frequency ω , order parameter P , damping constant Γ , relaxation time τ , dielectric susceptibility χ and the activation energy U of some ferroelectric materials such as KDP, BaTiO_3 , NaNO_2 , PbTiO_3 , PZT-x, CNO, SrZrO_3 and LiNbO_3 have been investigated in the ferroelectric and/or paraelectric phases in this thesis. We used the mean field theory (soft mode concept), the Landau theory, the pseudospin-phonon coupled model and the energy fluctuation model during this investigation of those ferroelectric materials mentioned above. In

Table 3.33 we summarize the calculated activation energy values of some ferroelectric materials studied here below the transition temperatures.

Table 3.33 Values of the activation energy U , which were calculated within the temperature ranges indicated for some ferroelectric materials studied in this here. $k_B T_C$ values are also given for comparison.

Ferroelectric Material	Transition Temperature (K)	Temperature Range (K)	Damping Constant	Activation Energy (eV)	$k_B T_C$ (eV)
CNO	196	151-179	Eq. 2.16	0.050	0.017
			Eq. 2.19	0.050	
BaTiO ₃	222	204.7-217.7	Eq. 2.16	0.570	0.020
			Eq. 2.19	0.320	
PZT-x (x=0.45)	657	644-656	Eq. 2.16	2.470	0.060
			Eq. 2.19	1.230	
LiNbO ₃	1260	479-1103	Eq. 2.16	0.100	0.110
			Eq. 2.19	0.100	
SrZrO ₃	1443	972-1321	Eq. 2.16	0.130	0.120
			Eq. 2.19	0.130	

CHAPTER 4

CONCLUSIONS

We calculated the Raman frequency ω_0 and its damping constant Γ_0 , pressure dependent, at 80 K and 90K constant temperatures in the ferroelectric mode of KDP. The “soft mode” concept was considered to predict the values of the Raman frequency. We used the “pseudospin-phonon coupled model” and the “energy fluctuation model” to calculate the damping constant values. Our prediction for the damping constant, as a function of pressure, can be compared with the experimental data when it is given in the literature.

We also examined the damping constant, temperature dependent, in the paraelectric phase of KDP at constant 6.54 kbar pressure. Comparison of the observed damping constant data and those calculated from the two models described here show that, the “energy fluctuation model” is more consistent than the “pseudospin-phonon coupled model”.

The temperature dependent damping constant was calculated using the “pseudospin-phonon coupled model” and the “energy-fluctuation model” for the hexagonal barium titanate. Our calculated Γ due to the pseudospin-phonon interactions can be compared with the experimental data below T_0 for this material. For calculation of the damping constant, the temperature dependence of the order parameter (bilinear coupling constant between acoustic and soft-optic modes) was obtained using the mean field theory. The order parameter increases and the damping constant decreases with decreasing temperature below T_0 , as expected. The relaxation time, temperature dependent, was also calculated using the values of the order parameter and of the damping constant below T_0 for the hexagonal barium titanate.

The relaxation time increases as the temperature decreases about 30K below T_0 in this ferroelectric material. The energy-fluctuation model gives better agreement with the experimental data. The extracted activation energy values are considerably large in comparison with the $k_B T_0$ near the transition temperature T_0 .

The soft mode Raman frequency and its damping constant was calculated above T_0 in $h-BaTiO_3$. The Raman frequency was calculated using the soft mode theory or the mean field theory. Calculation of the damping constant was performed using the pseudospin-phonon coupled model and the energy fluctuation model. It was obtained that the damping constant calculated from both models gives an adequate description of the observed behaviour above T_0 in $h-BaTiO_3$. Our results show that the soft mode behaviour can be explained as the main mechanism of an order-disorder transition in $h-BaTiO_3$.

The damping constant was calculated as a function of temperature for the tetragonal cubic transition at around 450 K in $BaTiO_3$. This calculation was performed for the tetragonal mode (308 cm^{-1}) using the pseudospin-phonon and the energy fluctuation models. The experimental data for the Raman intensity were used and the expressions for the damping constant were fitted to the bandwidth of this mode in the ferroelectric and paraelectric phases of $BaTiO_3$.

Our results show that the pseudospin-phonon coupled model agrees well with the experimental data for the ferroelectric-paraelectric transition in $BaTiO_3$. This indicates that the Raman intensity can be used as an order parameter to calculate the damping constant for the two models studied to predict the observed behavior of the tetragonal-cubic transition in $BaTiO_3$. Our calculated damping constant was also compared with the experimental data from the other sources given in the literature. From this comparison, it was found that our calculated values also follow the same trend as the observed data for the ferroelectric-paraelectric transition in $BaTiO_3$.

Raman frequencies of the tetragonal 310 cm^{-1} mode were analyzed at various temperatures for ferroelectric-paraelectric transition in BaTiO_3 . This temperature dependence of the Raman frequency was related to the spontaneous polarization in the tetragonal (ferroelectric) phase of BaTiO_3 . Using our mean field model, the temperature dependence of the dielectric susceptibility (dielectric constant) was calculated from the spontaneous polarization. It was found that the lattice mode studied here is associated with the ferroelectric-paraelectric phase transition in BaTiO_3 .

Our predictions for the spontaneous polarization and the dielectric constant at various temperatures can be examined using the experimental data for thin films studied when they are available in the literature.

The damping constant for the soft mode of E(1TO) was calculated at various temperatures using the pseudospin-phonon coupled model and the energy fluctuation model for the ferroelectric- paraelectric transition in PbTiO_3 . This calculation of the damping constant was performed by means of the Raman frequency of this mode associated with the order parameter in the ferroelectric PbTiO_3 on the basis of both models.

The damping constant predicted from both models for the soft mode studied, increases abruptly with increasing temperature as the T_C is approached, as also observed experimentally in PbTiO_3 . Our predicted values of the damping constant for both models agree with the experimental data in the ferroelectric phase ($T < T_C$) of a single crystal of PbTiO_3 .

We used the isobaric definition of the “mode Grüneisen parameter” to predict the frequencies of longitudinal optic (LO) and transverse optic (TO) modes in sodium nitrite. The constant values of the “Grüneisen parameter” and the bulk volume data of NaNO_2 was taken from the literature. Our calculated values of frequencies are in good agreement with the observed data. One can use this model to calculate the temperature dependence of the frequencies of some other ferroelectric materials.

Temperature dependence of the damping constant for the LA mode of PZT-0.45 was calculated by using the pseudospin-phonon coupled model (Eq. 2.16) and energy fluctuation model (Eq. 2.19) in the ferroelectric phase. This calculation was performed by associating the observed Brillouin frequency shift of this LA mode with the order parameter (spontaneous polarization). The damping constant values calculated from both models increase very rapidly close to the transition temperature as observed experimentally for the LA mode of PZT-0.45 in the ferroelectric phase. Our calculated values of the damping constant are in good agreement with the observed data in the ferroelectric phase of lead zirconate titanate. We also extracted the activation energy value of this LA mode of PZT-0.45 close to the transition temperature and we compared with the $k_B T_C$ value.

We calculated the damping constant, relaxation time and the activation energy of the LA mode of PZT-0.45 above the transition temperature in the paraelectric phase ($T_C=657$ K). We performed all these calculations by associating the observed Brillouin frequency shift to the order parameter. We then used both the pseudospin-phonon coupled model and the energy fluctuation model to predict the damping constant, relaxation time and the activation energy of this LA mode of PZT-0.45. Our results calculated from both models are in good agreement with the observed data of damping constant and the inverse relaxation time for the LA mode of PZT-0.45.

The temperature dependences of the Raman frequency, damping constant and the activation energy were calculated for the Raman soft mode of $\text{Cd}_2\text{Nb}_2\text{O}_7$ below the transition temperature (ferroelectric phase). Calculation of the Raman frequency was performed by using the mean field theory. We then predicted the damping constant values of this Raman mode by using both the pseudospin-phonon coupled model and the energy fluctuation model with the mean field theory. Our calculated values of the frequency and the damping constant are in good agreement with the observed data. Finally, we give the activation energy values of this Raman mode of

CNO in the temperature intervals studied here and they are compared with the $k_B T_C$ value.

The temperature dependence of the damping constant was calculated by using the soft mode concept for the E_g mode of SrZrO_3 in the ferroelectric phase. This calculation was performed by using the pseudospin-phonon coupled model and the energy fluctuation model. As the temperature approaches the transition temperature, damping constant increases very rapidly as expected. Although both models studied here seem to describe the observed behavior, the energy fluctuation model agrees better than the pseudospin-phonon coupled model. Finally, we calculated values of the activation energy from both models studied here and compared with the $k_B T_C$ value of SrZrO_3 crystal.

The temperature dependence of the order parameter (squared) was calculated by using the Landau theory for the $A_1(\text{TO}_1)$ Raman mode in LiNbO_3 . Our results indicate a first order phase transition for LiNbO_3 . The damping constant of this mode was then calculated using the pseudospin-phonon coupled model and the energy fluctuation model. The damping constant calculated from both models agrees well with the observed data. The inverse relaxation time of the $A_1(\text{TO}_1)$ Raman mode was then calculated and compared with the observed data. This calculation was performed by using the damping constant predicted from both models and the values of the order parameter (squared) predicted from the Landau theory. We also calculated values of the activation energy from both models studied here for a given temperature range and they were compared with the $k_B T_C$ value of LiNbO_3 crystal.

4.1 Summary

The dynamical properties such as frequency ω , order parameter P , damping constant Γ , relaxation time τ , dielectric susceptibility χ , and the activation energy U of various ferroelectric materials have been investigated in a wide range of temperatures in this thesis. The frequency ω was obtained to decrease as the transition temperatures approached in the ferroelectric phase while it increases above the transition temperatures for those ferroelectric materials studied here. The soft mode behavior of the frequency was considered in both ferroelectric and paraelectric phases.

The damping constant of those ferroelectric materials studied in this thesis, has been predicted by using the pseudospin-phonon coupled model and the energy fluctuation model below and/or above the transition temperatures. The damping constant increases very rapidly as the transition temperature is approached both in the ferroelectric and paraelectric phases. Those damping constant calculated from both models (at least one of them) agrees well with observed data.

Values of the activation energy of those ferroelectric materials have been extracted as we have given in Table 3.33. These activation energy values were then compared with the $k_B T_C$ values. For example, values of the the activation energy calculated from both models are much greater than the $k_B T_C$ value (5 times) of CNO ($T_C=196$ K), while the activation energy value and the $k_B T_C$ value are in the same order for SrZrO₃ ($T_C=1443$ K) and LiNbO₃ ($T_C=1260$ K). Our results show that as the transition temperatures increase, the $k_B T_C$ values increase and it reaches the same order of the values of the activation energy calculated through both models (Table 3.33).

REFERENCES

- [1] Karacali H. Kiraci A. and Yurtseven H. *Physica status solidi B*. 247, 927 (2010).
- [2] Kiraci A. and Yurtseven H. *Ferroelectrics*, 432, 14 (2012).
- [3] Yurtseven H. and Kiraci A. *Ferroelectrics*, 437, 137 (2012).
- [4] Kiraci A. and Yurtseven H. *Ferroelectrics*, 432, 193 (2013).
- [5] Yurtseven H. and Kiraci A. *Journal of Molecular Modeling*, 19, 3925-3930, (2013).
- [6] Kiraci A. and Yurtseven H. "Calculation of the Damping Constant and the Order Parameter for the Lattice Modes in Ferroelectric PbTiO₃", *Ferroelectrics "ISAF-PIA, Int. Symposium on the Applications of Ferroelectrics, 21-25 July, 2013, Prague"*, (2013).
- [7] Yurtseven H. and Kiraci A. *Ferroelectrics*, 460, 149 (2014).
- [8] L. E. Cross and R. E. Newnham, In *Ceramics and Civilization*, Vol. III, ed. W. D. Kingery, The American Ceramic Society, Ohio, p. 289, 1987.
- [9] Valasek J. *Phys. Rev.* 15 (1920) 537 – 538; 17 (1921) 475 – 481.
- [10] Busch G. Scherrer P., *Naturwiss.* 23, 737 (1935).
- [11] Wainer E., and Salomon N., *Electrical Reports Titanium Alloys Manufacturing Division National Lead Co. Reports No. 8,9, 10 (1938-1943)*.
- [12] Unruh, H.G. *Ferroelectrics*, *Ullmann's Encyclopedia of Industrial Chemistry*, 157 (2000).
- [13] Wells A.F. *Structural Inorganic Chemistry*, Oxford University Press. (1984).

- [14] Scott J. F, Reviews of Modern Physics, 46,83-125, (1974).
- [15] Sawyer C. B. and Tower C. H. Physical Review, 35, 269 (1930).
- [16] Lines M.E. and Glass A.M. (Clarendon Press, Oxford, 1977)
- [17] Kittel C, Introduction to solid state physics, 6 th ed., J. Wiley, New York, (1986).
- [18] Jona F. and Shirane G. Ferroelectrics Crystals (Pergamon, London, 1962).
- [19] Ishidate T. *et al*, Phys. Rev. Lett. 78, 2397 (1997).
- [20] Sawaguchi E. J. Phys. Soc. Jpn. 54, 480 (1985).
- [21] Yamaguchi M. *et al*, Phys. Rev. Lett. 75, 1399 (1995).
- [22] Samara G. A. Phys. Rev. 151, 378 (1966).
- [23] Sawaguchi E. Jpn. J. Appl. Phys. 24, Suppl. 24-2, 252 (1985).
- [24] Harada J. Phys. Rev. B4, 155 (1971).
- [25] Quittet A. M. and Lambert M., Solid St. Commun. 12, 1053 (1973).
- [26] Scalabrin A. Phys. Stat. Solidi (b) 79, 731 (1977).
- [27] Yamaguchi H. J. Phys. Soc. Jpn. 56, 589 (1987).
- [28] Begg B. D. *et al*, J. Am. Ceram. Soc. 79, 2666 (1996).
- [29] Luspín Y. J. Phys. C: Solid St. Phys. 13, 3761 (1980).
- [30] Sedykh P. and Michel D., Phys. Rev. B 79, 134119 (2009).
- [31] Yamaguchi H., J. Phys. Soc. Jpn. 57, 147 (1988).
- [32] Akishige Y. J. Phys. Soc. Jpn. 57, 718 (1988).
- [33] Burns G. and Scott B. A. Phys. Rev. B, 7, 3088 (1973).
- [34] Gavrilyachenko V. G. *et al*, Phys. Solid State, 40, 1402 (1998).
- [35] Sani A. J. Phys.: Condens. Matt. 14, 10601 (2002).
- [36] Fu D. S. *et al*, *et al*, J. Phys.: Condens. Matt. 12, 399 (2000).
- [37] Le Marrec F. J. Eur. Cer. Soc. 21, 1615 (2001).
- [38] Pytte E., Phys. Rev. B, 5, 3758 (1972).
- [39] Slater J. C. J. Chem. Phys. 9, 16 (1941).

- [40] Kobayashi K. K.J. Phys. Soc. Jpn. 24, 497 (1968).
- [41] Blinc R. and Zēks B. Adv. Phys. 21, 693 (1972).
- [42] Peercy P. S., Phys. Rev. B12, 2725 (1975).
- [43] Wilson C. M. and Cummins H. Z. (Springer, New York, 1969).
- [44] Kaminov I. P. and Damen T. C., Phys. Rev. Lett. 20, 1105 (1968).
- [45] Scott J. F. and Wilson C. M. Solid State Commun. 10, 597 (1972).
- [46] She C. Y. Phys. Rev. B6 1580 (1972).
- [47] Lamas A. da Costa, *et al*, Phys. Stat. Sol. (a) 68, 173 (1981).
- [48] Kay M. I., and Frazer B. C., Acta Crystal. 14, 56 (1961).
- [49] Tanisaki S. J. Phys. Soc. Jpn. 16, 579 (1961).
- [50] Komatsu K., *et al*, J. Phys. Soc. Jpn. 57, 2836 (1988).
- [51] Sawada S., Phys. Rev. Lett. 1, 320 (1958).
- [52] Tanisaki S. J. Phys. Soc. Jpn. 18, 1181 (1963).
- [53] Yamada Y., and Yamada T. J. Phys. Soc. Jpn. 21, 2167 (1966).
- [54] Takagi Y., and Gesi K., J. Phys. Soc. Jpn. 19. 142 (1964).
- [55] Hamano K. J. Phys. Soc. Jpn. 19, 945 (1964).
- [56] Sakiyama M., J. Phys. Soc. Jpn. 20, 2180 (1965).
- [57] Ema K., *et al*, J. Phys. Soc. Jpn. 39, 726 (1975).
- [58] Chisler E. V., and Shur M. S. Phys. Stat. Sol. 17 163 (1966).
- [59] Asawa C. K., and Barnoski K., Phys. Rev. B2 205 (1970).
- [60] Brehat F. and Wyncke B. J. J. Phys. C: Solid State Phys. 18 1705 (1985).
- [61] Fahim M. A., Thermochemica Acta. 363, 121 (2000).
- [62] Shimizu H., J. Phys. Soc. Jpn. 36 498 (1974).
- [63] Hatta I. J. Phys. Soc. Jpn. 48 160 (1980).
- [64] Buchheit W., Solid State Comm. 40 411 (1981).
- [65] Sakurai J., Cowley R. A. and Dolling G. J. J. Phys. Soc. Jpn. 28 1426 (1970).
- [66] Durand D. *et al*, Physica B136 325 (1986).

- [67] Jaffe B. *Piezoelectric Ceramics* (Academic, London, 1971).
- [68] Phelan D. *Phys. Rev. Lett.* 105, 207601 (2010).
- [69] Buixaderas E., *et al.* *Phys. Rev. B* 84, 184302 (2011).
- [70] Kim T. H. *et al.* *App. Phys. Lett.* 100, 082903 (2012).
- [71] Bokov A. A. *et al.* *Phys. Rev. B* 81, 172103 (2010).
- [72] Hlinka J., *et al.* *Phys. Rev. B* 83, 140101(R) (2011).
- [73] Gorfman S. *Phys. Rev. B* 84, 020102(R) (2011).
- [74] Cordero.F. *et al.* *Phys. Rev. Lett.* 98, 255701 (2007).
- [75] Zhang S.*et. al.* *Jpn. J. Appl. Phys.* 36, 2994 (1997).
- [76] Bouzid A. *et al.*,*J. Eur. Ceram. Soc.* 25, 3213 (2005).
- [77] Franke I. *et al.* *Phys. Rev. B* 73, 144114 (2006).
- [78] Ahtee M. *et al.* *Acta Crystallogr., Sect. B: Struct. Crystallogr. Cryst. Chem. B* 34, 752 (1978).
- [79] Carlsson L, *Acta Crystallogr.* 23, 901 (1967).
- [80] Zhao Y. and Weidner D. J., *Phys. Chem. Miner.* 18, 294 (1991).
- [81] Fujimori H. *et al.* *Phys. Rev. B* 61, 3971 (2000).
- [82] Tachibana M. *et al.* *Phys. Rev. B* 70, 064103 (2004).
- [83] Isupov V. A., *Phys. Solid State* 47, 2119 (2005).
- [84] Buixaderas E. *et al.* *Eur. Phys. J. B* 19, 9 (2001).
- [85] A. Küster, *Phasenübergänge bei ferroelektrischem Cd₂Nb₂O₇ und verwandten Substanzen* (Dissertationsschrift, Tübingen, Germany, 1992).
- [86] Salaev F. M. A. *et al.* *Fiz. Tverd. Tela.* 25, 163 (1983).
- [87] Markovin P. A. *et al.* *Fiz. Tverd. Tela.* 25, 3642 (1983).
- [88] Smolensky G. A *et al.* *Pis'ma v ZhET.* 37, 257 (1983).
- [89] Smolensky G. A *et al.* *Ferroelectrics.* 55, 321 (1984).
- [90] Salaev F. M. A. *et al.* *Pis'ma v ZhET.* 10, 600 (1984).
- [91] Taniguchi H. *et al.* *Phys. Rev. B* 77, 224104 (2008).

- [92] Ridah A. *et al.* Phys. Rev. B 56, 565967 (1997).
- [93] Servoin J. L and Gervais F. Solid State Commun. 31, 387 (1979).
- [94] Chowdhury M. R. J. Phys. C. 7, 99 (1974).
- [95] Abraham S. C. *et al.* J. Phys. Chem. Solids 34, 521 (1973).
- [96] Smolensky G. A *et al.* Phys. Status Solidi. 13, 309 (1966).
- [97] Gallagher P. K. and Jr O'Bryan H. M., J. Am. Ceram. Soc. 68, 147 (1985).
- [98] Thomas H. and Müller K. A. Phys. Rev. Lett. 21, 1256 (1968).
- [99] Cochran W. Phys. Rev. Lett. 3, 521, (1959).
- [100] de Gennes P.G. Solid State Commun. 1, 132 (1963).
- [101] Yamada Y. *et.al.* J. Phys. Soc. Jpn. 32 1565 (1972).
- [102] Matsushita M. J. Chem. Phys. 65 23 (1976).
- [103] Laulicht I. and Luknar N. Chem. Phys. Lett. 47 237 (1977).
- [104] Laulicht I. J. Phys. Chem. Solids 39 901 (1978).
- [105] Lahajnar G. Phys. Cond. Matter 18 301 (1974).
- [106] Schaack G. and Winterfelt V. Ferroelectrics 15, 35 (1977).
- [107] Brout R. Phase Transitions (Benjamin, New York, 1965) Chap. 2.
- [108] Grüneisen, E. Annals Physik, 12, 257 (1912).
- [109] Gillet, P. *et al.*J. Geophys. Res. 96(B7), 11805 (1991).
- [110] Rakov A. V. Opt. Spectrosc. 7, 128 (1959).
- [111] Bartoli F. F. and Litovitz T. A., J. Chem. Phys. 56, 413 (1972).
- [112] Sathiah, S., and Bist, H. D. Z. phys. Bcondensed Matter 84, 423 (1991).
- [113] Samara G. A. Phys. Rev. Lett. 27 103 (1971).
- [114] Inoue K. *et al.* Phys. Rev. B 38, 6352 (1988).
- [115] Luspín Y. *et al.* J. Phys. C: Solid St. Phys. 13, 3761 (1980).
- [116] Yurtseven H. Karacali H. and Kiraci A. Int. J. Mod. Phys. B. 25, 2063 (2011).
- [117] Bastow T. J. *J. Phys.: Condens.Matter.* 1, 4985 (1989).
- [118] Kanert O. *et al.**Solid State Commun.* 91, 465 (1994).

- [119] Karpov S. V. and Shultin A. A. *Soviet Physics-Solid State*. 17, 1915 (1976).
- [120] Karacali H, Yurtseven H. and Kiraci A. *Phys. Status Solidi B*. 246, 1124–1131 (2009).
- [121] Begg, B. D. *et al.* *J. Am. Ceram. Soc.* 79, 2666 (1996).
- [122] Akishige Y. *et al.* *Solid State Commun.* 60, 445 (1986).
- [123] Yurtseven H. and Sherman W. F. *Phase Trans.* 54, 165 (1995).
- [124] Marssi M. E. *et al.* *Ferroelectrics*. 291, 55 (2003).
- [125] Gupta S. J. *Raman Spectrosc.* 33, 42 (2002).
- [126] Wada S. *et al.* *Jpn. J. Appl. Phys.* 37, 5385 (1998).
- [127] Samara G. A. *Phys. Rev.* 151 151 (1968).
- [128] Ho Cho K and Lee H. Y. *IEEE*, CH3416-5, 566 (1995).
- [129] Yasmin S. *et al.* *J. Ceram. Process. Res.* 12, 387 (2011).
- [130] Heywang W. J. *Am. Ceram. Soc.* 47, 484 (1964).
- [131] Winterfeldt V. *et al.* *Ferroelectrics*. 15, 21 (1977).
- [132] Petzelt J. and Dvorak V. *Vibrational spectroscopy of phase transitions* (Acedemic pres, Orlando, 1984, Chapter 2).
- [133] Hossain M. A. *et al.* *J. Phys. Chem. Solids* 55 85 (1994).
- [134] Hossain M. A. *et al.* *Phys. Status Solidi A* 141, 335 (1994).
- [135] Fokin A. *et al.* *J. Electroceram.* 22, 270 (2009).

CURRICULUM VITAE

Ali Kiraci

Personel Information

Last name: Kiraci

First name: Ali

Date of birth: 5th August, 1981.

Title: Master of Science

Address: Cankaya University, Materials science and Engineering,

06530, Ankara / TURKEY

Tel: (+90)312 210 20 00

e-mail: akiraci@cankaya.edu.tr

Education

2009- Ph.D Middle East Technical University (GPA: 3.63/4.00).

2005-2008 M. Sc. in Physics, Abant Izzet Baysal University. (GPA: 3.86/4.00).

Supervisors: Dr. H. Karacali and Prof. Dr. H. Yurtseven

Thesis Title: *“Temperature Dependence Of The Damping Constant*

(Linewidth) Of Raman Modes In NaNO₂ And (NH₄)₂SO₄

Near The Phase Transitions.”

2000-2005 BSc Physics, Abant Izzet Baysal University. (GPA: 3.86/4.00).

Including oner year English preparation class (2000-2001), with a distinction (as the best bachelor in 2005).

Employment

- 2013\ Instructor, Cankaya University, Ankara, Turkey
- 2009-2013 Research Assistant, Dept. Physics , Middle East Technical University, Ankara, Turkey
- 2006 -2009 Research Assistant, Dept. Physics , Abant Izzet Baysal University, Bolu, Turkey

Computer Skills

Microsoft Office, Internet Explorer, Origin , Picker, Mathematica.

Teaching Skills:

Laboratory assistant: Freshman physics lab(Kinematics+Electricity).

Optics and waves, Applied Quantum physics, Modern physics,

Applied Electricity and Magnetism.

Languages

Turkish, English.

Publications Records

- 1) H.Yurtseven, C. Sisman Korkmaz and **A. Kiraci** “*Temperature dependence of the Brillouin frequency shift and the linewidth of the LA mode in the ferroelectric phase of PZT-x (PbZr_{1-x}Ti_xO₃).*”, ISAF-ISIF-PFM Joint Conference, Singapore, 2015. (Accepted).
- 2) H. Yurtseven, **A. Kiraci**, “*Calculation of the Infrared Frequencies as a Function of Temperature Using the Volume Data in the Ferroelectric Phase of NaNO₂*”, Ferroelectrics, 460:149–156, 2014.
- 3) **A. Kiraci**, H. Yurtseven, “*Calculation of the Damping Constant and the Order Parameter for the Lattice Modes in Ferroelectric PbTiO₃*”, Ferroelectrics "ISAF-PIA, Int. Symposium on the Applications of Ferroelectrics, 21-25 July, 2013, Prague", (2013).

- 4) H. Yurtseven, **A. Kiraci**, “*Temperature Dependence of the Polarization and the Dielectric Constant Near the Paraelectric- Ferroelectric Transitions in BaTiO₃*”, Journal of Molecular Modeling, 19, 3925-3930, (2013).
- 5) **A. Kiraci**, H. Yurtseven, “*Damping Constant Calculated as a Function of Temperature for the Tetragonal Raman Mode Close to the Paraelectric-Ferroelectric Transition in BaTiO₃*”, Ferroelectrics, 450:93–98, 2013.
- 6) H. Yurtseven, **A. Kiraci**, “*Calculation of the Damping Constant and the Relaxation Time for the Soft-Optic and Acoustic Mode in Hexagonal Barium Titanate*”, Ferroelectrics, 437, 137-148, (2012).
- 7) **A. Kiraci**, H. Yurtseven, “*Temperature dependence of the raman frequency, damping constant and the activation energy of a soft-optic mode in ferroelectric barium titanate*”, Ferroelectrics, 432, 14-21, 2012.
- 8) H. Karaçalı, H. Yurtseven, **A. Kiraci**, “*Calculation of the damping constant and activation energy for Raman mode in (NH₄)₂SO₄*”, International Journal of Modern Physics B. Vol. 25. No. 2063. 2011.
- 9) H. Karaçalı, **A. Kiraci**, H. Yurtseven, “*Calculation of the Raman frequency and the damping constant of a coupled mode in the ferroelectric and paraelectric phases in KH₂PO₄*”, Physica status solidi B. 247, No. 4, 927-936 (2010).
- 10) **A. Kiraci**, H. Karaçalı, H. Yurtseven, “*Temperature dependence of the order parameter, damping constant and activation energy close to phase transition in sodium nitrite*”, Journal of Optoelectronics and Advanced Materials - SYMPOSIA, Vol. 1, No. 3, 2009, p. 322 – 325.
- 11) H. Karaçalı, H. Yurtseven, **A. Kiraci**, “*Raman linewidths calculated as a function of temperature in NaNO₂*”, Physica status solidi B. 246, No. 5, 1124–1131 (2009).

Conferences, Meetings and Courses Attended

- **2015 JOINT ISAF-ISIF-PFM Conference**, Singapore, May 2015, presented poster.
- **2013 Joint UFFC, EFTF and PFM Symposium**, Prague, July 2013, presented poster.
- **The 8 th Asian Meeting on Ferroelectrics (AMF-8)**, Thailand, December 2012, presented poster.
- **ISAF-ECAPD 2010**, Edinburgh, August 2010, presented poster.
- **Condensed Matter Physics Conference of Balkan Countries**, Mugla, May 2008, presented poster.

- **APS 2008 March Meeting**, New Orleans, March 2008, oral session.
- “*Phase Transitions and renormalization groups*”, Feza Gursev Institute, Istanbul, **Summer school**, given by Prof. Dr. A. Nihat Berker, 8-19 June 2007.

Awards, Fellowships, and Grants

- The Scientific and Technological Research council of Turkey fellowship, 2009- 2014 (Ph. D)
- The Scientific and Technological Research council of Turkey fellowship, 2005-2007.(M. Sc)
- The top student Bachelor of Science, 2005.
- Turkish Physical Society fellowship, 2004-2005